BASIC SHIP-PLANNING SUPPORT SYSTEM USING BIG DATA IN MARITIME LOGISTICS FOR SIMULATING DEMAND GENERATION

(海上物流ビッグデータを活用した
船舶需要創出シミュレーションのための船舶基本計画支援システムの開発)

DIMAS ANGGA FAKHRI MUZHOFFAR
D195726

DISSERTATION

Submitted to the Graduate School of Engineering, Hiroshima University

September 2022
Higashi-Hiroshima

Hiroshima University
Graduate School of Engineering
Department of Transportation and Environmental System
Laboratory of Transportation System Innovation

this page intentionally left blank

TABLE OF CONTENT

TABLE OF CONTENT i
LIST OF TABLES v
LIST OF FIGURES vii
1. INTRODUCTION 1
1.1. Research Background 1
1.2. Objective in This Study 2
1.3. Structure of This Dissertation 2
2. LITERATURE REVIEW 5
2.1. Related Studies utilizing Big Data in Maritime Logistics 5
2.1.1. Overview of Studies discussing Cargo Throughput Forecasting 5
2.1.2. Overview of Studies discussing Shipping and Newbuilding Markets 8
2.1.3. Overview of Studies discussing Optimization Studies in Ship Deployment and Contracts 9
2.2. Originalities in This Study 11
3. BASIC CONCEPT 13
3.1. Big Data in Maritime Logistics used in This Study 13
3.1.1. Description of Ship Movement Data 13
3.1.2. Description of Ship Data 17
3.1.3. Description of Port Data 17
3.1.4. Description of Route Data 18
3.2. Configuration of Ship Basic-Planning Support System 19
3.2.1. Description of Global Network Model 21
3.2.2. Description of Cargo Movement Model 22
3.2.3. Description of Ship Model 22
3.2.4. Description of Ship Allocation Algorithm 23
4. MODEL DEVELOPMENT 24
4.1. Overview of Model Development 25
4.2. Development of Global Network Model 26
4.2.1. Overview of Global Network Model 26
4.2.2. Methodology to define Global Network Model 26
4.2.3. Results of Global Network Model 28

4.3. Development of Cargo Movement Model 31
4.3.1. Overview of Cargo Movement Model 31
4.3.2. Methodology to define Cargo Movement Model 31
4.3.3. Results of Cargo Movement Model 33
4.4. Development of Ship Model 35
4.4.1. Overview of Ship Model 35
4.4.2. Description of Ship Specifications 36
4.4.3. Methodology to predict Operation Condition 37
4.4.4. Evaluation of Predicted Operation Condition 40
4.5. Methodology to Calculate GHG emissions 41
4.5.1. Overview of GHG emissions Calculation 41
4.5.2. Calculation Process of GHG Emissions 43
4.5.3. Evaluation of GHG Emissions Calculation 49
4.6. Methodology to Calculate COST 50
4.6.1. Overview of COST Calculation 50
4.6.2. Calculation Process of COST 50
4.4.1. Evaluation of COST Calculation 60
4.7. Development of Ship Allocation Algorithm 60
4.7.1. Algorithm 1: Ship Replacement while Preserving the Existing Ship Allocation 60
4.7.2. Algorithm 2: An Optimization for Reconstructing Ship Allocation in Time-Charter Contract 61
4.7.3. Algorithm 3: An Optimization for Reconstructing Ship Allocation in Voyage-Charter Contract 63
4.7.4. Methodology to visualize Simulation Results 64
5. CASE STUDIES AND DISCUSSIONS 69
5.1. Case Studies intended for Capesize Dry Bulk Carrier 69
5.1.1. Overview of Case Studies intended for Capesize Dry Bulk Carrier 69
5.1.2. Definition of New Ships Instances in Case Studies intended for Capesize Dry Bulk Carrier 70
5.1.3. Actual Ship Allocation of Capesize Dry Bulk Carrier 72
5.1.4. Case study 1: Ship Replacement while Preserving the Existing Ship Allocation 73
5.1.5. Case study 2: Optimization of Ship Allocation in Time-Charter Contract using Existing Ships 75
5.1.6. Case study 3: Optimization of Ship Allocation in Time-Charter Contract with New Ships Instance 78
5.1.7. Discussion 1: Significance of the Total COST and GHG Emissions Reductions 81
5.1.8. Discussion 2: New Ship Demand 83

5.2. Case Studies intended for Panamax and MiniCape Dry Bulk Carriers 86
5.2.1. Overview of Case Studies intended for Panamax–MiniCape Dry Bulk Carriers 86
5.2.2. Definition of New Ships Instance in Case Studies intended for Panamax–MiniCape Dry Bulk Carriers 87
5.2.3. Actual Ship Allocation of Panamax–MiniCape Dry Bulk Carriers 89
5.2.4. Case study 4: Ship Replacement while Preserving the Existing Ship Allocation 91
5.2.5. Case study 5: Optimization of Ship Allocation in Time- and Voyage-Charter Contracts using Existing Ships 93
5.2.6. Case study 6: Optimization of Ship Allocation in Time- and Voyage-Charter Contracts with New Ships Instance 98
5.2.7. Discussion 3: Significance of the Total COST and GHG Emissions Reductions in Time- and Voyage-Charter Contracts 103
5.2.8. Discussion 4: New Ship Demand in Time- and Voyage-Charter Contracts 105
5.3. Case Studies intended for Panamax Dry Bulk Carrier of Specific Ship Operator 109
5.3.1. Overview of Case studies intended for Future Scenario 109
5.3.2. Actual Ship Allocation of Panamax Dry Bulk Carriers of Ship Operator **A** 110
5.3.3. Case study 7: Optimization of Ship Allocation in Time- and Voyage-Charter Contracts using Existing Ships 111
5.3.4. Case study 8: Optimization of Ship Allocation in Voyage-Charter Contract with New Ships Instance 112
5.4. Case Studies intended to examine Competitive Ship Dimension of Panamax and MiniCape Dry Bulk Carriers 115
5.3.5. Overview of Case Studies intended to examine Competitive Ship Dimension of Panamax Dry Bulk Carrier 115
5.3.6. Case study 9: Optimization of Ship Allocation in Time- and Voyage-Charter Contracts using only New Ships 116
5.5. Case Studies intended for Future Scenario 118
5.4.1. Overview of Case studies intended for Future Scenario 118
5.4.2. Case study 10: Optimization of Ship Allocation in Time- and Voyage-Charter Contracts intended for Future Scenario 119
5.4.3. Discussion 5: Future Potential Emissions Reductions by using Fuels with Lower Emissions Factors 130
6. CONCLUDING REMARKS 133
REFERENCES 135
ACKNOWLEDGEMENTS 139

this page intentionally left blank

LIST OF TABLES

Table 1. Related studies utilizing big data in maritime logistics. 5
Table 2. Resemblance between Arifin et al. [30] and this study. 11
Table 3. Features of MINT database [39]. 14
Table 4. Features of AXSDry database [40]. 16
Table 5. Features of Sea-web Ships database [42]. 17
Table 6. Features of Sea-web Port and Ports and Terminal Guide databases [43,44]. 18
Table 7. Features of distance table [44]. 19
Table 8. Overview of the global network model. 26
Table 9. Country list of the global network model of Capesize dry bulk carrier. 29
Table 10. Country list of the global network model of Panamax–MiniCape dry bulk carrier. 30
Table 11. Top exporters and importers of iron ore and coal in 2018 [31]. 30
Table 12. Overview of the cargo movement model. 31
Table 13. A sample of 2018 annual iron ore origin–destination (OD) table of Capesize dry bulk carrier [39]. 33
Table 14. A sample of 2018 annual iron ore OD table of Panamax–MiniCape dry bulk carrier [40]. 34
Table 15. A sample of 2018 monthly iron ore OD table of Panamax–MiniCape dry bulk carrier [40]. 35
Table 16. Overview of the ship model. 36
Table 17. A sample of recorded operation conditions in AXSDry data [40]: laden voyage. 39
Table 18. A sample of recorded operation conditions in AXSDry data [40]: ballast voyage. 39
Table 19. Mean absolute error of DL model predictions. 40
Table 20. Mean absolute error of route-base average (R-AVG). 41
Table 21. Correction factors of weather and fouling of various ship types [28,29]. 44
Table 22. Specific fuel oil consumption of various main engine and fuel types [28,29]. 45
Table 23. Emission factors for various fuel types [28,29]. 48
Table 24. Obtainable GHG emissions from main engine for various fuel types [28,29]. 49
Table 25. Evaluation of GHG calculation. 49
Table 26. Bunker prices for various fuel types in 2030–2050 [28]. 51
Table 27. Stockpile cost units for various cargo types [52]. 58
Table 28. Evaluation of COST calculation. 60
Table 29. Defined region for simulation results visualization. 66
Table 30. Overview of case studies of Capesize dry bulk carrier. 70

Table 31. Assumed specifications of the new ships. 72
Table 32. Results of case studies 1, 2, and 3. 82
Table 33. Significant main port limitations of West Australia and China. 85
Table 34. Overview of case studies of Panamax–MiniCape dry bulk carrier. 86
Table 35. Assumed specifications of the new ships. 88
Table 36. Results of case studies 4, 5, and 6. 103
Table 37. Average economic days taken from case study 5 104
Table 38. Size limitations of significant routes with highest annual cargo movement demand. 108
Table 39. Size categories consisted in ship list of Ship Operator **A**. 110
Table 40. Results of case studies 7a and 7b. 111
Table 41. Proposed new ship specifications. 113
Table 42. Allocated ships and operation numbers in case study 8. 114
Table 43. Assumed specifications of the new ships. 116
Table 44. Results of case study 9. 117
Table 45. Overview of case studies intended for future scenario. 118
Table 46. Defined specifications of the new ships in 2030 and 2050. 120
Table 47. Properties of various main engine's fuel types in 2030–2050 [28]. 121
Table 48. Total GHG emissions of case study 10. 130

LIST OF FIGURES

Figure 1. Structure of this dissertation. 3
Figure 2. The forecasting method proposed by Yang and Chang [13]: Convolutional neural network and long short-term memory (CNN-LSTM). 6
Figure 3. The AIS-based estimated iron ore payload by Zhou and Hu [18]:China's Monthly Iron Ore Imports in 2018 (%). 8
Figure 4. System configuration of Arifin et al. [30]. 19
Figure 5. System configuration of this study. 20
Figure 6. Worldwide ports of the global network model of Capesize dry bulk carrier. 27
Figure 7. Worldwide ports of the global network model of Panamax–MiniCape dry bulk carrier.. 28
Figure 8. Deep learning (DL) model to predict operation conditions. 38
Figure 9. Calculation process of cargo movement, GHG emissions, and ship cost. 43
Figure 10. Daily average fuel consumption of auxiliary engine and boiler [28,29]. 45
Figure 11. Bunker prices of high-Sulphur fuel oil 380 cSt and marine diesel oil in various bunker hubs [48]. 51
Figure 12. Bulk carrier daily operation cost for the given ship deadweight tonnage (DWT) and ship age [1,29,46,47]. 53
Figure 13. Bulk carrier ship prices for the given ship DWT and ship age [1,29,46,47]. 54
Figure 14. Response surfaces of bulk carrier operation cost: 3D and 2D visualizations [1,29,46,47]. 55
Figure 15. Response surfaces of bulk carrier depreciation cost: 3D and 2D visualizations [1,29,46,47]... 56
Figure 16. A sample of the COST composition. 59
Figure 17. Specified region of worldwide ports of Capesize dry bulk carrier. 65
Figure 18. Specified region of worldwide ports of Panamax–MiniCape dry bulk carriers. 65
Figure 19. A sample of great circle visualization: (**a**) average DWT, (**b**) average sailing speed, and (**c**) average ship age. 67
Figure 20. Ship admiralty coefficient (ADM) of Capesize dry bulk carrier before and after common structural rules for bulk carriers (CSR-BC) [42,56,57]. 70

Figure 21. Actual ship allocation of Capesize dry bulk carrier: (**a**) Average DWT and (**b**) sailing speed. 73
Figure 22. Ship replacement while preserving existing ship allocation of Capesize dry bulk carrier: Allocated new ship rate of (**a**) case study 1a (COST-optimized) and (**b**) case study 1b (GHG-optimized). 74
Figure 23. Ship allocation optimization in time-charter contract using existing ships of Capesize dry bulk carrier: Case study 2a (COST-optimized) (**a**) average DWT and (**b**) sailing speed. 76
Figure 24. Ship allocation optimization in time-charter contract using existing ships of Capesize dry bulk carrier: Case study 2b (GHG-optimized) (**a**) average DWT and (**b**) sailing speed..... 77
Figure 25. Ship allocation optimization in time-charter contract of Capesize dry bulk carrier with new ships instance: Case study 3a (COST-optimized) (**a**) average DWT and (**b**) sailing speed. 79
Figure 26. Ship allocation optimization in time-charter contract of Capesize dry bulk carrier with new ships instance: Case study 3b (GHG-optimized) (**a**) average DWT and (**b**) sailing speed..... 80
Figure 27. Average sailing distances of case study 2: ship allocation optimization in time-charter contract using existing ships of Capesize dry bulk carrier..... 81
Figure 28. Ship allocation optimization of Capesize dry bulk carrier with new ships instance: Allocated new ship rate of (**a**) case study 3a (COST-optimized) and (**b**) case study 3b (GHG-optimized). 84
Figure 29. COST- and GHG-optimized ship allocation with new ships instance (case study 3): Composition of operations in the routes of West Australia–China..... 85
Figure 30. Ship ADM of Panamax–MiniCape dry bulk carriers before and after CSR-BC [42,56,57]. 87
Figure 31. Actual ship allocation of Panamax–MiniCape dry bulk carriers: (**a**) Average DWT, (**b**) sailing speed, and (**c**) ship age. 90
Figure 32. Ship replacement while preserving existing ship allocation of Panamax–MiniCape dry bulk carriers: Allocated new ship rate of (**a**) case study 4a (COST-optimized) and (**b**) case study 4b (GHG-optimized). 92
Figure 33. Ship allocation optimization in time-charter contract using existing ships of Panamax–MiniCape dry bulk carriers: Case study 5a (COST-optimized) (**a**) average DWT and (**b**) ship age. 94
Figure 34. Ship allocation optimization in time-charter contract using existing ships of Panamax–MiniCape dry bulk carriers: Case study 5b (GHG-optimized) (**a**) average DWT and (**b**) ship age. 95

Figure 35. Ship allocation optimization in voyage-charter contract using existing ships of Panamax–MiniCape dry bulk carriers: Case study 5c (COST-optimized) (**a**) average DWT and (**b**) ship age. 96
Figure 36. Ship allocation optimization in voyage-charter contract using existing ships of Panamax–MiniCape dry bulk carriers: Case study 5d (GHG-optimized) (**a**) average DWT and (**b**) ship age. 97
Figure 37. Ship allocation optimization in time-charter contract of Panamax–MiniCape dry bulk carriers with new ships instance: Case study 6a (COST-optimized) (**a**) average DWT and (**b**) ship age. 99
Figure 38. Ship allocation optimization in time-charter contract of Panamax–MiniCape dry bulk carriers with new ships instance: Case study 6b (GHG-optimized) (**a**) average DWT and (**b**) ship age. 100
Figure 39. Ship allocation optimization in voyage-charter contract of Panamax–MiniCape dry bulk carriers with new ships instance: Case study 6c (COST-optimized) (**a**) average DWT and (**b**) ship age. 101
Figure 40. Ship allocation optimization in voyage-charter contract of Panamax–MiniCape dry bulk carriers with new ships instance: Case study 6d (GHG-optimized) (**a**) average DWT and (**b**) ship age. 102
Figure 41. Ship replacement while preserving existing ship allocation of Panamax–MiniCape dry bulk carrier: Allocated new ship rate of (**a**) case study 6a (COST-optimized), (**b**) case study 6b (GHG-optimized) (**c**) case study 6c (COST-optimized), (**d**) case study 6d (GHG-optimized). 106
Figure 42. COST- and GHG-optimized ship allocation with new ships instance (case study 6): Composition of operations in the worldwide routes. 107
Figure 43. Average monthly cargo movement demand used in the ship allocation with new ships instance (case studies 6c and 6d). 109
Figure 44. Visualization of actual ship allocation of panamax dry bulk carrier of Ship Operator **A**. 110
Figure 45. Economic days of a sample ship of Ship Operator **A**. 112
Figure 46. Admiralty coefficient of ships of Ship Operator A. 113

Figure 47. Visualization of actual ship allocation and ship allocation optimization of case study 8. 114
Figure 48. Ship age of ships in the actual ship allocation of Ship Operator **A**. 115
Figure 49. Changes in the allocated ships dimension of case study 9. 118
Figure 50. Linear projection of the GHG emissions target from 2008 to 2050 [49-51]. 119
Figure 51. ADM of Panamax and MiniCape in 2030 and 2050 [42,56,57]. 120
Figure 52. Projection of Cargo Movement Demand [40,58]: (**a**) annual and (**b**) monthly. 121
Figure 53. Ship allocation optimization in time-charter contract using new ships in 2030: Case study 10a (GHG-optimized) average DWT using (**a**) HFO, (**b**) LNG, and (**c**) MeOH. 123
Figure 54. Ship allocation optimization in voyage-charter contract using new ships in 2030: Case study 10b (GHG-optimized) average DWT using (**a**) HFO, (**b**) LNG, and (**c**) MeOH. 124
Figure 55. Ship allocation optimization in time-charter contract using new ships in 2050: Case study 10c (GHG-optimized) average DWT using (**a**) HFO, (**b**) LNG, and (**c**) MeOH. 128
Figure 56. Ship allocation optimization in voyage-charter contract using new ships in 2050: Case study 10d (GHG-optimized) average DWT using (**a**) HFO, (**b**) LNG, and (**c**) MeOH. 129
Figure 57. Annual GHG emissions reductions by using LNG (case studies 9a and 9b). 131
Figure 58. The extended ADM by 10% and 20% projected from the linear ADM of Panamax–MiniCape dry bulk carriers. 132
Figure 59. Annual GHG emissions reductions by using LNG (case studies 9a and 9b) with an extended ADM by 10% and 20%. 132

1. INTRODUCTION

1.1. Research Background

Economic growth creates dynamic changes in the global market, including the maritime industry. On a worldwide scale, huge demand for industrial cargo transport promotes intense ship movement and replacement [1]. As the demand for newbuilding specifications also changes according to the circumstances, developing a ship with adequate specifications to satisfy this demand is essential.

Meanwhile, the use of digital infrastructure to alter a business model and implement value-producing opportunities naturally generates a large data stream called big data. With the reduction in cost of data collection tools, a large amount of data can be obtained from various sources and formats [2,3]. This is significant for a broader understanding of the current and future conditions of various industries. Therefore, big data analytics will be a critical advantage in the future [4].

In the maritime industry, big data are being generated through advancements in navigation systems [5,6]. Together with the voyage data recorder, an automatic identification system (AIS) is required by the International Convention for the Safety of Life at Sea to aid navigation and avoid collisions of ocean-going ships. Towards its development, the deployment of satellite-based AIS receiver enables an accurate ship's geospatial monitoring on a worldwide scale [7]. From the ship side, an AIS transponder also transmits a ship's identification number, position, course, speed, and destination. These systems uphold the digitalization of previously analog-stored data, such as ship specifications, port limitations, and sailing routes [8].

The collection of static and dynamic big data in maritime logistics has allowed various studies to be conducted. Safety improvement, energy efficiency, logistics optimization, and predictive analysis have been broadly discussed [9-12]. Similarly, many data-driven studies have introduced a demand forecasting application for both regional and global scales. Forecasting analyses, such as the cargo throughput and shipbuilding market, have also been presented in some studies [13-25]; however, the demand for new ship specifications is unlikely to have been covered.

1.2. Objective in This Study

With big data in maritime logistics, ship operation monitoring is becoming relevant. Besides, shipbuilding tends to apply risk-based design rather than rules-based design, with aims of compatibility of design and performance [26,27]. Likewise, the International Maritime Organization (IMO) greenhouse gas (GHG) reduction strategy [28,29] set out a new future guideline. Therefore, it is crucial to examine the actual ship operation characteristics in the particular route to optimize its future ship design, both cost- and GHG-effectively.

Our prior studies examined the demand for new ship specifications by proposing a basic ship-planning support system using big data in maritime logistics [30]. We built the system and conducted the simulations in the form of a basic study. The proposed system was applied to the target ship of Capesize dry bulk carrier, which operated on relatively fixed routes, such as Australia and Brazil to East Asia routes [31]. Assuming the target ship operated in a time-charter contract manner, we built an algorithm to replicate its ship bidding scheme. However, the scope of that study was limited by the target routes and ship allocation considerations. The previous system delivered the simulations by only considering the ships' fuel costs; by contrast, this study has proposed an enhancement to our basic ship-planning support system. Additionally, we have broadened the scope of the geographical area to a global scale to understand the ship specifications in demand. Furthermore, we proposed the voyage-charter contract in addition to the assumed time-charter contract scheme. Finally, we suggest two attributes to be considered in the ship allocation algorithm: ship cost (COST) aspects and GHG emissions.

1.3. Structure of This Dissertation

Accordingly, Figure 1 provides an overview of structure of this dissertation. The content of each chapter are summarized, as follows:

- Chapter 1: This chapter described an overview of the dynamic changes in the global market and the significance of big data in maritime logistics. Moreover, the objective of the basic-ship planning support system is clarified.
- Chapter 2: In this chapter, we discussed several studies and originalities in this study. We covered related studies utilizing big data in maritime logistics, which examined the forecasting of the cargo throughput, shipbuilding and new ship, and optimization in ship deployment. Additionally, we described the novel aspects of this study, including an improvement and originally proposed features compared to the prior study.

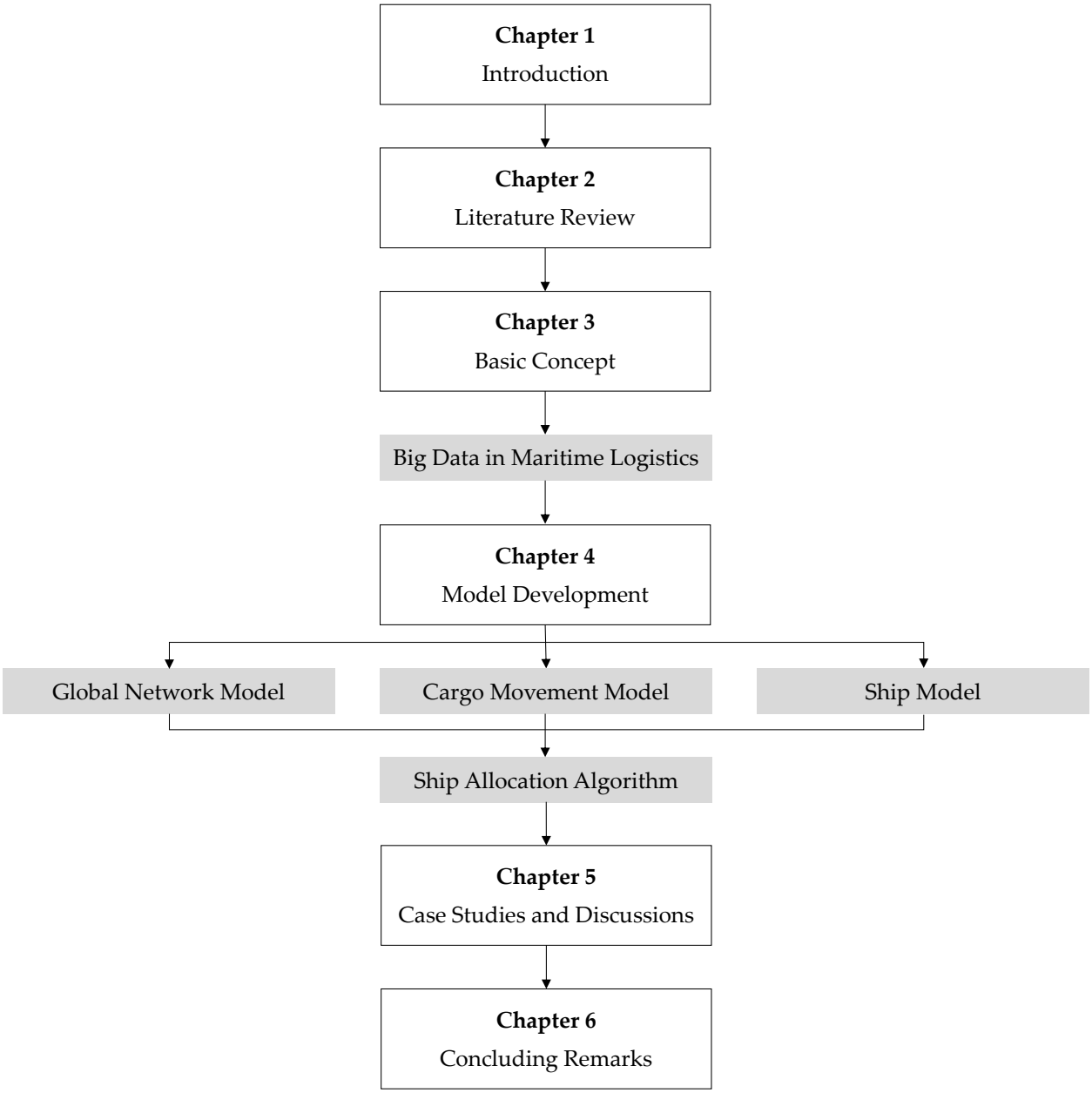

Figure 1. Structure of this dissertation.

- Chapter 3: This chapter provided the basic concept for developing the basic-ship planning support system. We defined the accessible big data in maritime logistics used in this study, including ship movement data, ship data, port data, and route data. Moreover, we clarified that the system configuration consists of the developed model, such as the global network model, cargo movement model, ship model, and ship allocation algorithm.

- Chapter 4: This chapter gives an account of the detailed model development configured in the basic-ship planning support system. Using the available data, we modeled the global network model, cargo movement model, and ship model. The results produced by these models were then arranged as an input to calculate GHG and COST, and the ship allocation algorithm. Moreover, the defined algorithms to simulate ship allocation are discussed.
- Chapter 5: This chapter presents the case studies and discussions. We propose case studies intended for Capesize and Panamax–MiniCape dry bulk carriers, and future scenarios of the IMO GHG reduction strategy. We conducted case studies utilizing the defined algorithms; ship replacement while preserving existing ship allocation, optimization of ship allocation using existing ships and with new ships instance, in time- and voyage-charter contracts.
- Chapter 6: This last chapter summarizes the discussions mentioned above and future tasks considered.

2. LITERATURE REVIEW

2.1. Related Studies utilizing Big Data in Maritime Logistics

In recent years, studies utilizing big data in maritime logistics have emerged as predictive analytics tools. These have mainly discussed energy efficiency improvement, accident avoidance, and logistics optimization. Focusing on regional and global scales, some studies have examined the forecasting of the cargo throughput, shipbuilding market, and new ship specifications [9-12]. Table 1 lists several studies on these topics.

Table 1. Related studies utilizing big data in maritime logistics.

Author	Forecasting Scope	Logistical Context [1]	Shipping Market [2]	Used Data [3]
[13]	Cargo Throughput	*Country*	*Co*	*Po*
[14–16]	Cargo Throughput	*Country*	*Co*	*Po, St*
[17]	Cargo Throughput	*Global*	*Bu*	*Ai*
[18,19]	Cargo Throughput	*Global*	*Bu*	*Ai, Sh*
[20]	Shipping Market	*Global*	*Ta*	*Ai, St*
[21]	Shipbuilding Market	*Global*	*Co, Bu, Ta*	*St*
[22–24]	Shipbuilding Market	*Global*	*Bu*	*Sh, St*
[25]	Shipbuilding Market	*Global*	*Co, Bu*	*Ai, Sh, St*
[30]	New Ship Specification	*Region*	*Bu*	*Sm, Sh, Po, Ro, St*
This Study	New Ship Specification	*Global*	*Bu*	*Sm, Sh, Po, Ro, St*

[1] *Country*: From or to a country; *Region*: Connections between more than two countries; *Global*: Worldwide scale; [2] *Co*: Container; *Bu*: Bulk Carrier; *Ta*: Tanker; [3] *Ai*: AIS data; *Sm*: ship movement data; *Sh*: ship data; *Po*: port data; *Ro*: route data; *St*: statistical data.

2.1.1. Overview of Studies discussing Cargo Throughput Forecasting

A number of studies constructed a long-term model predicting cargo demand based on regression analysis and neural networks using a combination of ship and port data. Yang and Chang [13] researched forecasting the demand for container throughput in five ports in Taiwan. This study is composed mixed-precision neural network consisting of a convolutional neural network for the learning process and long short-term memory to identify the significant features. The proposed method can predict container throughput effectively compared to other forecasting approaches, as shown in Figure 2. This finding gives potential future cost reduction in the planning and development of ports.

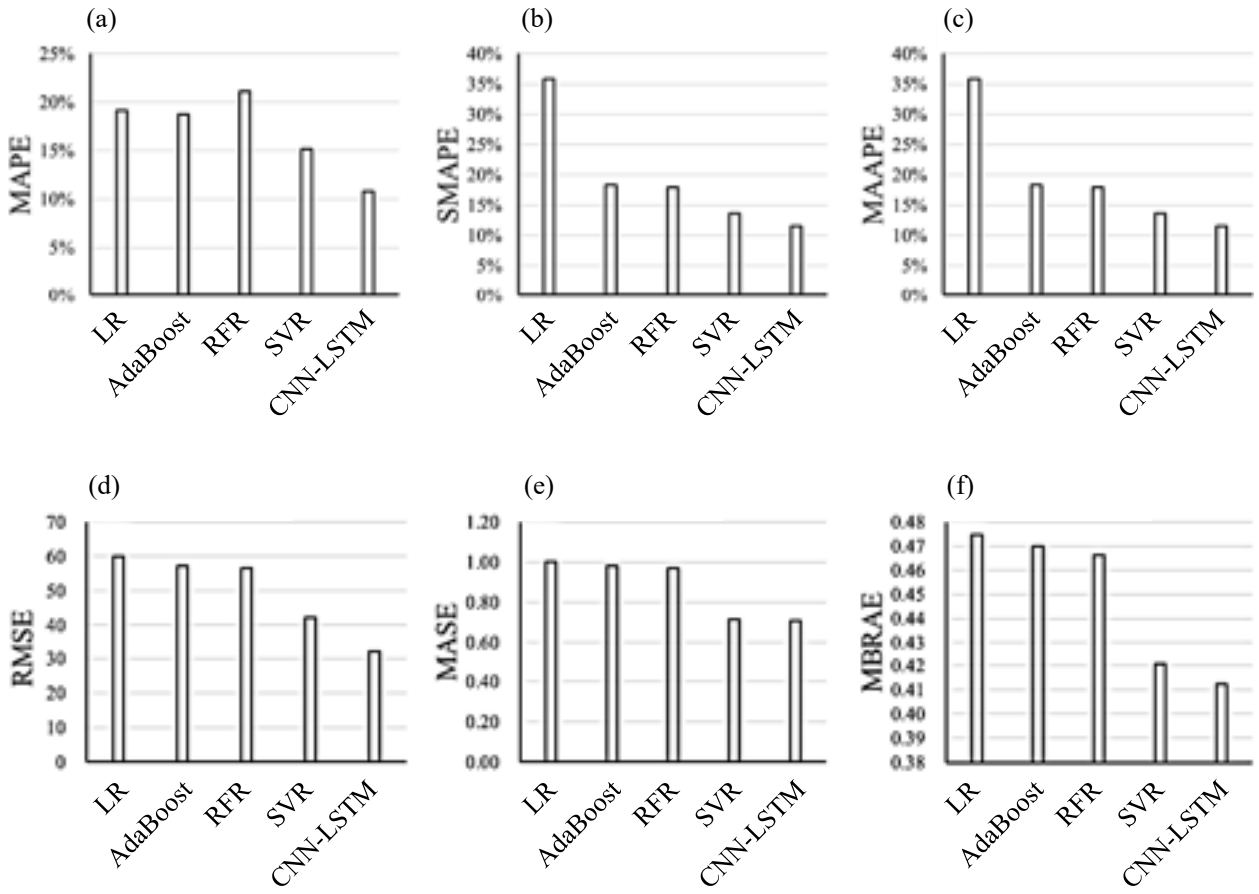

Figure 2. The forecasting method proposed by Yang and Chang [13]: Convolutional neural network and long short-term memory (CNN-LSTM).

Furthermore, Jugović et al. [14] discussed the aspects that influence maritime shipping markets. This study presents three key economic concepts to analyze the supply and demand in the freight market: supply function, demand function, and equilibrium price. In the case of short-term equilibrium, the balance of supply and demand is determined by the effectiveness of ships in operation. Moreover, long-term equilibrium conditions have fluctuated following the order of new ships and a scrap of old ships. This is related to the sale and purchase market, new buildings, and demolition.

Akar and Esmer [15] investigated the container volume forecasting of container ports in Turkey. Multi regression analysis is proposed, and the cargo handling capacity of these ports until 2023 was analyzed. In this perspective, the predicted cargo amount varies depending on the location of ports. Assuming no changes in the container ships' size category, the expected container throughput in 2023, 12.7 million TEU, can be handled by the target ports.

Similarly, Gökkuş et al. [16] examined the accuracy of four forecasting models to forecast the annual container throughput in the ports of Istanbul, Izmir, and Mersin. The proposed models include Artificial Neural Network with Artificial Bee Colony and Levenberg-Marquardt Algorithms, Multiple Nonlinear Regression with Genetic Algorithm (MNR-GA), and Least Square Support Vector Machine. All proposed models but MNR-GA results in moderate forecasts for all target ports. To conclude, this study reported an increase in 2023 container traffic by 67% and 95% at target ports Izmir, Mersin, and Instanbul, respectively.

Moreover, Jia et al. [17] estimated the payload of bulk carriers based on the AIS-reported draught data. Initially, this study verifies the quality of AIS data by using the port calls from ship agents. Moreover, this study estimated the ships' payload and evaluated the estimation through a multi-factor regression model. The findings described that the draught information captured and evaluated in AIS data and port calling data are reliable in estimating the ships' payload. In addition, the future global carbon footprint per transport mode is measured considering the estimated payload. However, this study does not compare the estimation results to the cargo amount sourced from alternative statistical data.

Similarly, Zhou and Hu [18] examined an AIS-based iron ore trade volume estimation. The actual shipment was obtained by inputting the static and dynamic data, in the form of ship and AIS data, into the constructed back-propagation neural network (BP-NN). This study estimated the trade volume of iron ore in 2018. In the annual context, the error of estimated value in China is statistically less than 0.5%, as shown in Figure 3. Despite its dependency on the ship size category and cargo type, this study confirmed the practicability of BP-NN to estimate the trade volume of iron ore bulk carriers.

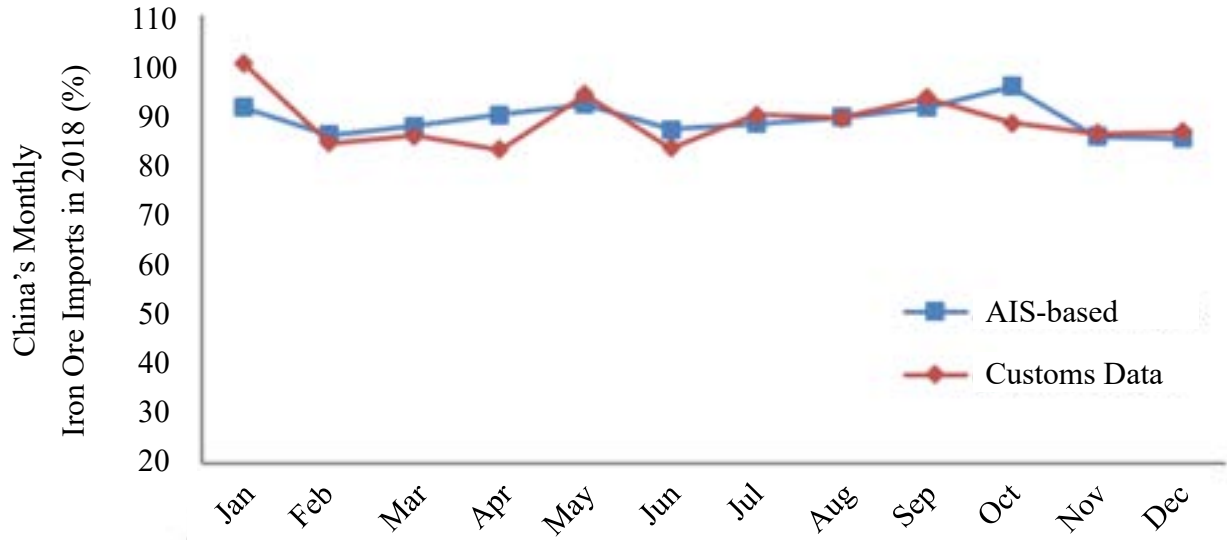

Figure 3. The AIS-based estimated iron ore payload by Zhou and Hu [18]:China's Monthly Iron Ore Imports in 2018 (%).

In addition, Kanamoto et al. [19] discussed the applicability of the AIS data of dry bulk carriers to forecast future cargo movement. This study estimated the dry bulk cargo movement, such as iron ore, coal, grain, fertilizers, and iron and steel products. The available database of AIS data is used to forecast the future cargo movement for each cargo type by using the logit model. This study clarified the relationship between significant routes with large cargo movement, ship sizes, and sailing distances for the observed cargo type. The proposed model forecasted the cargo movement of iron ore and coal in 2030. The findings pointed out the growth of imports towards developing countries, generating the demand for the smaller size of the dry bulk carrier. The results of estimated cargo movement allow future studies to analyze the ships' allocation and charter contracts.

2.1.2. Overview of Studies discussing Shipping and Newbuilding Markets

For the case of shipping and newbuilding markets, Prochazka et al. [20] analyzed the effectiveness of AIS data to comprehend the characteristics of the crude oil tanker spot-market charterer. This study provided the spatial pattern of contracting to represent the actual fixtures, which were determined by several factors: shipping market conditions, seasonality, charterers' condition, and ships' age and flag. The effectiveness of the carbon pricing policy has been reported to reduce GHG emissions. The experimental condition indicated that charterers own the main role of allocating ships based on their geographical position, allowing lower sailing speed. This study put forward future tasks considering a ship allocation reflected by the market

conditions. This scheme is described to dynamically reallocate ship allocation depending on the available ship capacity, dwelling time, and current position in the existing and future conditions.

Using statistical data, Sharma and Sha [21] formulated the forecasting model to predict the newbuilding index. The proposed model was composed of the integration of neural networks (NN), weighted fuzzy logic (WF), and genetic algorithms (GA). The economic conditions in five years span are predicted by using NN. Next, the output of NN, together with other statistical data, was inputted to WF and GA. This study presented discrete case studies: global container throughput, newbuilding index, and newbuilding market share. The findings allow shipbuilders and industrial partners to comprehend the current and forecasted shipbuilding market.

Similarly, Wada et al. [22-24] suggested a system dynamics model forecast the shipbuilding market demand and long-term GHG emissions reduction measures. Several simulations were conducted using the proposed demand-forecasting model, including the ship price prediction model, to prove the constructed system. Focusing on the supply and demand in the shipbuilding market, this study discussed the scenarios of shipbuilding capacity adjustment.

Finally, Lee and Jung [25] built a platform to collect big data in the shipbuilding market and forecast the ship order quantity of container ships and bulk carriers. This study proposed an autoregressive model and carried out distinctive analyses of the ship demand estimation model, analysis of ship satellite navigation information, customer profiling, and unstructured data analysis. The further application of the proposed model is to simulate case studies considering the business plans of shipbuilders.

The abovementioned studies have discussed a macro-level forecasting model for fluctuations in the shipping and shipbuilding markets. However, they have not examined the operation-level demand forecasting to understand competitive ship specifications following market changes.

2.1.3. Overview of Studies discussing Optimization Studies in Ship Deployment and Contracts

Several studies proposed an optimization method for ship deployment and contracts. Zhang et al. [32] analyzed the cold chain shipping mode selection, ship selection, and ship deployment between containerized and bulk reefers. Each ship is deployed considering the economic and environmental objectives of adopting the value-based management. In this context, the proposed decision framework allows optimization of ships' sailing speed following its contract scheme and cargo value depreciation of perishable goods. The two decision models have

been executed in this scheme: the sensitivity scenario analyses. This study evaluated GHG emitted from the cold chain shipping. When the goods are less perishable, the results indicated that the average sailing speed tends to decrease along with an increase in bunker prices. This indicates that the importance of sailing speed differs depending on the cargo type.

Similarly, Venturini et al. [33] discussed the berthing times and positioning optimization in container terminals. A novel mathematical formulation is introduced to integrate the berth allocation problem and sailing speed optimization. It investigates the trade-off between fuel consumption reductions and dwelling time extension. Up to 40% potential GHG emissions reduction is reported compared with when the ship sails at its design speed. These studies reported the correlation between the ship's sailing speed and GHG emissions.

Arslan and Papageorgiou [34] adopted multi-stage stochastic programming to deal with the bulk carrier renewal problem, focusing on ship-sizing and deployment. It was reported to provide a total cost reduction. Lin and Liu [35] developed a genetic algorithm to solve the tramp shipping routing problem of the Handymax dry bulk carrier. The combined mathematical model was proposed to overcome ship allocation and cargo movement problems. These studies formulated a novel method to optimize the operation-level ship allocation. However, a particular case study of an actual ship allocation was not considered.

Yang et al. [36] discussed the diverse applications of AIS data, including the ship performance evaluation. Dynamic route planning in the Baltic Sea Region to reduce ship owners' COST and GHG emissions were examined [37]. The reported benefit can surpass the cost in the proposed cost-benefit analysis by reducing sailed distances and GHG emissions. It proved the applicability of AIS data to evaluating ship allocation in a specific region. Dynamic optimization was specified as a future research opportunity to optimize ship allocation considering various routes and external factors.

Bai et al. [38] examined the potency of financial hedging and operational risk management strategies to overcome significant earning risks in the tramp shipping scheme. Ordinary least square regression and the Bayesian belief network were proposed to account for the data of 31 tramp shipping companies, such as ship age, sailing distances, and AIS data. Operational risk management strategies were reported to effectively mitigate bunker price and freight rate fluctuation risks. It confirmed that ship allocation optimization is attainable by utilizing big data in maritime logistics.

2.2. Originalities in This Study

According to our literature review, no study has been carried out on demand forecasting at the particular operational level to recognize the benefit of new ship specifications in the future. Therefore, Arifin et al. [30] proposed a basic ship-planning support system by integrating big data in maritime logistics (see Table 1). We have explored the possibility of simulating operation-level ship allocation and successfully built a ship allocation algorithm as the core of our system. Table 2 shows the resemblance between Arifin et al. [30] and this study.

Table 2. Resemblance between Arifin et al. [30] and this study.

Author	Target Ship [1]	Cargo Types [2]	Route [3]	Operation Period	Ship Allocation Consideration	
					COST [4]	*GHG* [5]
Arifin et al. [30]	*Iron*	*Ir*	Australia, Brazil–Japan, *Korea*	2014 [39]	*Fuel*	*na*
This Study	*Cape*; *Pana*	*Ir; Co; Gr; Ot*	Worldwide	2018 [39,40]	*Fuel*; *Ops*; *Dep*; *Stoc*	*ME*; *AE*

[1] *Iron*: iron ore bulk carrier; *Cape*: Capesize dry bulk carriers with deadweight tonnage more than 100,000; *Pana*: Panamax–MiniCape dry bulk carriers with deadweight tonnage 65,000–140,000.
[2] *Ir*: iron ore; *Co*: coal; *Gr*: grain; *Ot*: others.
[3] *Korea*: South Korea.
[4] Ships' costs of *Fuel*: fuel; *Ops*: operation; *Dep*: depreciation; *Stoc*: stockpile.
[5] *COST*: ship's cost; *GHG*: ship's GHG emissions; *na*: not available; *na*: not available–no consideration of GHG; ships' GHG emitted from of *ME*: main engine; *AE*: auxiliary machineries.

Arifin et al. [30] have concentrated on iron ore bulk carriers operating on limited routes. Further, this study explores wider target ships, including Capesize and Panamax–MiniCape dry bulk carriers. We expand our model to comprise the worldwide routes of iron ore, coal, grain, and others. In our system, the ship allocation algorithm is constructed independently, covering the attributes of COST and GHG emissions. In this context, COST consists of the costs of fuel, operation, depreciation, and stockpile. In addition, GHG emissions comprise the GHG emitted by ships' main engine and auxiliary machinery.

The following improvements have been suggested by the Arifin et al. [30]:

- Target route and cargo type: Prior simulations [30] were executed on limited target routes and cargo types, such as Australia, Brazil, Japan, and South Korea routes of iron ore. In contrast, this study has broadened the scope of simulations to accommodate iron ore, coal, grain, and other cargo type routes worldwide.
- Ship allocation algorithm: The key performance index (KPI) in the prior ship allocation algorithm [30] considered only the fuel cost as the COST variable. Therefore, the previously generated ship allocation simulation directly reflected the estimated fuel cost, which was a fraction of the actual COST. This study has proposed more realistic COST attributes [1], such as the costs of fuel, operation, depreciation, and stockpiling.

3. BASIC CONCEPT

3.1. Big Data in Maritime Logistics used in This Study

3.1.1. Description of Ship Movement Data

This dataset presents dynamic data of the ship movement and its attributes. In this study, the port calling data of ships were obtained from the Market Intelligence Network (MINT) database of IHS Markit Ltd. [39] and the AXSDry database of AXSMarine [40]. These databases are defined as the ship movement data, which provide the historical ship position in a port-level manner for various ship types. Moreover, the quality of the database of port calling data has been discussed by Wada et al. [41]. This study evaluated the data acquisition between the port calling data of the MINT database [39] and the operation reports of the ship's operator. The findings of this study confirm that 95% of the ship operation reports from 2015 to 2018 are covered in the ship movement data.

We then extracted the ship movement data of the Capesize and Panamax–MiniCape dry bulk carriers, which are dry bulk carriers with a deadweight tonnage (DWT) of more than 100,000 and 65,000–140,000, respectively [39,40]. The time range of Capesize dry bulk carriers (DWT more than 100,000) port calling data extracted from the MINT database [39] was from January 2015 to May 2019. Table 3 provides the content enclosed in this data, such as the ship specification, route information, and operation conditions. The ship specification in this data includes the variables of administration and principal particulars, such as ships' IMO number, name, type, group owner, registered owner, manager, operator, and DWT. The route information in this data poses the voyage information in both loading and unloading, namely voyage calling type, country of origin and destination, zone of origin and destination, port of origin and destination, terminal of origin and destination, and indicated destination. Lastly, the operation conditions in this data hold date and draught data, including dates of arrival and departure, estimated time arrival, and draughts of arrival and departure. Furthermore, we aggregated the data into voyage records. Initially, the ship movement data contained 328,670 entries, including calling types of anchorage, port, and terminal.

They were defined as the set of a ship origin port's departure data and destination port's arrival date. Hence, any operation between these entries was considered an outlier by referring to Arifin et al. [30]. Later, the entry numbers were reduced to 36,849 entries of laden and ballast.

Table 3. Features of MINT database [39].

Features [1]	Variables	Attributes
Ship *IMO Number*	Administration	Ship Specification
Ship Name	Administration	
Ship Type	Administration	
Ship Group Owner	Administration	
Ship Registered Owner	Administration	
Ship Manager	Administration	
Ship Operator	Administration	
Ship *DWT*	Principal Particulars	
Voyage Calling Type	Voyage Information	Route Information
Origin Country	Loading Information	
Origin Zone	Loading Information	
Origin Port	Loading Information	
Origin Terminal	Loading Information	
Indicated Destination	Loading Information	
Destination Country	Discharge Information	
Destination Zone	Discharge Information	
Destination Port	Discharge Information	
Destination Terminal	Discharge Information	
Voyage Departure Date	Date and Time	Operation Conditions
Voyage Arrival Date	Date and Time	
Voyage *ETA*	Date and Time	
Arrival Draught	Draught Rate	
Departure Draught	Draught Rate	

[1] *IMO Number*: International Maritime Organization number; *DWT*: deadweight tonnage; *ETA*: estimated time arrival.

In the case of Panamax–MiniCape dry bulk carriers (DWT 65,000–140,000), the port calling data extracted from the AXSDry database [40] ranged from August 2017 to September 2018. This dataset contained 31,527 entries (January 2013 to December 2020: 1,812,635 entries) of cargo throughput in laden and ballast operations. Table 4 provides the content in the AXSDry database [40], such as the ship specification, route information, operation conditions, and cargo information. These attributes are similar to the previously discussed MINT database [39], except for the cargo information. The ship specification in this data includes the variables of administration, principal particulars, and performances, namely ships' name, type, DWT, design speed, and maximum draught.

The route information in this data poses the voyage information in loading and unloading, such as the zone of loading and discharge, country of loading and discharge, port of loading and discharge, and berth of loading and discharge. The operation conditions in this data include dates of loading and discharge, the draught of loading and discharge, average speed of laden and ballast voyages, voyage duration of laden and ballast, and duration of loading and discharge. Lastly, cargo information holds commodity name and group, charter, and voyage intake (cargo movement).

Table 4. Features of AXSDry database [40].

AXS Features	Variables	Attributes
Ship Name	Administration	Ship Specification
Ship Type	Administration	
Ship *DWT*	Principal Particulars	
Ship Design Speed	Performances	
Ship Max Draught	Performances	
Loading Zone	Loading Information	Route Information
Loading Country	Loading Information	
Loading Port	Loading Information	
Loading Berth	Loading Information	
Discharge Zone	Discharge Information	
Discharge Country	Discharge Information	
Discharge Port	Discharge Information	
Discharge Berth	Discharge Information	
Commodity Name	Cargo Type	Cargo Information
Commodity Group	Cargo Type	
Voyage Intake	Cargo Movement	
Voyage Loading Date	Date and Time	Operation Conditions
Voyage Discharge Date	Date and Time	
Loading Draught	Laden Draught Rate	
Laden Voyage Avg Speed	Laden Avg. Sailing Speed	
Laden Voyage Duration	Laden Sailing Days	
Loading Duration	Laden Port Staying Time	
Discharge Draught	Ballast Draught Rate	
Ballast Voyage Avg Speed	Ballast Avg Sailing Speed	
Ballast Voyage Duration	Ballast Sailing Days	
Discharge Duration	Ballast Port Staying Time	

[1] *DWT*: deadweight tonnage.

3.1.2. Description of Ship Data

This dataset presents static data of the ships' specifications. The ship data from the Sea-web Ships database of IHS Markit Ltd. were used in this study [42]. We downloaded the ship data of dry bulk carriers with DWT ranging from 10,000 to 400,000 [31], for ships built or expected to be delivered from 1942 to 2023. This dataset contained 11,744 entries, including the technical and non-technical attributes, as shown in Table 5.

Table 5. Features of Sea-web Ships database [42].

Ships' Attributes	Variables [1]
Administration	*IMO Number*; Callsign; Flag; Class; Shipbuilder; Registered Owner; Ship Manager; Operator.
Principal Particular	*DWT*; *GT*; Displacement (t); Length (m); Breadth (m); Draught (m); Depth (m).
Performance	Built Year; Main Engine Power (kW); Design Speed (kn)

[1] *IMO Number*: International Maritime Organization number; *DWT*: deadweight tonnage; *GT*: gross tonnage.

Several attributes of each ship are included in this data, such as ships' administration, principal particular, and performance. The administration attributes enclosed ships' IMO number, callsign, flag, class, shipbuilder, registered owner, ship manager, and operator. The principal particular attributes hold ships' DWT, gross tonnage (GT), displacement, length, breadth, draught, and depth. Finally, the performance attributes include ships' built year, main engine power, and design speed.

3.1.3. Description of Port Data

This dataset presents static data of the port and its specifications. The port data from the Sea-web Ports of IHS Markit Ltd. and the IHS Fairplay Ports and Terminals Guide were used in this study [43,44]. We downloaded the worldwide port data containing 5918 entries, including 2098 ports. Table 6 presents the attributes of each port comprised in this data, such as ports' administration, facility information, location information, and ship size limitation.

Table 6. Features of Sea-web Port and Ports and Terminal Guide databases [43,44].

Ports' Attributes	Variables [1]
Administration	Port Name, World Port Number; *UNLOCODE*, *ISPS* Compliant, Time Zone (*GMT*).
Facility Information	Facilities of Break Bulk; Container; Dry Bulk; Dry Dock; Liquid; *LNG*, *LPG*; Multipurpose; Passenger; *RoRo*.
Location Information	Country; Coordinates of Latitude and Longitude; Decimals of Latitude and Longitude.
Ship Size Limitation	Max. *DWT*; Max. Length (m); Max. Breadth (m); Max. Draught (m).

[1] *UNLOCODE*: United Nations Code for Trade and Transport Locations; *ISPS*: International Ship and Port Facility Security Code; *GHT*: Greenwich Mean Time; *LNG*: liquefied natural gas; *LPG*: liquefied petroleum gas; *RoRo*: roll-on roll-off; *DWT*: deadweight tonnnage.

The administration attributes enclose ports' name, world port number, United Nations Code for Trade and Transport Locations (UNLOCODE), International Ship and Port Facility Security Code (ISPS) compliant, and time zone. The facility information attributes contained ports' facilities of break bulk, container, dry bulk, and other cargo types. The location information attributes included ports' country, coordinates of latitude and longitude, and decimals of latitude and longitude. Finally, the size limitation attributes hold ships' DWT, length, breadth, and draught.

3.1.4. Description of Route Data

This dataset presents static data on the routes and their sailing distances. The distance table of the IHS Fairplay Ports and Terminals Guide was used in this study [44]. Table 7 presents the features of this data. Three attributes are attached to each route: port of origin, destination, and distances. The port of origin and destination attributes enclosed ports' name, country, coordinates of latitude and longitude, and decimals of latitude and longitude.

Moreover, the distances hold the shortest direct distances and distances via Panama Canal. In this context, we consider the shortest direct distances since it sets out the distance of sailing directly and via a canal. This distance is presumed to be able to be served by the largest dry bulk carriers possible [45]. We extracted the worldwide sailing distances served by dry bulk carriers containing 53,592 entries.

Table 7. Features of distance table [44].

Routes' Attributes	Variables
Port of Origin and Destination	Port Name; Country; Coordinates of Latitude and Longitude; Decimals of Latitude and Longitude.
Distances	Shortest Direct Distances (nm); Distances via Panama Canal (nm).

3.2. Configuration of Ship Basic-Planning Support System

Arifin et al. [30] proposed a maritime logistics database (MLDB) and ship allocation model in the previous study. These were assembled in the previously built basic ship-planning support system, as shown in Figure 4. In this context, MLDB integrates the available big data in maritime logistics, such as ship movement data, ship data, port data, and route data. The MLDB was defined as a relational database; for example, the operation conditions can be clarified by integrating the ship movement data and ship data.

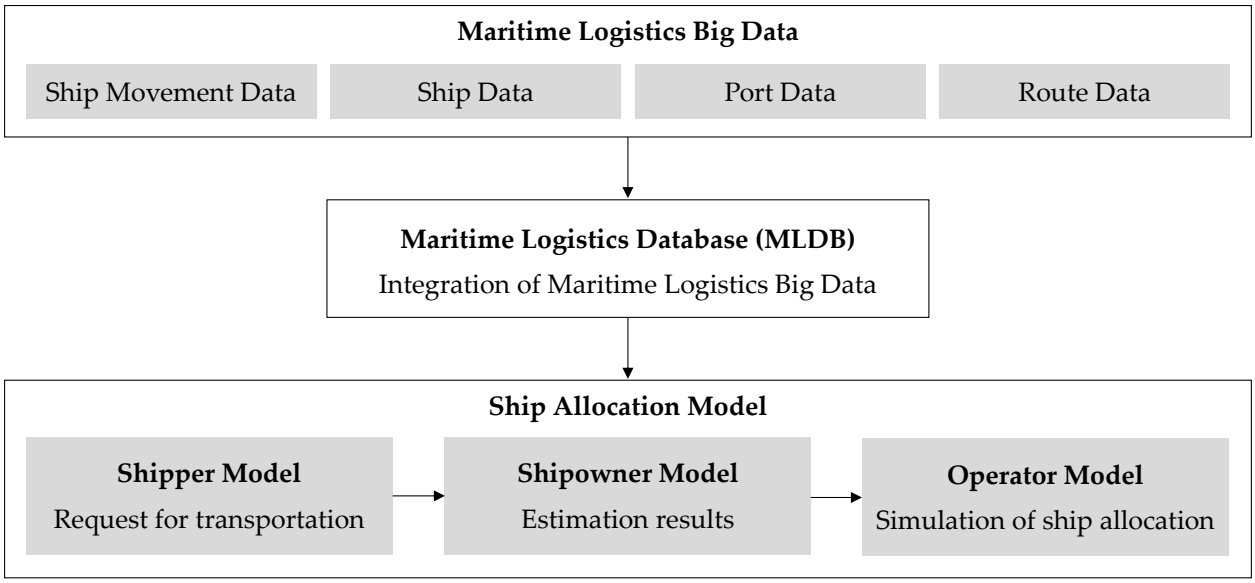

Figure 4. System configuration of Arifin et al. [30].

Moreover, the following error cleaning methods were performed to ensure the reliability and quality of the data used to construct the MLDB:

- Keeping the first recorded instance in the ship movement data based on its arrival date and time and considering its duplicated instances as an outlier.
- An instance with an average sailing speed more than its design speed, calculated by considering the sailing days and sailing distance between origin and destination ports, is treated as an outlier.

- An instance with unavailable data, such as the missing voyage data and draught data, is considered an outlier

Moreover, the abovementioned data are inputted into the ship allocation model. Three distinct models were developed in the ship allocation model by Arifin et al. [30], as follows:

- Shipper model: This model issues a request for transporting a certain cargo amount between origin and destination ports. This model is defined using cluster analysis. •
- Shipowner model: This model represents each ship and its operation conditions. This model estimates the draught rate (%), average sailing speed (kn), and port staying time (d) by using the deep learning (DL) model. These variables were later used to calculate the voyage attributes; transported cargo movement (t), sailing days (d), and fuel cost (USD).
- Operator model: This model includes the voyage attributes calculation and allocates ships to transport the cargo movement demand.

Furthermore, three discrete models and a ship allocation algorithm were assembled in our basic ship-planning support system, as shown in Figure 5. We modeled a global network model, cargo movement model, and ship model using the available big data in maritime logistics. The global network model defines the ports worldwide and their attributes in its sailing network. The cargo movement model covers an estimation of cargo movement between ports. The ship model includes each ship and its specifications and predicts the ships' operation conditions.

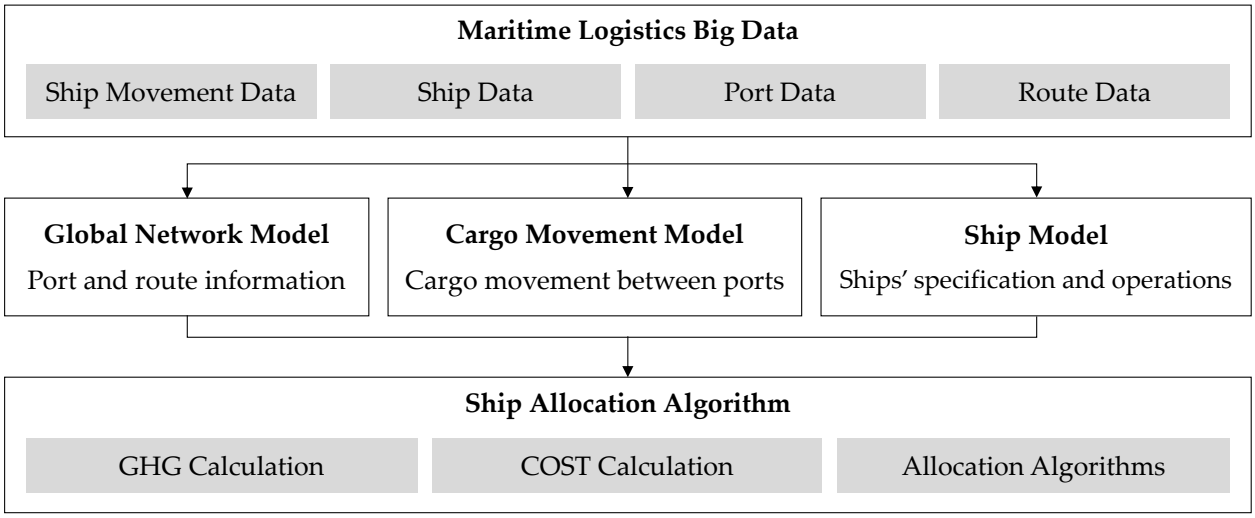

Figure 5. System configuration of this study.

The ship allocation algorithm reconstructs the ship allocation, which is the core of our basic ship-planning support system. An input of the cargo movement demand, route list, and existing ship list are needed to observe the changes in ship allocation by adding future scenarios, such as presenting the new ships in the ship list. We can also identify new ships that are replacing existing ships from their results, making it possible to assess competitive ships in demand.

The resemblance between Arifin et al. [30] and this study is shown in Table 2. Arifin et al. [30] have concentrated on iron ore bulk carriers operating in the Australia, Brazil, Japan, and South Korea routes of iron ore. Meanwhile, the developed ship allocation model considers only fuel cost to allocate a ship to serve a certain route. Further, this study explores wider target ships, including Capesize and Panamax–MiniCape dry bulk carriers. In this study, we expanded our previously constructed model to comprise the worldwide routes of iron ore, coal, grain, and others. In our system, the ship allocation algorithm is constructed independently, covering the attributes of COST and GHG emissions. In this context, COST attributes consist of fuel, operation, depreciation, and stockpile costs. In addition, GHG emissions comprise the GHG emitted by ships' main engine and auxiliary machinery.

3.2.1. Description of Global Network Model

This model was called the shipper model in Arifin et al. [30] containing the ports' specifications, sailing routes, and sailing distances. Formerly, this model specified limited target routes and cargo types, namely Australia, Brazil, Japan, and South Korea routes of iron ore. Prior study fails to acknowledge the potential of available maritime logistics big data to expand the scope of this model.

Therefore, we extended its scope to include a worldwide sailing network served by Capesize and Panamax–MiniCape dry bulk carriers accommodating iron ore, coal, grain, and other cargo types worldwide. Additionally, we characterized these ports into main ports and port clusters. For case studies conducted in this study, this model was composed of the available ship movement data [39,40]. Thus, this model contained 593 ports (52 main ports and 79 port clusters) of Capesize dry bulk carriers and 1234 ports (147 main ports and 85 port clusters) of Panamax–MiniCape dry bulk carriers. This model also contains the sailing distances considering the 2018 ship movement data. Hence, this model comprised 1085 sailing routes of Capesize dry bulk carriers and 3338 sailing routes of Panamax–MiniCape dry bulk carriers [44].

3.2.2. Description of Cargo Movement Model

This model was not defined independently and constructed in the prior study [30], consisting of the cargo movement and type between the ports. Previously, this model described the cargo movement towards the limited scope of transported iron ore in the Australia, Brazil, Japan, and South Korea routes. However, the previous study cannot cover the global cargo movement trend using the available maritime logistics big data.

On a worldwide scale, we used the arrival draught in the MINT ship movement data [39] of Capesize dry bulk carrier in 2018 to estimate the cargo amount. Moreover, for the case studies of Panamax–MiniCape dry bulk carriers, we adopted the documented cargo throughput in the AXSDry ship movement data [40]. This was recorded in the discrete date and time, allowing us to form OD tables containing monthly and annual cargo movement. Later, this model results in cargo movement towards various routes arranged in origin-destination (OD) tables and is used as the cargo amount to be transported in the ship allocation algorithm.

3.2.3. Description of Ship Model

This model was called the shipowner model in Arifin et al. [30], containing the ships' specifications and operation conditions. Formerly, this model characterized ships that operated in limited target routes, particularly Australia, Brazil, Japan, and South Korea routes of iron ore. This scope resulted in an inadequate perspective to perceive the ships' characteristics worldwide using the accessible maritime logistics big data.

This model depicts the ships' specifications in this study, covering the technical and non-technical variables, such as the principal dimensions and ownership information. In this study, this model was created specifically for ships instance that occurred in 2018 ship movement data. Thus, this model contained 1647 ships of Capesize dry bulk carriers and 2479 ships of Panamax–MiniCape dry bulk carriers. In addition, this model generates the operation conditions, which include draught rate, average sailing speed, and port staying time when a ship is allotted to a particular route. This model also predicts the operation conditions for each ship's laden and ballast voyages, namely draught rate (%), average sailing speed (kn), and port staying time (d), which were later inputted into the GHG and COST calculations.

For the case of Capesize dry bulk carrier, operation conditions were defined using the DL model, taking into account the MINT ship movement data [39]. On the other hand, we adopted the route-base average (R-AVG) to specify the operation conditions of Panamax–MiniCape dry bulk carriers since the ship's operation conditions were explicitly stated in the AXS ship movement data [40].

3.2.4. Description of Ship Allocation Algorithm

This model was labeled the ship allocation model in Arifin et al. [30], consisting of the KPI in each set of ships and route. Previously, this model calculated KPI considering each ship's fuel cost when allocated to a certain route. These ships were later offered for Australia, Brazil, Japan, and South Korea routes of iron ore. In this context, this scheme will simulate the selection of ships to carry certain cargo amounts and routes. However, the previously proposed mechanism fails to give sufficient consideration to ship allocation, such as other COST variables and the emitted GHG caused by the allocated ships' operation.

Accordingly, this model computes the GHG emissions [28,29] and COST [1,29,46,47] when a ship is designated to a specific route. Then, this model allocates a ship onto a route with the highest merit to transport a certain cargo amount in a time- and voyage-charter contract manner by adopting a greedy algorithm that considers the COST- and GHG-optimized ship allocation. Thus, this model optimizes the ship allocation and the global COST and GHG emissions, which are visualized regionally to understand the changes in the new ship allocation.

this page intentionally left blank

4. MODEL DEVELOPMENT

4.1. Overview of Model Development

Following what has already been discussed, we developed several models: the global network model, cargo movement model, and ship model. The global network model characterizes each port and route served by the target ships. The Cargo movement model describes the worldwide port-to-port cargo movement demand (CARGO) served by the target ships. The ship model represents individual target ships' data and operation conditions. Further, the results of these models are used as input to the calculations of GHG emissions [28,29] and COST [1,29,46,47]. The total GHG emissions consist of the GHG emitted from ships' main engine, auxiliary engine, and boiler, whereas the total COST contains the costs of ships' fuel, operation, depreciation, and stockpile.

Further to the calculated attributes of ships toward certain routes, we proposed three discrete algorithms as the ship allocation algorithm following a specific scheme: existing ships replacement by using new ships without changing their allocation, ship allocation optimization in a time-charter contract manner, and ship allocation optimization in a voyage-charter contract manner. Algorithm 1 proposes an optimization by offering a direct clone of the existing ship, a new ship with the exact specifications and operation conditions that serve the same annual allocations. Algorithm 2 reconstructs the ship allocation to transport the cargo movement demand using the offered ships in a time-charter contract manner. Algorithm 3 reconstructs the ship allocation to transport the cargo movement demand using the offered ships in a voyage-charter contract manner. Hence, using the defined algorithm, the following were the objectives of the conducted simulations:

- Target ship: Capesize dry bulk carrier (DWT 100,000 or more, 1647 ships); Panamax–MiniCape dry bulk carriers (DWT 65,000-140,000, 2479 ships);
- Cargo types: Iron ore, coal, grain, and others;
- Route: Worldwide (sailing routes served by target ship);
- Operation period: 2018;

Finally, we summarized the results of the average DWT, sailing speed, and ship age graphically in a great circle format [53-55].

4.2. Development of Global Network Model

4.2.1. Overview of Global Network Model

This model defines each port and route served by the Capesize and Panamax–MiniCape dry bulk carriers. We extracted a list of ports visited by such carriers from the ship movement data worldwide. In addition, we provided an overview of this model in Table 8.

Table 8. Overview of the global network model.

Target Ship [1]	Capesize	*Panamax–MiniCape*
Ship Movement Data	MINT [39]	AXSDry [40]
Operation Period	2013–2019	2013–2020
Cargo Types [2]	*Ir, Co*	*Ir, Co, Gr, Ot*
Port Numbers	593	1234
Main Port Numbers	52	147
Other Port Numbers	541	1087
Port Cluster Numbers	79	85
2018 Route Numbers	1085	3338

[1] *Capesize*: dry bulk carriers with deadweight tonnage more than 100,000; *Panamax–MiniCape*: dry bulk carriers with deadweight tonnage 65,000–140,000.
[2] *Ir*: iron ore; *Co*: coal; *Gr*: grain; *Ot*: others.

4.2.2. Methodology to define Global Network Model

The various ports that occurred in the operation period were divided into main ports and port clusters. Main ports represented each port with significant port calling numbers, whereas port clusters included all the other ports served by the Capesize and Panamax–MiniCape dry bulk carriers. Capesize's port and route network contain 52 main ports and 541 other ports as 79 port clusters, as shown in Figure 6. Moreover, the Panamax–MiniCape's port and route network contains 147 main ports and 1087 other ports as 85 port clusters, as shown in Figure 7.

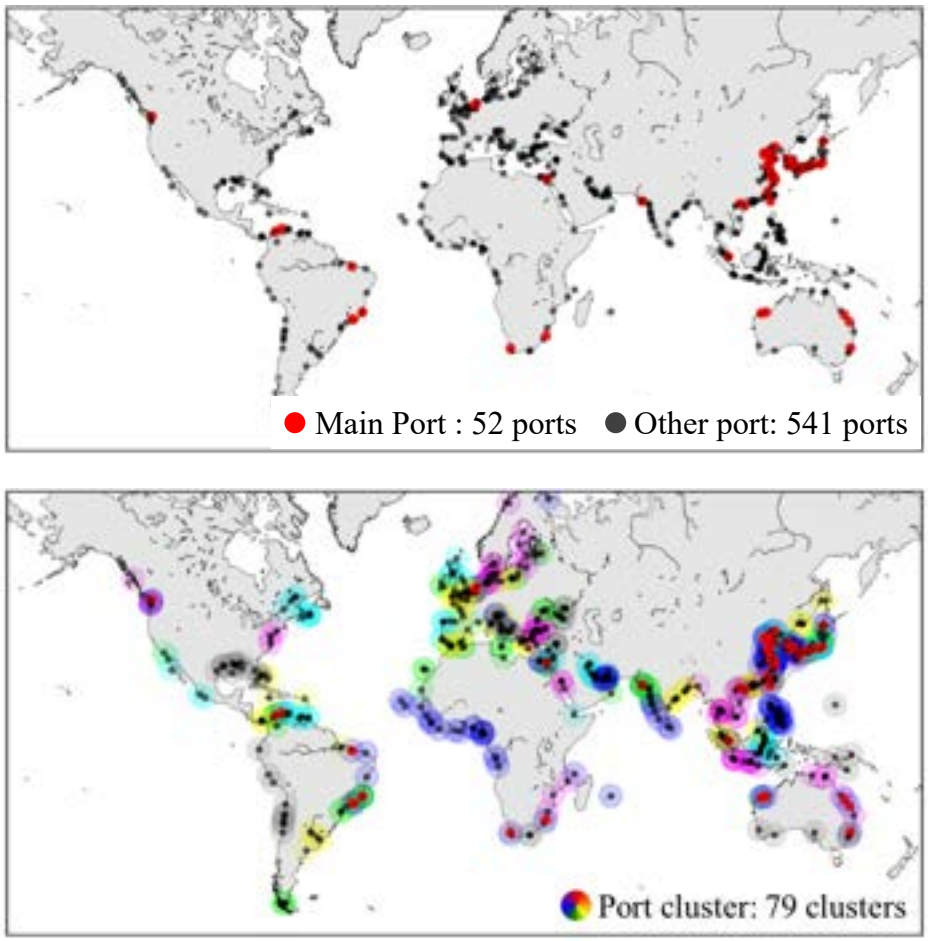

Figure 6. Worldwide ports of the global network model of Capesize dry bulk carrier.

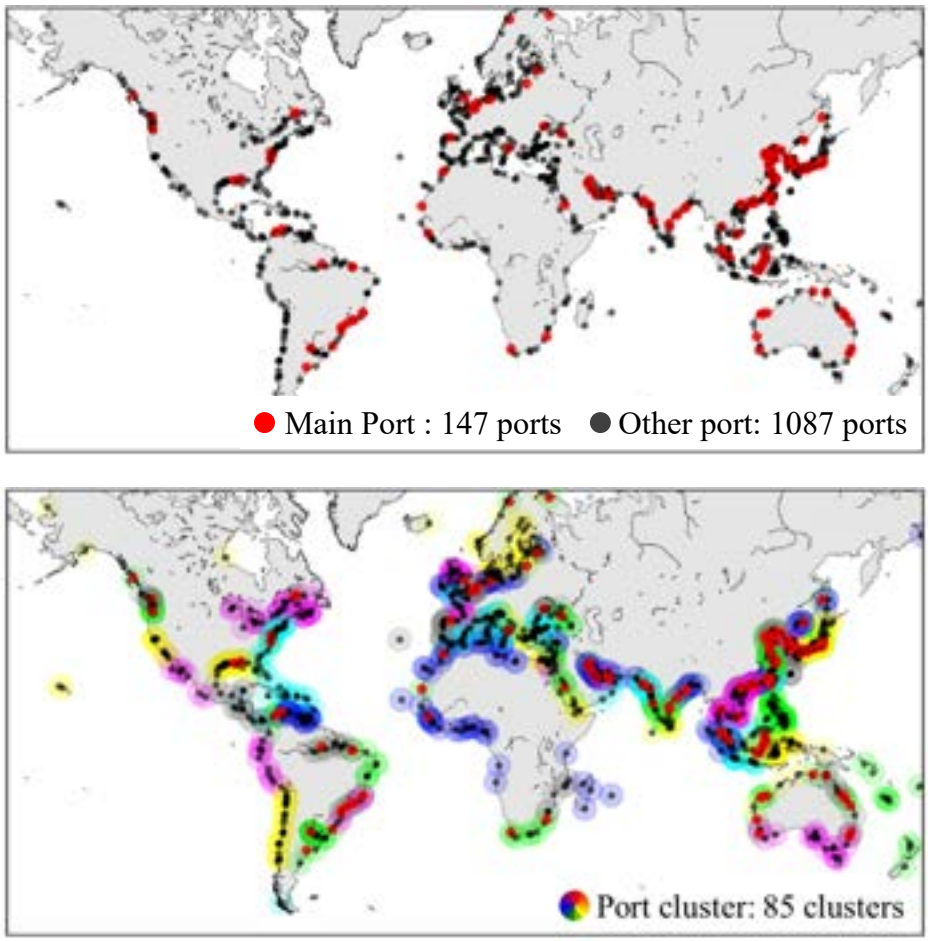

Figure 7. Worldwide ports of the global network model of Panamax–MiniCape dry bulk carrier..

4.2.3. Results of Global Network Model

The main port and other port numbers consisted in the global network model of Capesize dry bulk carrier are presented in Table 9. The main ports are mainly located in China (21 ports), Japan (7 ports), Australia (6 ports), and Brazil (4 ports) and accounted for 77.2% of the iron ore and coal trade in 2018, as seen from the worldwide port calling numbers of the Capesize dry bulk carriers in MINT ship movement data [39].

Table 9. Country list of the global network model of Capesize dry bulk carrier.

Country	Main Port Numbers	Other Port Numbers
China	21	63
Japan	7	46
Australia	6	12
Brazil	4	11
South Korea	3	14
Colombia	2	6
Netherlands	2	9
South Africa	2	4
Canada	1	14
Chinese Taipei	1	5
Egypt	1	7
India	1	21
Singapore	1	0
Others	0	329

In Table 10, the main port and other port numbers in the global network model of Panamax–MiniCape dry bulk carrier. The main ports are mainly located in China (28 ports), Australia (14 ports), Brazil (11 ports), Indonesia (11 ports), India (10 ports), Japan (9 ports), United States of America (7 ports), and South Korea (7 ports) and accounted for 71.3% of the iron ore and coal trade in 2018, as seen from the worldwide port calling numbers of the Panamax–MiniCape dry bulk carriers in AXSDry ship movement data [40]. Similar to Capesize's port calling numbers, these rates indicate that most port calling numbers were served in these countries. This tendency matches the worldwide top exporters and importers ranking of iron ore and coal in 2018 [31], as shown in Table 11.

Table 10. Country list of the global network model of Panamax–MiniCape dry bulk carrier.

Country [1]	Main Port Numbers	Other Port Numbers
China	28	93
Australia	14	28
Brazil	11	24
Indonesia	11	76
India	10	36
Japan	9	80
South Korea	7	12
USA	7	95
Russia	5	16
Canada	4	36
Malaysia	4	17
Netherlands	3	6
Taiwan	3	8
Colombia	3	4
South Africa	2	6
UAE	2	13
Argentina	2	14
Saudi Arabia	2	8
Others	20	515

[1] *USA*: United States of America; *UAE*: United Arab Emirates.

Table 11. Top exporters and importers of iron ore and coal in 2018 [31].

Iron Ore Exporters		Iron Ore Importers		Coal Exporters		Coal Importers	
Country Name [1]	Market Share (%)	Country Name [1]	Market Share (%)	Country Name [1]	Market Share (%)	Country Name [1]	Market Share (%)
Australia	57	China	71	Indonesia	33	China	19
Brazil	26	Japan	8	Australia	30	India	18
Africa	4	Europe	7	Russia	11	Japan	15
Canada	3	*Korea*	5	*USA*	8	*Korea*	11
Others	10	Other	9	Others	18	Others	37

[1] *Africa*: South Africa; *Korea*: South Korea; *USA*: United States of America.

This model also contains each port limitation and the sailing distance between the ports. The port limitations are set by port data and the largest possible ship visiting a port. Following the sailing routes included in the 2018 ship movement data [39,40], the sailing distances were extracted from the IHS Fairplay Ports and Terminals Guide [44]. Finally, this model comprised 1085 sailing routes of Capesize dry bulk carriers and 3338 sailing routes of Panamax–MiniCape dry bulk carriers.

4.3. Development of Cargo Movement Model

4.3.1. Overview of Cargo Movement Model

This model defines the worldwide port-to-port CARGO served by the Capesize and Panamax–MiniCape dry bulk carriers. This study defined the CARGO between ports based on the estimated cargo movement for the case of Capesize dry bulk carrier (DWT more than 100,000) and the reported voyage intake for Panamax–MiniCape (DWT 65,000–140,000). Additionally, we provided an overview of this model in Table 12.

Table 12. Overview of the cargo movement model.

Target Ship [1]	Capesize	*Panamax–MiniCape*
Ship Movement Data	MINT [39]	AXSDry [40]
Operation Period	2018	2018
Cargo Types [2]	*Ir, Co*	*Ir, Co, Gr, Ot*
2018 Route Numbers	1085	3338
Cargo Movement Estimation	Equations (1) and (2)	Equations (3) and (4)
Origin-Destination Tables	Annual	Annual and Monthly
2018 Cargo Movement (MT)	1652	1168

[1] *Capesize*: dry bulk carriers with deadweight tonnage more than 100,000; *Panamax–MiniCape*: dry bulk carriers with deadweight tonnage 65,000–140,000.

[2] *Ir*: iron ore; *Co*: coal; *Gr*: grain; *Ot*: others.

4.3.2. Methodology to define Cargo Movement Model

For the case of Capesize dry bulk carrier, CARGO was estimated by considering the ship's DWT and draught when it arrived at the destination port, which was included in the 2018 MINT ship movement data [30]. The set of available Capesize dry bulk carriers and its iron ore and coal routes are represented as I and J, respectively.

The cargo movement (CM_{ij}) per trip for each ship i serving the route j (t), and the annual cargo movement (CA_j) of the route j (t/y), are calculated as follows:

$$\boldsymbol{CM_{ij} = DWT_i \times \frac{\left({d'_{ij}}/{D_i}\right)}{(1-0.2)} \quad \forall i \in I, \quad \forall j \in J,} \tag{1}$$

$$\boldsymbol{CA_j = \sum_i (CM_{ij}) \quad \forall i \in I, \quad \forall j \in J,} \tag{2}$$

where DWT_i is the ship i DWT, d'_{ij} is the ship i arrival draught (m), and D_i is the ship i maximum draught (m), i is an individual ship (1647 Capesize dry bulk carriers operating in 2018), and j is an individual route (1085 routes of iron ore and coal in 2018). The CA_j for each cargo type was collected later in the OD tables. Hence, these tables contained the annual cargo movement in a port-level manner.

This study classified the ship movement data into two voyage modes by referring to Arifin et al. [30]; laden and ballast. We applied Equation (1) to calculate the cargo movement (CM_{ij}) carried by ship i only for its laden voyage. Then, the transported annual cargo movement (CA_j) is calculated by using Equation (2). It summarized all the laden instances in the route j towards the target year.

Furthermore, this model also defines the worldwide port-to-port CARGO served by the Panamax–MiniCape dry bulk carriers. For the case of the mentioned ship type, CARGO between ports were defined based on the operational-level voyage intake (cargo movement, cm_{ijm}) was reported in AXSDry database [40]. The calculation using Equation (1) to estimate the cargo movement demand is redundant since the cargo movement information is already stated.

Moreover, the cargo type was previously categorized based on the arrival port of this data. Hence, this data records discrete cargo types on each operation, such as iron ore, coal, grain, and others, making it possible to group certain cargo types into specific time ranges. Thus, the OD tables for each cargo type could be collected monthly- and annual-basis.

The set of months in a year is represented as M. The cargo movement (cm_{ijm}) per trip for each ship i serving the route j in month m (t) was collected to form the monthly cargo movement (cm_{jm}) of the route j (t/m), and annual cargo movement (CA_j) of the route j (t/y), as follows:

$$\boldsymbol{cm_{jm} = \sum_{i} (cm_{ijm}) \quad \forall i \in I, \quad \forall j \in J, \quad \forall m \in M,} \tag{3}$$

$$\boldsymbol{CA_j = \sum_{m} (cm_{jm}) \quad \forall i \in I, \quad \forall j \in J, \quad \forall m \in M,} \tag{4}$$

where cm_{ijm} is the cargo movement per trip for each ship i serving the route j (t), i is an individual ship (2479 Panamax–MiniCape dry bulk carriers operating in 2018), j is an individual route (3338 routes of iron ore, coal, grain, and others in 2018), and m is an individual month in a year (1: January (Jan), 2: February (Feb), 3: March (Mar), 4: April (Apr), 5: May, 6: June (Jun), 7: July (Jul), 8: August (Aug), 9: September (Sep), 10: October (Oct), 11: November (Nov), 12: December (Dec)).

4.3.3. Results of Cargo Movement Model

Finally, Table 13 shows a sample of the annual iron ore OD table of Capesize dry bulk carrier [39]. The data enclosed in this table was used as the cargo movement demand in the case studies intended for ship allocation in the time-charter contract.

Table 13. A sample of 2018 annual iron ore origin–destination (OD) table of Capesize dry bulk carrier [39].

Origin Ports [1]	Destination Ports Cargo Movement (MT) [2]					
	Caofeidian	Zhoushan	Tianjin	Ningbo	Rizhao	Yingkou
Port Hedland	57.79	30.70	39.10	26.11	34.18	19.49
Port Walcott	8.47	14.62	8.91	11.13	8.31	3.22
Itaqui	12.42	12.56	2.78	4.34	2.83	3.21
Dampier	10.77	11.35	12.65	9.56	8.04	6.95
Tubarao	*na*	6.06	0.35	0.83	*na*	*na*
Sepetiba	4.06	2.41	1.05	5.07	2.21	0.34
Saldanha Bay	0.36	4.87	1.24	2.16	2.94	0.90
Canada-B	*na*	2.74	*na*	1.27	*na*	*na*
Guaiba Island	3.33	1.36	1.88	0.57	0.57	0.36
Cape Preston	0.81	9.39	1.40	0.46	*na*	0.11

[1] Port cluster of *Canada-B*: ports of Baie-Comeau, Canso, Halifax, Port Cartier, Quebec, and Sept-Iles.
[2] *na*: not available–no cargo movement.

For the case of Panamax–MiniCape dry bulk carriers, Table 14 shows a sample of the annual iron ore OD table, whereas Table 15 presents a sample of the monthly iron ore OD table of Panamax–MiniCape dry bulk carriers [40]. The data enclosed in these OD tables were used as the cargo movement demand in the case studies intended for ship allocation in time- and voyage-charter contracts, respectively.

Table 14. A sample of 2018 annual iron ore OD table of Panamax–MiniCape dry bulk carrier [40].

Origin Ports [1]	Destination Ports Cargo Movement (MT) [2]					
	Ningbo	Ghent	Dunkirk	Rotterdam	Tangshan	China-B
Cape Preston	8.06	*na*	*na*	*na*	0.95	0.43
Port Hedland	0.40	*na*	*na*	*na*	0.49	1.70
Geraldton	0.06	*na*	*na*	*na*	2.27	0.93
Tubarao	*na*	0.70	0.23	0.23	*na*	*na*
Port Cartier	*na*	1.66	2.60	*na*	*na*	0.07
Europe	*na*	0.10	0.21	1.17	*na*	*na*
Richards Bay	0.08	*na*	*na*	*na*	0.51	0.49
Pd. Madeira	*na*	1.32	0.26	*na*	*na*	*na*
Milne Inlet	*na*	0.19	0.86	1.92	*na*	*na*
Sept-Iles	*na*	1.02	0.58	0.32	*na*	*na*

[1] Port cluster of *Europe*: ports of Aaheim, Bremanger Quarry, Fredericia, Klaipedia, Kokkola, Kotka, Liepaja, Lulea, Mo I Rana, Muuga, Tahkoluoto, and Ventspils.

[2] *na*: not available–no cargo movement.

Table 15. A sample of 2018 monthly iron ore OD table of Panamax–MiniCape dry bulk carrier [40].

Origin Ports [1]	Cargo Movement (x100,000 t) of Ningbo [2]											
	Jan	*Feb*	*Mar*	*Apr*	*May*	*Jun*	*Jul*	*Aug*	*Sep*	*Oct*	*Nov*	*Dec*
Cape Preston	7.4	5.3	6.5	6.4	4.2	8.5	6.4	8.4	7.4	6.4	9.4	4.4
Port Hedland	0.7	1.1	*na*	*na*	1.1	1.1	*na*	*na*	*na*	*na*	*na*	*na*
Geraldton	*na*	*na*	*na*	*na*	*na*	0.6	*na*	*na*	*na*	*na*	*na*	*na*
Tubarao	*na*	*na*	*na*	*na*	*na*	*na*	*na*	*na*	*na*	*na*	*na*	*na*
Port Cartier	*na*	*na*	*na*	*na*	*na*	*na*	*na*	*na*	*na*	*na*	*na*	*na*
Europe	*na*	*na*	*na*	*na*	*na*	*na*	*na*	*na*	*na*	*na*	*na*	*na*
Richards Bay	*na*	*na*	*na*	*na*	*na*	*na*	*na*	*na*	*na*	0.8	*na*	*na*
Pd. Madeira	*na*	*na*	*na*	*na*	*na*	*na*	*na*	*na*	*na*	*na*	*na*	*na*
Milne Inlet	*na*	*na*	*na*	*na*	*na*	*na*	*na*	*na*	*na*	*na*	*na*	*na*
Sept-Iles	*na*	*na*	*na*	*na*	*na*	*na*	*na*	*na*	*na*	*na*	*na*	*na*

[1] Port cluster of *Europe*: ports of Aaheim, Bremanger Quarry, Fredericia, Klaipedia, Kokkola, Kotka, Liepaja, Lulea, Mo I Rana, Muuga, Tahkoluoto, and Ventspils.

[2] *Jan*: January (Jan); *Feb*: February; *Mar*: March; *Apr*: April; *May*: May, *Jun*: June; *Jul*: July; *Aug*: August; *Sep*: September; *Oct*: October; *Nov*: November; *Dec*: December*; na*: not available–no cargo movement.

4.4. Development of Ship Model

4.4.1. Overview of Ship Model

This model contains the individual ship data, Capesize and Panamax–MiniCape dry bulk carriers, and their operation condition. We extracted a list of dry bulk carriers that operated in the ship movement data worldwide. This model encloses each ship and its static information, such as principal particulars and performances. In the ship movement data, these ships were coupled with their operation conditions; draught rate, average sailing speed, and port staying time. Later, we adopted a mechanism to predict the operation conditions for each available ship and port. Table 16 gives an overview of this model.

Table 16. Overview of the ship model.

Target Ship [1]	*Capesize*	*Panamax–MiniCape*
Ship Movement Data	MINT [39]	AXSDry [40]
Operation Period	2013–2019	2013–2020
Cargo Types [2]	*Ir, Co*	*Ir, Co, Gr, Ot*
2018 Route Numbers	1085	3338
2018 Ship Numbers	1647	2479
Operation Condition Prediction	Deep Learning	Route-Base Average

[1] *Capesize*: dry bulk carriers with deadweight tonnage more than 100,000; *Panamax–MiniCape*: dry bulk carriers with deadweight tonnage 65,000–140,000.
[2] *Ir*: iron ore; *Co*: coal; *Gr*: grain; *Ot*: others.

4.4.2. Description of Ship Specifications

This model contains each ship and its attributes. In the 2018 ship movement data [39,40], the Capesize and Panamax–MiniCape dry bulk carriers consisted of 1647 and 2479 ships, respectively. These ships are individually attached to several technical and non-technical variables, as shown in Table 5. Each ship is tied to several attributes, such as administration, principal particulars, and performance. The administration attributes include ships' IMO number, callsign, flag, class, shipbuilder, registered owner, ship manager, and operator. The principal particular attributes identify ships' DWT, gross tonnage (GT), displacement, length, breadth, draught, and depth. Finally, the performance attributes present ships' built year, main engine power, and design speed.

From the abovementioned variables, we obtained both static and dynamic variables. The static variable is the one that is commonly fixed toward the operation period of the ships [1]. This variable covers the ships' administration, principal particulars, and performances. Further, these features are used to calculate the GHG emissions and COST and to assess the compatibility of ships' dimensions and ports' size limitations.

On the contrary, the dynamic variable represented the condition at only the current operation period of the ships. This term is generally attached to the administration variables of the ships, except its IMO number and shipbuilder since these variables are attached to a ship towards its lifetime. The administration variables that include ownership information, such as flag, registered owner, ship manager, and operator, are subject to change towards the operation period of the ships.

4.4.3. Methodology to predict Operation Condition

In addition to what has already been discussed, each ship is tied to its operation condition whenever a ship is assigned to a certain route. Therefore, it is necessary to know this information for all available routes. A ship's operation conditions throughout a particular route are assumed to be its typical performance, despite of the operation terms in the practiced contract. This study defines the operation conditions as follows:

- Draught rate: The ratio between the arrival draught and the ship's design draught at the destination port;
- Average sailing speed: The ship's average sailing speed starting from its departure time at the origin port to its arrival time at the destination port;
- Port staying time: The ship's port staying time starts from its arrival time until its departure time at the destination port.

For the Capesize dry bulk carrier, we constructed a DL model distinctively to predict the operation conditions in each voyage mode: laden and ballast. We proposed DL as the prediction method in this case by referring to our previous studies [30]. Figure 8 shows an overview of the proposed DL model. With each operation condition as the target feature, the model takes into account the following Capesize dry bulk carrier features as an input:

- Ship specifications [42]: 1658 entries, which consist of DWT, length, breadth, draught, design speed, main engine power, and built year;
- Port data [43]: 564 entries, which consist of port limitations of length, breadth, and draught;
- Ship movement data [39,44]: 36,596 entries of worldwide operations from January 2015 to May 2019, which consist of dates of arrival and departure, ports of origin and destination, and sailing distances;
- Statistical data [48]: 49 entries, which consisting of monthly average high-sulphur fuel oil (HSFO) bunker prices in various bunker hubs.

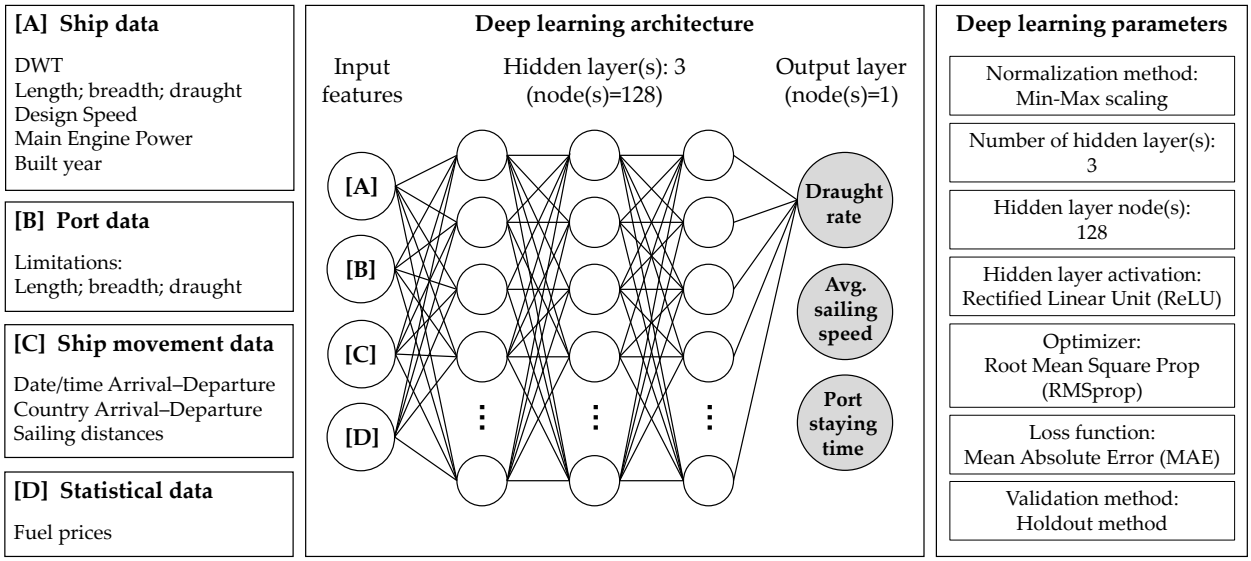

Figure 8. Deep learning (DL) model to predict operation conditions.

The same architecture is used to predict the abovementioned operation conditions. Its input features are represented as binary vectors by using the one-hot encoding. These are normalized using Min-Max scaling before the training process.

The proposed DL model is comprised of three hidden layers of 128 nodes equipped with Rectified Linear Unit activation functions. We applied the optimizer of the Root Mean Square prop and the loss function of mean absolute error loss. Finally, we applied the holdout method to train our model, in which 70% was for the training data, 20% for the validation data, and 10% for the test data.

The same applies to Panamax–MiniCape dry bulk carriers; we estimated the operation conditions for the laden and ballast voyage mode. We predicted the operation conditions of this dry bulk carrier size category by adopting the R-AVG since the transported cargo types at the operational level are distinctively reported in AXSDry ship movement data [40]. A sample of the recorded operation conditions in this data is shown in Table 17 and Table 18.

Table 17. A sample of recorded operation conditions in AXSDry data [40]: laden voyage.

Ship Name [1]	Voyage Loading Port	Voyage Discharge Port	Voyage Loading Date	Voyage Discharge Date	Laden Voyage [2]			
					DR	*SS*	*SD*	*PS*
Ship A	Port Hedland	Rizhao	2017-12-15	2018-01-07	100%	10.4	27.5	1.3
	Port Hedland	Tianjin	2018-01-30	2018-02-16	100%	9.9	21.2	1.1
	Port Hedland	Taicang	2018-03-05	2018-04-08	100%	10.8	35.4	1.4
	Port Hedland	Lianyungang	2018-04-26	2018-05-12	100%	10.7	20.0	1.5
	Port Hedland	Zhenjiang	2018-07-10	2018-08-09	101%	11.8	31.4	1.4
	Port Hedland	Jiangyin	2018-09-11	2018-10-02	99%	11.4	22.4	1.3
Ship B	Gladstone	Haimen	2018-05-25	2018-06-14	92%	11.3	22.7	1.5
	Newcastle	Yuhuan	2018-07-28	2018-08-20	92%	10.5	25.8	0.9
	Newcastle	Yuhuan	2018-09-07	2018-09-26	92%	10.5	21.9	1.3
	Newcastle	Yuhuan	2018-10-16	2018-11-11	92%	10.2	29.4	1.3
	Brisbane	Longkou	2018-12-02	2018-12-22	94%	9.8	22.4	0.0

[1] *Ship A*: dry bulk carriers with deadweight tonnage 99,000 transporting iron ore; *Ship B*: dry bulk carriers with deadweight tonnage 105,000 transporting coal.

[2] *DR*: draught rate (%); *SS*: average sailing speed (kn); *SD*: sailing days (days); *PS*: port staying time (days).

Table 18. A sample of recorded operation conditions in AXSDry data [40]: ballast voyage.

Ship Name [1]	Voyage Loading Port	Voyage Discharge Port	Voyage Loading Date	Voyage Discharge Date	Ballast Voyage [2]			
					DR	*SS*	*SD*	*PS*
Ship A	Port Hedland	Rizhao	2017-12-15	2018-01-07	49%	12.5	24.0	4.6
	Port Hedland	Tianjin	2018-01-30	2018-02-16	60%	12.6	18.7	4.0
	Port Hedland	Taicang	2018-03-05	2018-04-08	52%	14.0	19.7	2.3
	Port Hedland	Lianyungang	2018-04-26	2018-05-12	51%	12.2	14.3	4.0
	Port Hedland	Zhenjiang	2018-07-10	2018-08-09	51%	12.7	35.2	2.0
	Port Hedland	Jiangyin	2018-09-11	2018-10-02	50%	13.0	23.7	1.7
Ship B	Gladstone	Haimen	2018-05-25	2018-06-14	53%	12.9	12.7	2.9
	Newcastle	Yuhuan	2018-07-28	2018-08-20	53%	10.9	19.8	2.8
	Newcastle	Yuhuan	2018-09-07	2018-09-26	52%	11.9	22.1	3.7
	Newcastle	Yuhuan	2018-10-16	2018-11-11	53%	11.1	19.4	4.1
	Brisbane	Longkou	2018-12-02	2018-12-22	52%	10.9	22.3	2.7

[1] *Ship A*: dry bulk carriers with deadweight tonnage 99,000 transporting iron ore; *Ship B*: dry bulk carriers with deadweight tonnage 105,000 transporting coal.

[2] *DR*: draught rate (%); *SS*: average sailing speed (kn); *SD*: sailing days (days); *PS*: port staying time (days).

Next, this section applied the R-AVG by gathering the operation conditions on all available routes worldwide. We have provided an example of the R-AVG of draught rate case only since the scheme of R-AVG for average sailing speed and port staying time cases are the same. The port calling data instances and cargo types are represented as U and C, respectively. Moreover, the number of U is described as U'. The average draught rate (DR_{jc}) for each route j transporting cargo type c (%) is calculated as follows:

$$(22) \quad \boldsymbol{DR_{jc} = \frac{1}{U'} \times \sum_{i} \sum_{u} \left(DR_{uijc}\right) \quad \forall u \in U, \quad \forall i \in I, \quad \forall j \in J, \quad \forall c \in C,} \tag{5}$$

where U' is the number of U, DR_{uijc} is the draught rate of a port calling data instance, u is an individual port calling instance (16,110 Panamax–MiniCape dry bulk carriers operating in 2018), i is an individual ship (2479 Panamax–MiniCape dry bulk carriers operating in 2018), j is an individual route served by Panamax–MiniCape dry bulk carriers (3338 routes of iron ore, coal, grain, and others in 2018), and c is an individual cargo type served by Panamax–MiniCape dry bulk carriers (1: iron ore, 2: coal, 3: grain, 4: others).

4.4.4. Evaluation of Predicted Operation Condition

The average operation conditions of the worldwide routes (AVG) are the baselines that affirm the benefits of adopting the DL model. In the case of Capesize dry bulk carrier, the mean absolute error (MAE) is applied to compare the DL prediction and AVG results, as shown in Table 19.

Table 19. Mean absolute error of DL model predictions.

Operation Condition	Mean Absolute Error (MAE) of			
	Deep Learning (DL) Model		Worldwide Average (AVG)	
	Laden Voyage	Ballast Voyage	Laden Voyage	Ballast Voyage
Draught rate (%)	1.686	3.923	4.115	4.721
Avg. sailing speed (kn)	1.181	1.427	1.318	1.434
Port staying time (d)	1.273	2.439	1.819	3.129

The DL prediction results indicate a higher accuracy than the AVG. In the case of draught rate, DL returned MAE of 1.686 and 3.923 in laden and ballast voyages, respectively. These values prove 59% and 17% higher precision than AVG for both voyage modes. Similarly, port staying time predicted by using DL resulted in MAE of 1.273 and 2.439 in laden and ballast voyages, respectively. These suggest 30% and 22% more definitive values compared to AVG. Later, we will use the operation condition prediction results of the DL model to calculate the CARGO, GHG, and COST variables for each Capesize dry bulk carrier.

Furthermore, similar to the Capesize dry bulk carrier, AVG is used as the baselines to confirm the advantage of adopting the R-AVG. The R-AVG results indicate a higher accuracy than the AVG, as shown in Table 20.

Table 20. Mean absolute error of route-base average (R-AVG).

Operation Condition	MAE of			
	Route-Base Average (R-AVG)		AVG	
	Laden Voyage	Ballast Voyage	Laden Voyage	Ballast Voyage
Draught rate (%)	2.133	1.374	4.714	2.120
Avg. sailing speed (kn)	1.049	1.037	1.468	1.248
Port staying time (d)	0.431	0.516	0.885	0.882

Table 20 suggests that R-AVG owns a lower MAE compared to the AVG. The draught rate in R-AVG yielded MAE of 2.133 and 1.374 in laden and ballast voyages, justifying an advancement of 55% and 35% compared to AVG, respectively. Similarly, port staying time delivered using R-AVG resulted in MAE of 0.431 and 0.516 in laden and ballast voyages, respectively. These outcomes confirm 51% and 42% improvement comparatively to AVG. Finally, we will use the annual R-AVG of operation conditions to calculate the GHG and COST variables for each Panamax–MiniCape dry bulk carrier.

4.5. Methodology to Calculate GHG emissions

4.5.1. Overview of GHG emissions Calculation

In this section, we have provided an overview of the calculation process of cargo movement (CM), GHG emissions (GH), and total COST (TC). Figure 9 illustrates the calculation process and its correlated variables. The variables and constants which were taken as the input, the used equations, and the resulted output were explained in this section.

For these calculations, ship movement data [39,40], ship data [42], and the assumed constants [1,28,29,48] were used as the input. Constants were defined based on ship movement and ship data attributes. Next, we processed these data by applying Equations (1)–(4) and Equations (6)–(15) to calculate CM and GH, respectively. In this study, these were calculated for both cases of Capesize and Panamax–MiniCape dry bulk carriers but CM, since AXSDry ship movement data [40] of Panamax–MiniCape dry bulk carriers comprised voyage intake (CM).

Cargo movement (CM) was calculated by inputting actual draught (d), ship deadweight tonnage (DWT), and ship maximum draught (D) using Equations (1) and (2). Making use of Equation (6), the actual power of the main engine (p) can be calculated. Moreover, fuel consumption of main engine and auxiliary machinery (A, B) are defined using Equations (7) and (8). We can calculate the total GHG emissions (GH) by applying Equation (15).

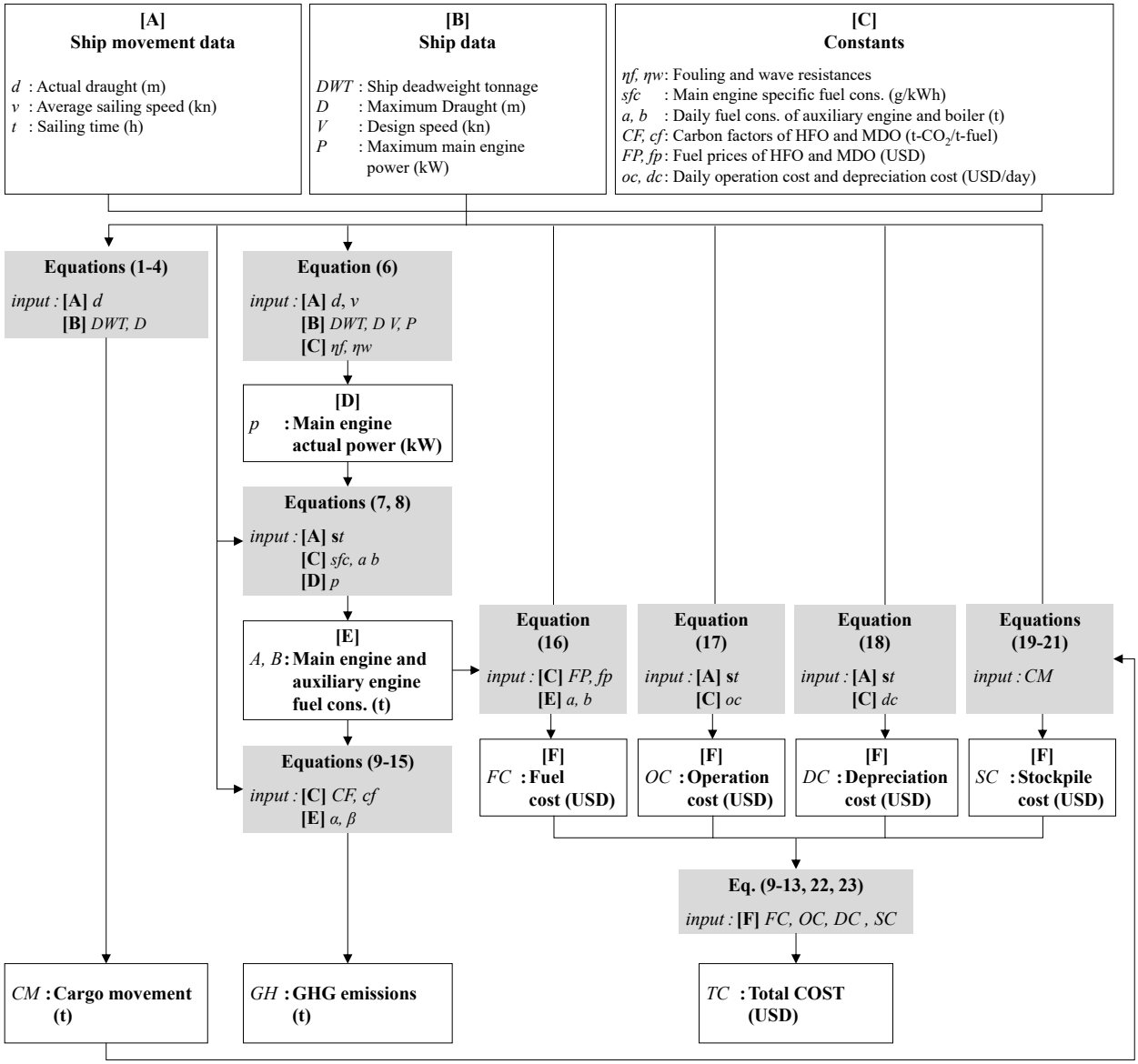

Figure 9. Calculation process of cargo movement, GHG emissions, and ship cost.

4.5.2. Calculation Process of GHG Emissions

We calculated the total GHG referred to in prior IMO GHG studies [28,29]. It comprised the GHG emissions from the main engine and auxiliary machinery (an auxiliary engine and a boiler). This calculation used ship data [42] and port data [43], as well as the global network model and ship model results. First, we calculated the actual power the main engine operated on average in sailing mode.

The actual power of the main engine (p_{ij}) of a ship i operating in the route j (kW) is calculated as follows [28,29,32,33]:

$$\boldsymbol{p_{ij}} = \frac{\boldsymbol{P_i} \times \left(\boldsymbol{d_{ij}}/\boldsymbol{D_i}\right)^{\left(\frac{2}{3}\right)} \times \left(\boldsymbol{v_{ij}}/\boldsymbol{V_i}\right)^{3}}{\boldsymbol{\eta w_{ij}} \times \boldsymbol{\eta f_{ij}}} \quad \forall \boldsymbol{i} \in \boldsymbol{I}, \quad \forall \boldsymbol{j} \in \boldsymbol{J}, \tag{6}$$

where P_i is the ship i maximum main engine power (kW), d_{ij} is the ship i actual draught (m), D_i is the ship i maximum draught (m), v_{ij} is the ship i average sailing speed (kn), V_i is the ship i design speed (kn), and ηw_{ij} and ηf_{ij} are the correction factors of weather and fouling, respectively, i is an individual ship (1647 Capesize and 2479 Panamax–MiniCape dry bulk carriers operating in 2018), and j is an individual route (1085 routes of Capesize's iron ore and coal and 3338 routes of Panamax–MiniCape's iron ore, coal, grain, and others in 2018). The P_i, D_i, and V_i of each ship were acquired from the ship data [42], d_{ij} and v_{ij} were generated by the ship model, ηw_{ij} and ηf_{ij} were considered constants with values 0.909 and 0.917, respectively, as shown in Table 21 [28,29].

Table 21. Correction factors of weather and fouling of various ship types [28,29].

Ship Type	Ship Capacity [1]		Weather correction factor (ηw)	Fouling correction factor (ηf)
Bulk carrier; General cargo; Tanker	0–9,999	*DWT*	0.909	0.917
	10,000–+	*DWT*	0.867	0.917
Container Ship	0–999	*TEU*	0.909	0.917
	1000–+	*TEU*	0.867	0.917

[1] *DWT*: deadweight tonnage; *TEU*: twenty equipment unit.

After calculating p_{ij}, the main engine fuel consumption (A_{ij}) for a ship i serving the route j (t) is calculated as follows:

$$\boldsymbol{A_{ij}} = \left(\boldsymbol{p_{ij}} \times \boldsymbol{sfc_i} \times \boldsymbol{st_{ij}}\right) \quad \forall \boldsymbol{i} \in \boldsymbol{I}, \quad \forall \boldsymbol{j} \in \boldsymbol{J}, \tag{7}$$

where p_{ij} is the actual power of the main engine (kW), sfc_i is the ship i specific fuel oil consumption of the main engine (g/kWh), st_{ij} is the round-trip sailing time (d), i is an individual ship (1647 Capesize and 2479 Panamax–MiniCape dry bulk carriers operating in 2018), and j is an individual route (1085 routes of Capesize's iron ore and coal and 3338 routes of Panamax–

MiniCape's iron ore, coal, grain, and others in 2018). In this study, the main engine of ship i was assumed to be a slow-speed diesel engine fueled by heavy fuel oil (HFO), as shown in Table 22. Thus sfc_i, for ships built before and after 2001 were assumed to be 185 and 175 g/kWh, respectively [28,29].

Table 22. Specific fuel oil consumption of various main engine and fuel types [28,29].

Main Engine Type	Fuel Type [1]	Specific Fuel Consumption (g/kWh) [2]		
		Before 1984	1984–2000	After 2000
Slow-speed Diesel (SSD)	*HFO*	205	185	175
	MeOH	*na*	*na*	350
LNG-Otto (Slow-speed Dual-fuel)	*LNG*	*na*	*na*	148

[1] *HFO heavy fuel oil*; *MeOH*: methanol; *LNG*: liquefied natural gas.
[2] *na*: not available–no information.

In addition to the main engine, we estimated the auxiliary machinery fuel consumption (an auxiliary engine and a boiler). The daily average fuel consumption of the auxiliary engine (a_i) and boiler (b_i) were determined by a linear correlation between the ship size and the average fuel consumption of the auxiliary machinery [28,29], as shown in Figure 4.

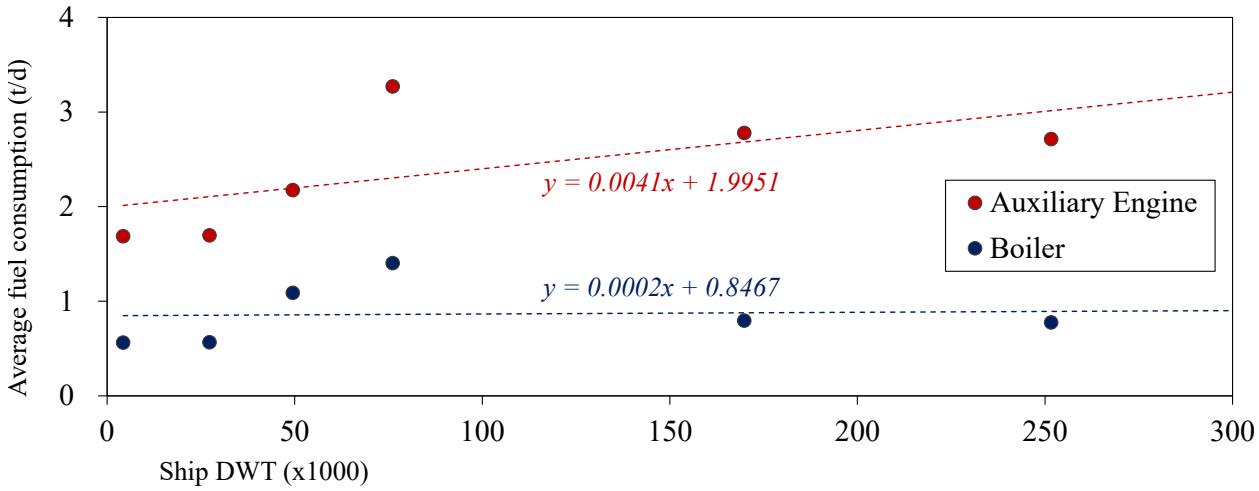

Figure 10. Daily average fuel consumption of auxiliary engine and boiler [28,29].

The auxiliary machinery fuel consumption (B_{ij}) for a ship i operating on the route j (t) is calculated as follows:

$$\boldsymbol{B_{ij} = (a_i + b_i) \times st_{ij} \quad \forall i \in I, \quad \forall j \in J,} \tag{8}$$

where a_i is the ship i auxiliary engine daily average fuel consumption of the ship's auxiliary engine (t/d), b_i is the ship i boiler daily average fuel consumption of the ship (t/d), st_{ij} is the round-trip sailing time (d), i is an individual ship (1647 Capesize and 2479 Panamax–MiniCape dry bulk carriers operating in 2018), and j is an individual route (1085 routes of Capesize's iron ore and coal and 3338 routes of Panamax–MiniCape's iron ore, coal, grain, and others in 2018). Next, the possible annual trip numbers (n_{ij}) of a ship i serving the route j is defined as follows:

$$\boldsymbol{nx_{ij} = \frac{(yd - md_i)}{(st_{ij} + ps_{ij})} \quad \forall i \in I, \quad \forall j \in J,} \tag{9}$$

$$\boldsymbol{ny_{ij} = \left(\frac{CA_j}{CM_{ij}}\right) \quad \forall i \in I, \quad \forall j \in J,} \tag{10}$$

$$\boldsymbol{n_{ij} = \begin{cases} nx_{ij} \; if \; (nx_{ij} \leq ny_{ij}) \\ ny_{ij} \; if \; (nx_{ij} > ny_{ij}) \end{cases} \quad \forall i \in I, \quad \forall j \in J,} \tag{11}$$

where nx_{ij} and ny_{ij} are the possible trip numbers considering the annual economic days and annual cargo movement, respectively, i is an individual ship (1647 Capesize and 2479 Panamax–MiniCape dry bulk carriers operating in 2018), and j is an individual route (1085 routes of Capesize's iron ore and coal and 3338 routes of Panamax–MiniCape's iron ore, coal, grain, and others in 2018). The yd is the number of days in a year, taken as 365 (d), md_i is the assumed annual maintenance days (d), st_{ij} is the round-trip sailing time (d), ps_{ij} is the loading–unloading time (d), CA_j is the annual transported cargo movement of route j (t/y), and CM_{ij} is the ship i cargo movement per trip serving the route j (t).

Likewise, using the assembled monthly OD tables in the case of Panamax–MiniCape dry bulk carriers [40], we can managed to calculate the possible monthly trip numbers (n_{ijm}) of a ship i serving the route j as follows:

$$\boldsymbol{ny_{ijm}} = \left(\frac{\boldsymbol{cm_{jm}}}{\boldsymbol{cm_{ijm}}}\right) \quad \forall \boldsymbol{i} \in \boldsymbol{I}, \quad \forall \boldsymbol{j} \in \boldsymbol{J}, \quad \forall \boldsymbol{m} \in \boldsymbol{M}, \tag{12}$$

$$\boldsymbol{n_{ijm}} = \begin{cases} \boldsymbol{nx_{ij}\ if\ (nx_{ij} \leq ny_{ijm})} \\ \boldsymbol{ny_{ijm}\ if\ (nx_{ij} > ny_{ijm})} \end{cases} \quad \forall \boldsymbol{i} \in \boldsymbol{I}, \quad \forall \boldsymbol{j} \in \boldsymbol{J}, \quad \forall \boldsymbol{m} \in \boldsymbol{M}, \tag{13}$$

where nx_{ij} and ny_{ijm} are the possible trip numbers considering the annual economic days and monthly cargo movement, respectively, cm_{jm} is the monthly transported cargo movement of route j (t/m), cm_{ijm} is the ship i cargo movement per trip serving the route j in month m (t), i is an individual ship (2479 Panamax–MiniCape dry bulk carriers operating in 2018), and j is an individual route (3338 routes of Panamax–MiniCape's iron ore, coal, grain, and others in 2018).

Finally, we define the total GHG emissions, which cover the GHG emissions of the main engine and auxiliary machinery. We calculate the annual GHG emissions (GH_{ij}) for a ship i operating in the route j (t/y) as follows:

$$\boldsymbol{GH_{ij}} = \Big(\big(\boldsymbol{A_{ij}} \times \boldsymbol{CF}\big) + \big(\boldsymbol{B_{ij}} \times \boldsymbol{cf}\big)\Big) \times \boldsymbol{n_{ij}} \quad \forall \boldsymbol{i} \in \boldsymbol{I}, \quad \forall \boldsymbol{j} \in \boldsymbol{J}, \tag{14}$$

where A_{ij} is the main engine fuel consumption (t), B_{ij} is the auxiliary machinery fuel consumption (t), CF and cf are the HFO and marine diesel oil (MDO) carbon factors (t-CO2/t-fuel), respectively, n_{ij} is the possible annual trip numbers, i is an individual ship (1647 Capesize and 2479 Panamax–MiniCape dry bulk carriers operating in 2018), and j is an individual route (1085 routes of Capesize's iron ore and coal and 3338 routes of Panamax–MiniCape's iron ore, coal, grain, and others in 2018). Furthermore, the monthly GHG emissions (GH_{ijm}) for a ship i operating in the route j (t/m) is calculated as follows:

$$\boldsymbol{GH_{ijm}} = \Big(\big(\boldsymbol{A_{ij}} \times \boldsymbol{CF}\big) + \big(\boldsymbol{B_{ij}} \times \boldsymbol{cf}\big)\Big) \times \boldsymbol{n_{ijm}} \quad \forall \boldsymbol{i} \in \boldsymbol{I}, \quad \forall \boldsymbol{j} \in \boldsymbol{J}, \quad \forall \boldsymbol{m} \in \boldsymbol{M}, \tag{15}$$

where A_{ij} is the main engine fuel consumption (t), B_{ij} is the auxiliary machinery fuel consumption (t), CF and cf are the HFO and marine diesel oil (MDO) carbon factors (t-CO2/t-fuel), respectively, n_{ijm} is the possible monthly trip numbers, i is an individual ship (2479

Panamax–MiniCape dry bulk carriers operating in 2018), and j is an individual route (3338 routes of Panamax–MiniCape's iron ore, coal, grain, and others in 2018). Table 23 shows the emission factors defined in the IMO GHG study [28,29], CF and cf were taken as 3.114 and 3.206 t-CO2/t-fuel, respectively.

Table 23. Emission factors for various fuel types [28,29].

Fuel Type [1]	Emission Factors (t-CO2/t-fuel)
HFO	3.114
MDO	3.206
LNG	2.750
MeOH	1.375

[1] *HFO heavy fuel oil*; *MDO*: marine diesel oil; *LNG*: liquefied natural gas; *MeOH*: methanol.

Moreover, we construct the case studies intended for future scenarios by following the target of the IMO GHG emissions reduction strategy [28,29]. The minimum goal of GHG emissions reduction is 50% in 2050 compared to 2008 [49-51]. Implementation programs of zero-carbon and low-carbon fuels were pointed out as a measure considering this scheme.

Furthermore, we offer that the main engine is fueled by fuels with lower emission factors for the case studies intended for future scenarios. These fuels own discrete sfc_i and CF compared to HFO, which was previously discussed in the calculation of main engine fuel consumption (A_{ij}, see Equation (**7**)). In this context, liquefied natural gas (LNG) and methanol (MeOH) were proposed as lower emission factors by referring to IMO GHG studies [28,29].

Table 22 highlights the specific fuel oil consumption (sfc_i) of various main engines and fuel types, including the proposed fuel types [28,29]. In this context, sfc_i is an extension of its engine types; slow-speed diesel engines utilized MeOH, and slow-speed dual-fuel engines utilized LNG. The value of sfc_i (g/kWh) for LNG and MeOH were 148 and 350, respectively. These numbers suggest different fuel consumption for the same main engine power after 2000 rather than HFO. The fuel consumption by using LNG as fuel renders 15% less consumption compared to HFO. In contrast, two times fuel is consumed by using MeOH as the main engine fuel. Later, these were used as sfc_i of Equation (7).

However, the reduction of total GHG emissions is not directly generated by sfc_i. In this context of the proposed fuel, the emission factors of LNG and MeOH are presented in Table 23. These fuel types hold emission factors (t-CO2/t-fuel) of 2.750 and 1.375, respectively. These values depicted 12% and 56% emissions factors compared to HFO. Accordingly, these were used as CF of Equation (14) in the case studies intended for future scenarios. Finally, Table 24 presents the obtainable reduction in total GHG emissions of the main engine, delivered by each fuel type.

Table 24. Obtainable GHG emissions from main engine for various fuel types [28,29].

Fuel Type	Specific Fuel Consumption *(sfc,* in g/kWh)	Emission Factors (*CF,* g-CO2/g-fuel)	Total GHG Emissions (*GH,* g) [1]	Obtainable Reduction (%)
HFO	175	3.114	545	0
LNG	148	2.750	407	25.3
MeOH	350	1.375	481	11.7

[1] Calculated by using Equation (4) where the actual power of the main engine (p_{ij}) and the round-trip sailing time (st_{ij}) were assumed constants as 1.

As previously discussed, MeOH holds 1.375, the lowest emission factor compared to other fuel types. However, a drawback of this fuel type is the large specific fuel consumption of 350. On the other hand, LNG placed moderate emissions factors in the middle of HFO and MeOH but with the lowest specific fuel consumption compared to other fuel types. Hence, these attributes allowed 25.3% and 11.7% GHG emissions reduction compared to HFO.

4.5.3. Evaluation of GHG Emissions Calculation

In this section, we will evaluate the GHG emissions calculation scheme. An evaluation of the GHG calculation is shown in Table 25. We calculated the main engine GHG emissions using the 2018 worldwide average ship age and draught rate of the Capesize dry bulk carriers [39] and the average variables depicted in the IMO GHG study [28]. For the following size categories, an error margin of less than 4% indicated the applicability of our GHG calculation scheme.

Table 25. Evaluation of GHG calculation.

Size Category (DWT x1000)	GHG Emissions (MT)		Error (%)
	IMO GHG Study [28]	This Study	
100–199	39	38.8	0.5
200–+	22	22.7	3.2

4.6. Methodology to Calculate COST

4.6.1. Overview of COST Calculation

In the previous section, we have provided an overview of the calculation process of cargo movement (CM), GHG emissions (GH), and total COST (TC). The variables and constants taken as the input, the used equations, and the resulting output are explained in Figure 9. For these calculations, ship movement data [39,40], ship data [42], and the assumed constants [1,28,29,48] were used as the input. Constants were defined based on ship movement and ship data attributes. In the COST context, fuel cost (FC) by applying Equations (16). Later, refer to the response surface presented in Figure 10 and Figure 11, with the Equations (17)–(18), operation cost (OC) and depreciation cost (DC) are calculated. Further, stock cost (SC) is determined by using Equation (19)–(21). Finally, the annual total COST (TC) is calculated using Equation (22).

4.6.2. Calculation Process of COST

In this study, the total COST considers the fuel, operation, depreciation, and stockpile costs [1]. The fuel cost represents the cost of the fuel needed to transport specific cargo from the origin port to the destination port. The operation cost describes the cost of operating the ship. It comprises the crew, consumables, repairs, and insurance costs. The depreciation cost is the reduction in the ship's resale price after a year. The stockpile cost depicts the cost of stockpiling transported cargo at the destination port until the cargo is consumed based on the port's daily cargo movement demand.

4.6.2.1. Calculation Process of Fuel Cost

The fuel cost is calculated from the fuel consumption. The fuel cost (FC_{ij}) for a ship i serving the route j (USD) is calculated as the total GHG emissions equation by replacing the GHG emissions carbon factor (CF, cf) with fuel price constants (FP, fp), as follows:

$$\boldsymbol{FC_{ij} = \left(\left(A_{ij} \times FP\right) + \left(B_{ij} \times fp\right)\right) \quad \forall i \in I, \quad \forall j \in J,} \tag{16}$$

where A_{ij} is the main engine fuel consumption (t), B_{ij} is the auxiliary machinery fuel consumption (t), FP and fp are the HFO and MDO prices (USD/t-fuel), respectively, i is an individual ship (1647 Capesize and 2479 Panamax–MiniCape dry bulk carriers operating in 2018), and j is an individual route (1085 routes of Capesize's iron ore and

coal and 3338 routes of Panamax–MiniCape's iron ore, coal, grain, and others in 2018). After observing the fluctuation in maritime fuel price, Figure 11 presents the HFO and MDO prices from various bunker site [48]. FP and fp were assumed to be USD 300 and USD 600, respectively.

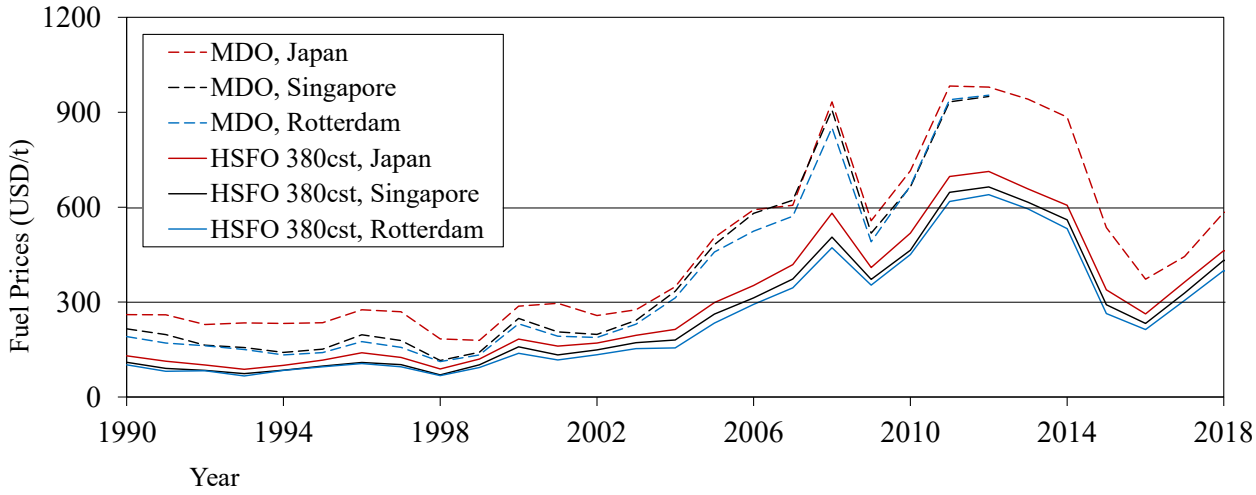

Figure 11. Bunker prices of high-Sulphur fuel oil 380 cSt and marine diesel oil in various bunker hubs [48].

Similar to what has already been discussed in the calculation of total GHG emissions, low-carbon fuels are later offered in the case studies intended for future scenarios. This study proposed LNG and MeOH as the fuel with lower emissions factors [28,29]. Thus, these fuel types are tied to their prices (FP) in the context of the main engine's fuel cost. Table 26 shows bunker prices for various fuel types in 2030–2050 by referring to the price-forecasting included in the recent IMO GHG study [28]. In this current insight, the increase in fuel costs can be ascertained by utilizing LNG- and MeOH-fueled main engines.

Table 26. Bunker prices for various fuel types in 2030–2050 [28].

Fuel Type [1]	Fuel Price in 2030–2050 (USD/t) [2]
HFO	375
LNG	590
MeOH	400

[1] *HFO heavy fuel oil*; *LNG*: liquefied natural gas; *MeOH*: methanol.
[2] Assumed no fluctuation of fuel prices toward these years.

4.6.2.2. Calculation Process of Operation Cost and Depreciation Cost

We composed response surfaces using the DWT and age of the dry bulk carrier ships to calculate the operation and depreciation costs. Considering Stopford [1], we expanded the correlation between the Capesize dry bulk carrier operation cost to other bulk carrier size classes [29,46,47]. Similarly, the depreciation cost was acquired by referring to the bulk carrier newbuilding and secondhand prices [48]. Figure 12 shows the daily operation cost for the given ship DWT and ship age which is defined by referring to the following attributes:

- Daily operation cost of Capesize bulk carriers [1].
- Operation cost ratios of various bulk carrier size categories in 2011; Capesize, Panamax, Handymax, and Handysize [46].
- Ship DWT range for various bulk carrier size categories in 2011; Capesize, Panamax, Handymax, and Handysize [47].
- Average ship DWT for various bulk carrier size categories in 2011; Capesize (205,000 DWT), Panamax (76,000 DWT), Handymax (51,000 DWT), and Handysize (27,000 DWT) [29].

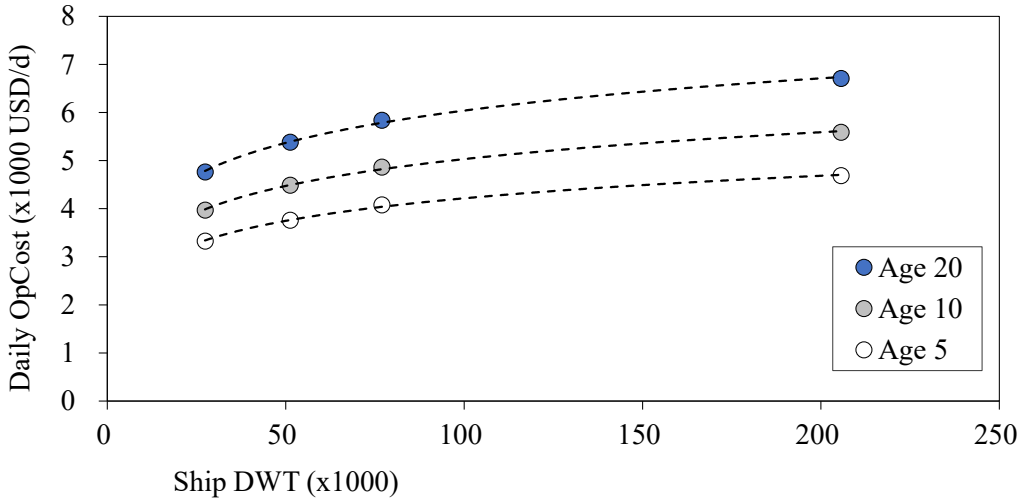

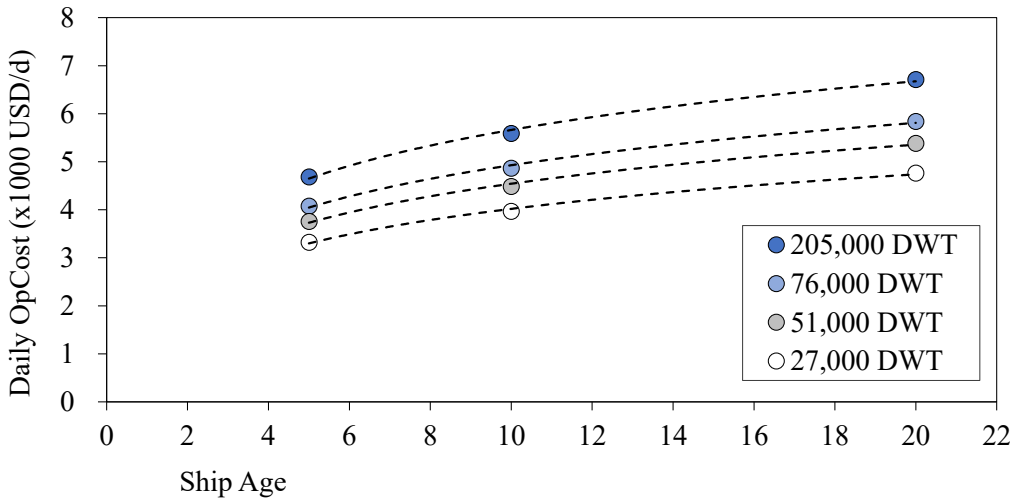

Figure 12. Bulk carrier daily operation cost for the given ship deadweight tonnage (DWT) and ship age [1,29,46,47].

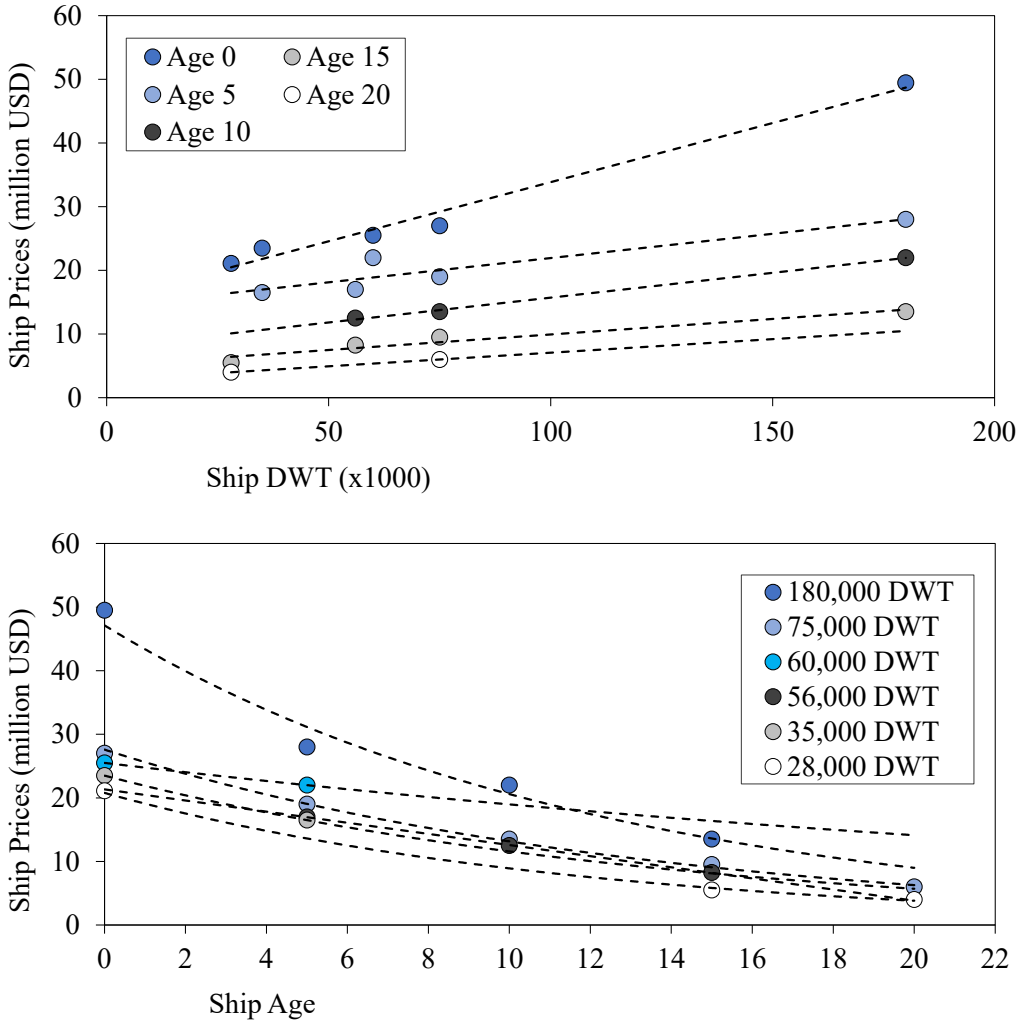

Figure 13. Bulk carrier ship prices for the given ship DWT and ship age [1,29,46,47].

Correspondingly, the depreciation cost is determined by referring to the bulk carrier newbuilding and secondhand ship prices in 2019 [48]. The ship prices for the given ship DWT and ship age are shown in Figure 13. The annual depreciation cost is obtained from the difference between the ship price in the current year and the previous year. Then, the daily depreciation cost was taken as the annual depreciation cost divided by the number of days in a year, taken as 365 days. Finally, we represent these attributes in the bulk carrier operation cost and depreciation cost response surfaces, as shown in Figure 14 and Figure 15.

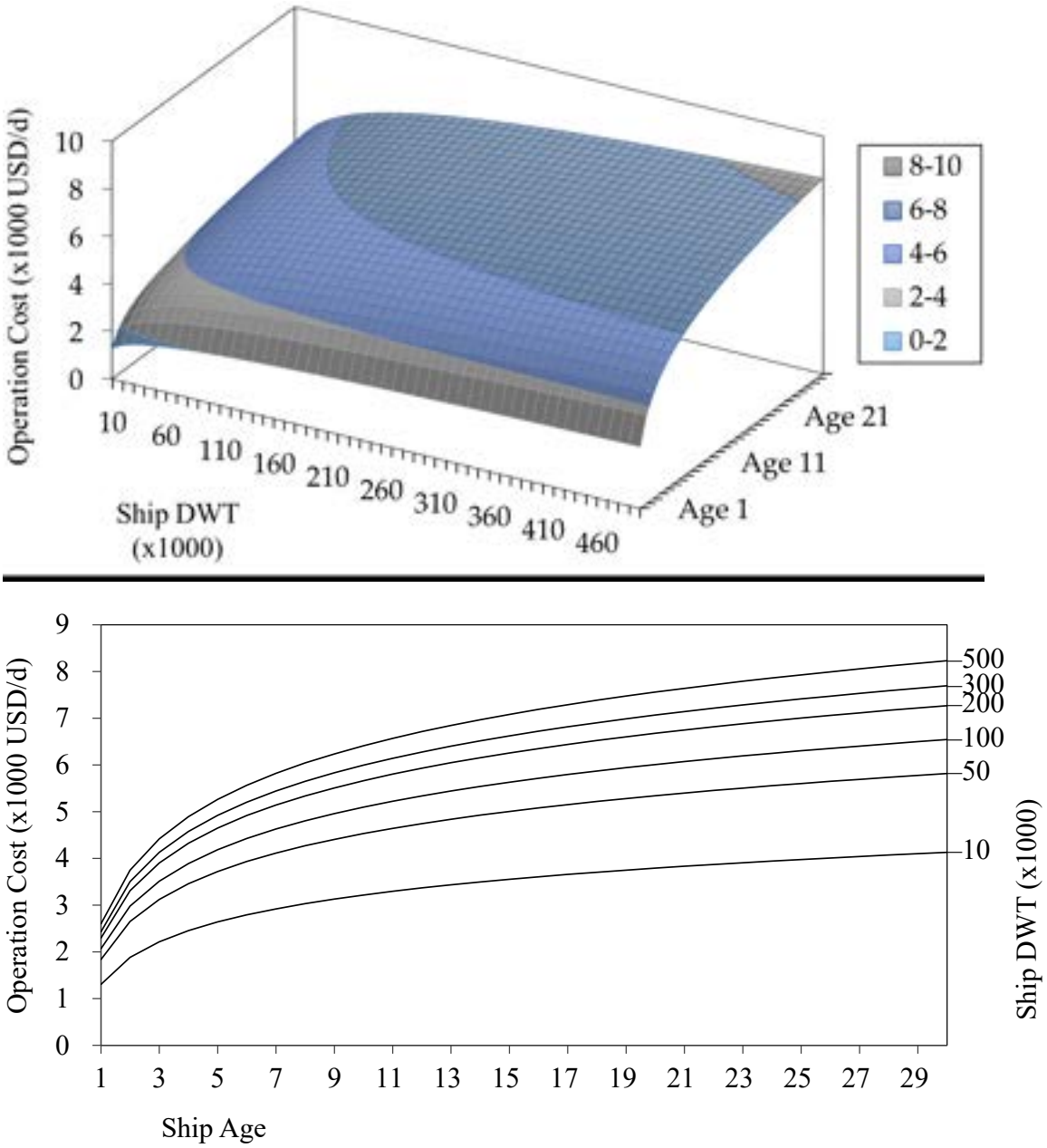

Figure 14. Response surfaces of bulk carrier operation cost: 3D and 2D visualizations [1,29,46,47].

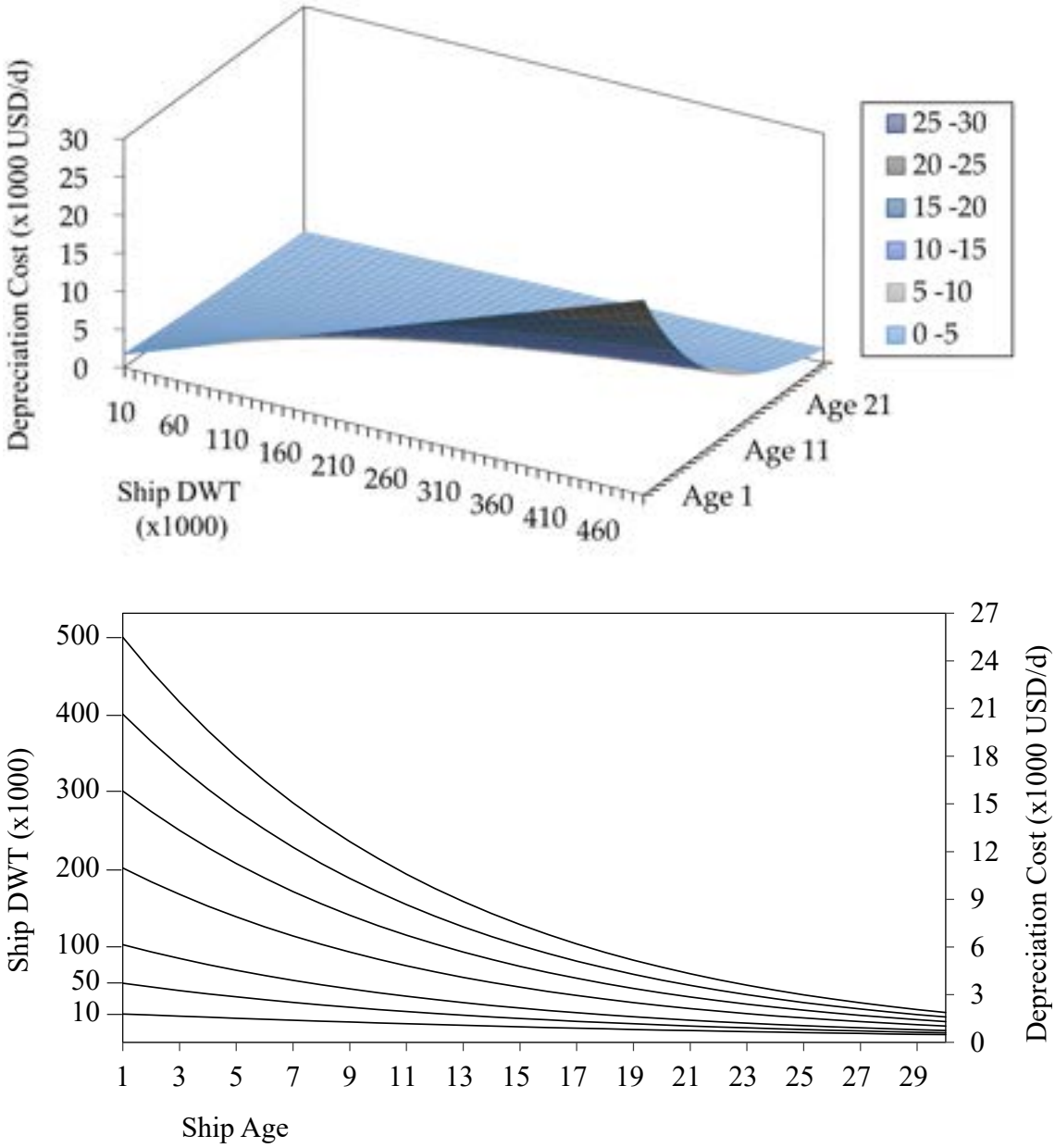

Figure 15. Response surfaces of bulk carrier depreciation cost: 3D and 2D visualizations [1,29,46,47].

Thus, the operation and depreciation costs (OC_{ij}, DC_{ij}) for a ship i operating on the route j (USD) are calculated using the following equation:

$$\boldsymbol{OC_{ij} = \left(oc_i \times st_{ij}\right) \quad \forall i \in I, \quad \forall j \in J,} \tag{17}$$

$$\boldsymbol{DC_{ij} = \left(dc_i \times yd\right) \quad \forall i \in I, \quad \forall j \in J,} \tag{18}$$

where oc_i is the ship i daily operation cost (USD/d), st_{ij} is the round-trip sailing time (d), dc_i is the ship i daily depreciation cost (USD/d), yd is the number of days in a year (d),

taken as 365, i is an individual ship (1647 Capesize and 2479 Panamax–MiniCape dry bulk carriers operating in 2018), and j is an individual route (1085 routes of Capesize's iron ore and coal and 3338 routes of Panamax–MiniCape's iron ore, coal, grain, and others in 2018). oc_i and dc_i for each ship i are shown in Figure 5a,b, respectively, based on each ship's DWT and age.

4.6.2.3. Calculation Process of Stockpile Cost

Additionally, this study establishes the stockpile cost to resemble the cargo stockpile cost at the destination port. Origin and destination ports of route j are defined as k and l, respectively. The stockpile cost is determined by referring to the daily destination port's cargo movement demand (CD_l, t/d), which is calculated as the sum of cargo movements ($\sum_k(CA_{kl})$) arriving at the destination port l divided by 365 days (yd). Then, the accumulated period (sd_{ij}, d) is calculated by rounding off the division of cargo movement (CM_{ij}) carried by a ship i to the destination port l by the daily destination port cargo movement demand (CD_l) as follows:

$$\boldsymbol{CD_l = \left(\sum_{k}(CA_{kl})\right) \times \left(\frac{1}{yd}\right) \quad \forall (j,l) \in J,} \tag{19}$$

$$\boldsymbol{sd_{ij} = \left\lfloor \frac{CM_{ij}}{CD_l} \right\rfloor \quad \forall i \in I, \quad \forall (j,l) \in J,} \tag{20}$$

where i is an individual ship (1647 Capesize and 2479 Panamax–MiniCape dry bulk carriers operating in 2018), j is an individual route (1085 routes of Capesize's iron ore and coal and 3338 routes of Panamax–MiniCape's iron ore, coal, grain, and others in 2018), and l is destination port of route j. Hence, the stockpile cost (SC_{ij}) for a ship i serving the route j (USD) is calculated as follows:

$$\boldsymbol{SC_{ij} = \left(\sum_{x=0}^{sd_{ij}} CM_{ij} - (CD_l \times x)\right) \times sc_l \quad \forall i \in I, \quad \forall (j,l) \in J,} \tag{21}$$

where sc_l is the stockpile cost unit (USD/t/d), which depends on the port and cargo type, i is an individual ship (1647 Capesize and 2479 Panamax–MiniCape dry bulk carriers operating in 2018), and j is an individual route (1085 routes of Capesize's iron ore and

coal and 3338 routes of Panamax–MiniCape's iron ore, coal, grain, and others in 2018), and k and l are an individual port (1085 origin and destination ports of iron ore and coal in 2018). In this study, sc_l was defined as a constant by referring to the average stockpile cost of the Japan Port Association [52]. Table 27 presents the stockpile cost units (USD/t/d) for various cargo types. Hence, sc_l for the routes of Capesize's iron ore and coal were taken as 0.012 and 0.042 USD/t/day, respectively. Similarly, sc_l on Panamax–MiniCape's routes were considered for the cargo types of iron ore, coal, grain, and others.

Table 27. Stockpile cost units for various cargo types [52].

Cargo Type [1]	Stockpile Cost Units (USD/t/d)
Iron Ore	0.012
Coal	0.042
Grain	0.186
Others	0.186

[1] *Others*: other dry bulks.

4.6.2.4. Calculation Process of Total COST

Finally, we define the total COST, which includes the fuel, operation, depreciation, and stockpile costs. The annual total COST (TC_{ij}) for a ship i operating on the route j (USD/y) is obtained as follows:

$$\boldsymbol{TC_{ij} = \left(\left(FC_{ij} + OC_{ij} + SC_{ij}\right) \times n_{ij}\right) + DC_{ij} \quad \forall i \in I, \quad \forall j \in J,} \tag{22}$$

where FC_{ij} is the fuel cost (USD), OC_{ij} is the operation cost (USD), SC_{ij} is the stockpile cost (USD), DC_{ij} is the depreciation cost (USD), n_{ij} is the possible annual trip number, i is an individual ship (1647 Capesize and 2479 Panamax–MiniCape dry bulk carriers operating in 2018), and j is an individual route (1085 routes of Capesize's iron ore and coal and 3338 routes of Panamax–MiniCape's iron ore, coal, grain, and others in 2018).

Furthermore, the monthly total COST (TC_{ijm}) for a ship i operating on the route j (USD/m) is obtained as follows:

$$\boldsymbol{TC_{ijm} = \left(FC_{ij} + OC_{ij} + SC_{ij} + DC_{ij}\right) \times n_{ijm} \quad \forall i \in I, \quad \forall j \in J, \quad \forall m \in M,} \qquad (23)$$

where FC_{ij} is the fuel cost (USD), OC_{ij} is the operation cost (USD), SC_{ij} is the stockpile cost (USD), DC_{ij} is the depreciation cost (USD), n_{ij} is the possible annual trip number, i is an individual ship (2479 Panamax–MiniCape dry bulk carriers operating in 2018), and j is an individual route (3338 routes of Panamax–MiniCape's iron ore, coal, grain, and others in 2018). Finally, a sample of the COST composition (USD/t) is shown in Figure 16.

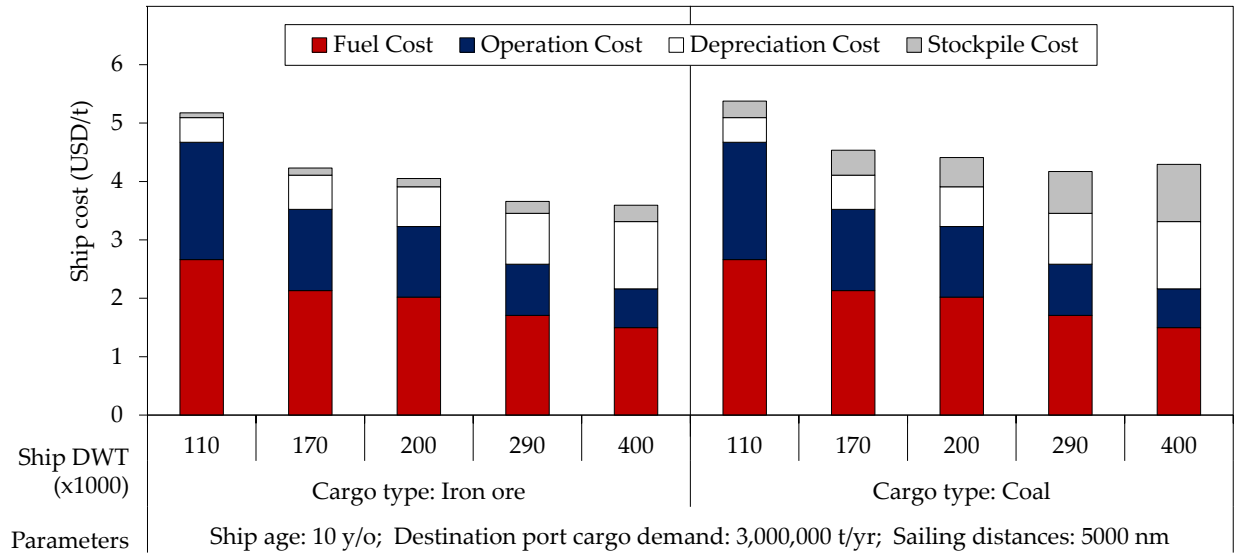

Figure 16. A sample of the COST composition.

A declining trend in the COST composition (USD/t) can be observed towards the larger ship DWT. The larger ship's fuel and operation costs to transport one-ton cargo are getting lower. On the contrary, it can be observed that the depreciation and stockpile cost significantly increase following the size of the ship. These values draw a tendency for larger ships to be economically-effective for both iron ore and coal cargo types.

4.4.1. Evaluation of COST Calculation

In this section, we will evaluate the COST calculation scheme. Table 28 presents an evaluation of the COST composition with the following COST item parameters [1]:

- Fuel: 2005 HSFO 380cst and MDO Rotterdam bunker prices (USD) [48];
- Depreciation: 2005 daily depreciation cost (USD/d) [48];
- Ship: Operation conditions of a ten years old ship in 2005 [42].

The error margin is between 0.7% and 4.1% for the COST item parameters, which justifies the practicability of our COST calculation scheme.

Table 28. Evaluation of COST calculation.

COST item	COST Composition (%)		Error
	Stopford [1]	This Study	(%)
Fuel	35.2	34.4	0.7
Operation	16.2	20.3	4.1
Depreciation	48.6	45.3	3.3

4.7. Development of Ship Allocation Algorithm

4.7.1. Algorithm 1: Ship Replacement while Preserving the Existing Ship Allocation

4.7.1.1. Definition of Algorithm 1

This algorithm proposes an optimization by offering a direct clone of the existing ship, a new ship with the exact specifications and operation conditions that serve the same annual allocations. The existing ship is replaced if the new ship offers practically lower COST or GHG emissions. Locally, a new ship justifies the replacement of an existing ship with the capability to reduce COST or GHG emissions. Globally, a collection of existing ships is replaced by new ship formations.

4.7.1.2. Methodology of Algorithm 1

In this scheme, for each instance of an existing ship i, we offered a new ship i' with the same specifications, operation conditions, and annual allocations as the ship i but with the admiralty coefficient (ADM) of the year 2021. Additionally, we proposed two optimization schemes: COST- and GHG-optimized. In this section, we have provided an example of a COST-optimized case.

Along with the calculation of the annual COST (TC_{ij}) per ton cargo (CM_{ij}) of a ship i, we also calculated the annual COST ($TC_{i'j}$) per ton cargo ($CM_{i'j}$) of an offered ship i'. Thus, the KPI ($w_{ij}, w_{i'j}$) for each ship i and i' serving the route j is defined as follows:

$$\boldsymbol{w_{ij}} = \left(\frac{\boldsymbol{TC_{ij}}}{\boldsymbol{CM_{ij}}}\right), \quad \boldsymbol{w_{i'j}} = \left(\frac{\boldsymbol{TC_{i'j}}}{\boldsymbol{CM_{i'j}}}\right) \quad \forall(\boldsymbol{i}, \boldsymbol{i'}) \in \boldsymbol{I}, \quad \forall \boldsymbol{j} \in \boldsymbol{J}, \tag{24}$$

Finally, we acquired the global merit (W_{ij}), for an offered new ship i' replacing an existing ship i by fulfilling the following conditions:

$$\boldsymbol{W_{ij}} = \begin{cases} \boldsymbol{w_{ij}\ if\ (w_{ij} - w_{i'j}) < 0} \\ \boldsymbol{w_{i'j}\ if\ (w_{ij} - w_{i'j}) > 0} \end{cases} \quad \forall(\boldsymbol{i}, \boldsymbol{i'}) \in \boldsymbol{I}, \quad \forall \boldsymbol{j} \in \boldsymbol{J}, \tag{25}$$

where W_{ij} represents a COST-effective ship, i and i' are an individual ship (1647 Capesize and 2479 Panamax–MiniCape dry bulk carriers operating in 2018), and j is an individual route (1085 routes of Capesize's iron ore and coal and 3338 routes of Panamax–MiniCape's iron ore, coal, grain, and others in 2018). A ship i' is determined to replace the ship i only if it offers a lower KPI. With the same ship allocation, these steps resulted in a new ship replacing the existing ship after conducting them for all the ships. Additionally, the seized COST reduction can be examined for an existing ship i replaced by a new ship i'.

4.7.2. Algorithm 2: An Optimization for Reconstructing Ship Allocation in Time-Charter Contract

4.7.2.1. Definition of Algorithm 2

Based on the greedy algorithm approach, this algorithm reconstructs the ship allocation to transport the worldwide cargo movement demand using the available ships in the existing ship allocation or with the new ships instance. Using the total COST and GHG emissions for each ship and route, the allocation algorithm transports the same cargo amount as the existing ship allocation in a time-charter contract manner. This algorithm allocates ships conforming to the limitations of port dimensions for certain ships.

4.7.2.2. Methodology of Algorithm 2

In this algorithm, a ship with the highest global merit is sequentially designated to transport cargo on a certain route on a one-year time-charter contract by replicating the ship bidding process to obtain the most advantageous ship. The allocation algorithm was adopted separately for both cases to achieve a global reduction in the total COST and GHG emissions. Next, we have provided an example of the ship allocation in the COST-optimized case since the allocation scheme for both the COST- and GHG-optimized cases are the same.

The annual COST (TC_{ij}) per ton cargo (CM_{ij}) was set as an individual ship KPI (y_{ij}). Additionally, the average KPI for the route j ($\bar{y}_j$) is known; therefore, the merit for each ship i operating in the route j (m_{ij}) is defined as follows:

$$\boldsymbol{y_{ij}} = \left(\frac{\boldsymbol{TC_{ij}}}{\boldsymbol{CM_{ij}}}\right) \quad \forall \boldsymbol{i} \in \boldsymbol{I}, \quad \forall \boldsymbol{j} \in \boldsymbol{J}, \tag{26}$$

$$\boldsymbol{\bar{y}_j} = \frac{\boldsymbol{1}}{\boldsymbol{I}} \times \sum_{\boldsymbol{i}} \left(\boldsymbol{y_{ij}}\right) \quad \forall \boldsymbol{i} \in \boldsymbol{I}, \quad \forall \boldsymbol{j} \in \boldsymbol{J}, \tag{27}$$

$$\boldsymbol{m_{ij}} = \left(\boldsymbol{\bar{y}_j} - \boldsymbol{y_{ij}}\right) \quad \forall \boldsymbol{i} \in \boldsymbol{I}, \quad \forall \boldsymbol{j} \in \boldsymbol{J}, \tag{28}$$

Finally, the global merit (M) is obtained as follows:

$$\boldsymbol{M} = \boldsymbol{max}\left(\boldsymbol{m_{ij}}\right) \quad \forall \boldsymbol{i} \in \boldsymbol{I}, \quad \forall \boldsymbol{j} \in \boldsymbol{J}, \tag{29}$$

where i is an individual ship (1647 Capesize and 2479 Panamax–MiniCape dry bulk carriers operating in 2018), and j is an individual route (1085 routes of Capesize's iron ore and coal and 3338 routes of Panamax–MiniCape's iron ore, coal, grain, and others in 2018).

A set of ships and routes with global merit M is the most COST-effective allocation. After that, the annual cargo movement demand of the route j (CA_j) is subtracted by the annual cargo carried by that ship (CM_{ij}). The allocation algorithm is then repeated until all the cargo movement demands are assigned to a particular ship, while the allocated ship (i) is removed from the available ship list (I). All these processes result in the operation-level ship allocation. The annual CARGO, total COST, and GHG

emissions were elaborated for each ship i allotted on a specific route j. Therefore, we could explain the reduction in the total COST and GHG emissions and visualize the results geographically.

4.7.3. Algorithm 3: An Optimization for Reconstructing Ship Allocation in Voyage-Charter Contract

4.7.3.1. Definition of Algorithm 3

Identical to Algorithm 2 that we have previously discussed, this algorithm is built based on the greedy algorithm approach. This algorithm was created to simulate the ship's bidding process in a monthly voyage-charter contract. This algorithm inputs the created monthly OD tables and the calculated COST and GHG emissions. Fulfilling the demand to transport all the worldwide cargo movement demand described in monthly OD tables, this algorithm sequentially allocates all available ships in the existing ship allocation and with new ships instance for some scenarios.

4.7.3.2. Methodology of Algorithm 3

In this algorithm, a ship can be allocated when its specifications, length, and breadth are under the limitations of port dimensions. Among these static limitations, this algorithm selects a ship with the highest global merit to transport cargo of each operation on a certain route. A ship is allocated individually by simulating the ship allocation in a monthly voyage-charter contract. This algorithm is utilized separately for both COST and GHG emissions cases to acquire the monthly optimized ship allocation.

In this section, we have discussed an application example in the COST-optimized case since the allocation mechanism for both the COST- and GHG-optimized cases are the same. The global merit selection (M) in this algorithm is similar to what has already been discussed in the prior section, by replacing the annual COST (TC_{ij}) with the monthly COST (TC_{ijm}) in the KPI calculation, as follows:

$$\boldsymbol{y_{ijm} = \left(\frac{TC_{ijm}}{cm_{ijm}}\right) \quad \forall i \in I, \quad \forall j \in J, \quad \forall m \in M,} \tag{30}$$

where y_{ijm} is the monthly KPI of an individual ship, TC_{ijm} is the monthly total COST (USD/m), cm_{ijm} is cargo amount (t) transported by ship i, i is an individual ship (2479

Panamax–MiniCape dry bulk carriers operating in 2018), and j is an individual route (3338 routes of Panamax–MiniCape's iron ore, coal, grain, and others in 2018). Next, a ship and route with global merit M is considered having the most COST-effective allocation. Afterward, the cargo movement in the operation carried by the selected ship (cm_{ijm}) is subtracted from the route's monthly cargo movement demand (cm_{jm}). These processes result in an allocation of a ship at the operational level.

Furthermore, the above scheme is then repeated until all the cargo movement demands are allocated to a particular ship. For each route j, the annual CARGO, total COST, and GHG emissions were summarized. Thus, the reduction in the total COST and GHG emissions from the optimized ship allocation could be explained and visualized.

4.7.4. Methodology to visualize Simulation Results

We visualize the ship allocation results in great circle format [53-55]. In this instance, visualization nodes are not defining one port but several ports based on their defined region. The region of available ports is shown in Figure 17 and Figure 18. Moreover, Table 29 presents our defined 24 geographical regions for both Capesize and Panamax–MiniCape dry bulk carriers, despite the number of available ports.

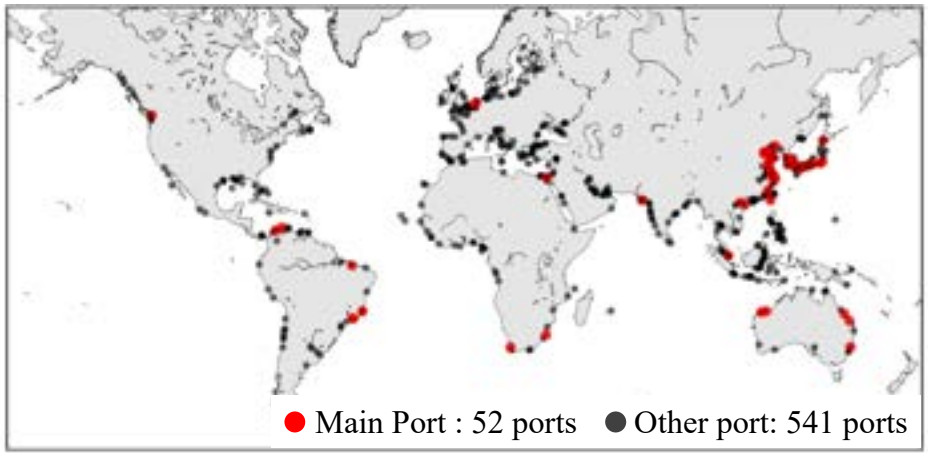

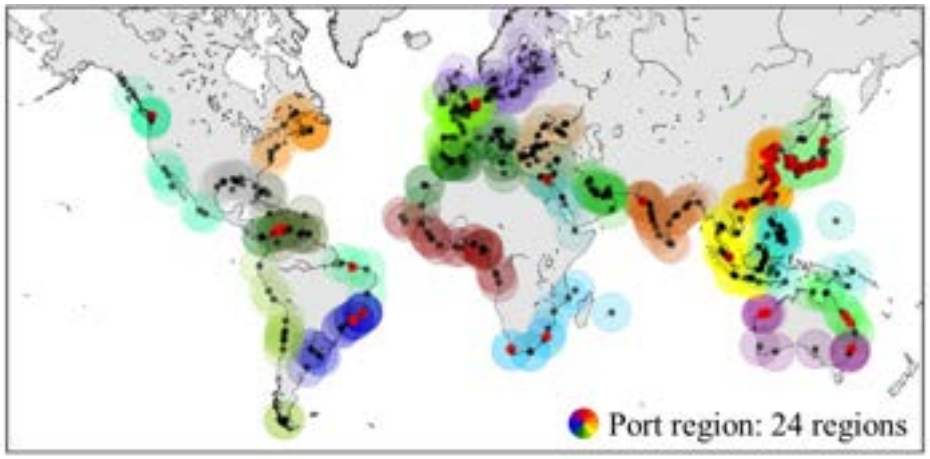

Figure 17. Specified region of worldwide ports of Capesize dry bulk carrier.

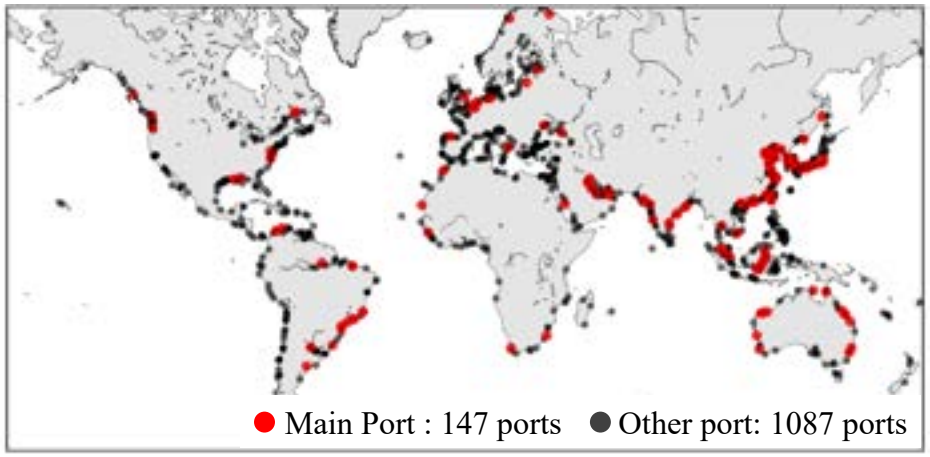

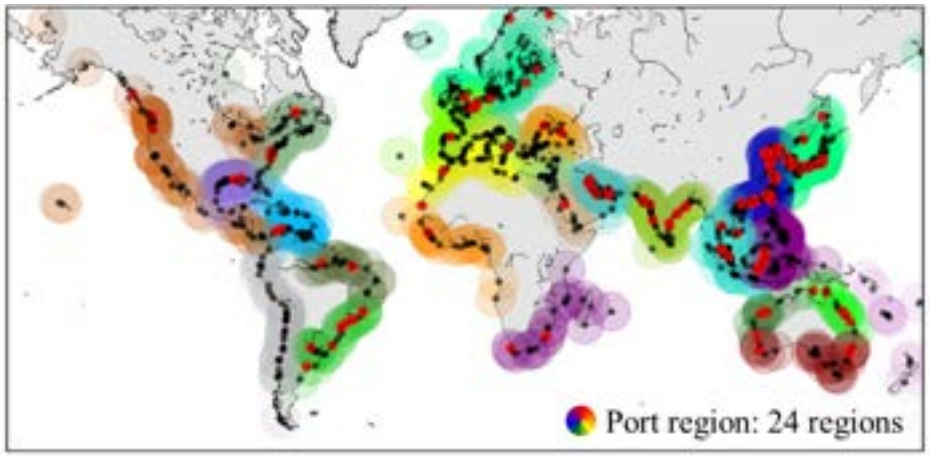

Figure 18. Specified region of worldwide ports of Panamax–MiniCape dry bulk carriers.

Table 29. Defined region for simulation results visualization.

Region [1]	Latitude	Longitude
North-Europe	54.28	17.40
West-Europe	47.58	-1.56
West-North America	46.36	-121.37
Black Sea	44.56	31.03
East-North America	39.98	-74.66
North-East Asia	34.30	133.72
East-Mediterranean	32.63	35.76
West-Mediterranean	32.02	-7.83
Red Sea	30.58	32.28
Gulf of Mexico	29.11	-93.47
South-East Asia	25.00	110.00
Persian Gulf	22.73	56.33
Indian subcontinent	12.80	76.19
Caribbean Sea	10.27	-65.43
West-Africa	4.27	0.99
East-South East Asia	-1.48	117.03
East-South America	-2.58	-44.37
West-South East Asia	-6.21	107.61
West-Australia	-20.67	116.70
East-Australia	-22.54	150.31
South-South America	-22.97	-43.93
South-Africa	-33.03	17.97
South-Australia	-33.76	142.92
West-South America	-35.00	-60.00

[1] *Region*: defined geographical region.

To give a better overview, we graphically summarize the simulation results, such as average DWT, average sailing speed (kn), and average ship age (y/o). The connections between visualization nodes present two attributes; thickness and color. In this study, the thickness represents cargo movement (MT), and the color variant represents average values.

A sample of great circle visualization is shown in Figure 19. The state of the allocated ships, average DWT, average sailing speed, and average ship age between nodes could co be clarified.

(a) Average DWT

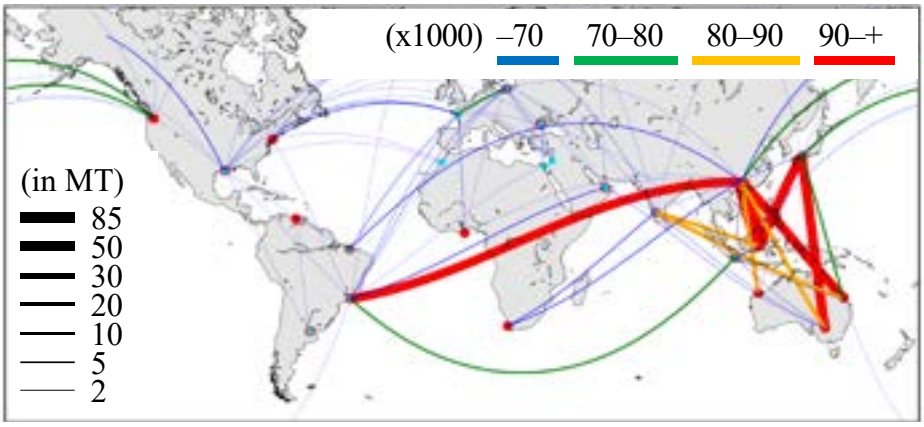

(b) Average Sailing Speed

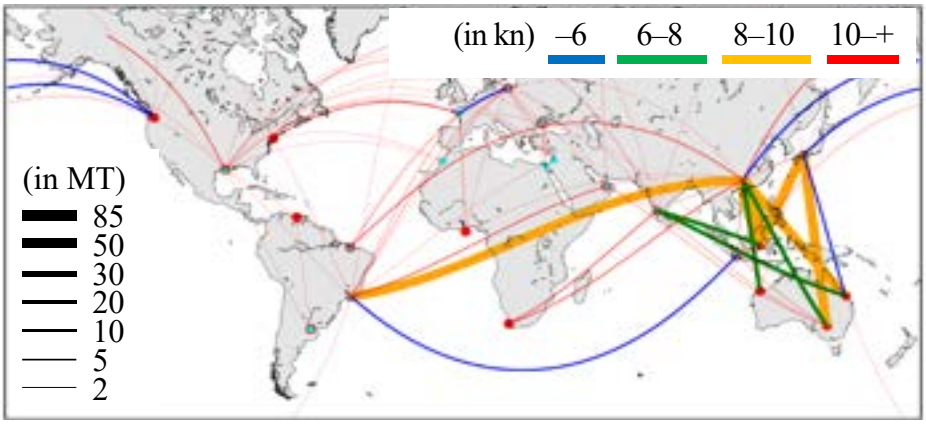

(c) Average Ship Age

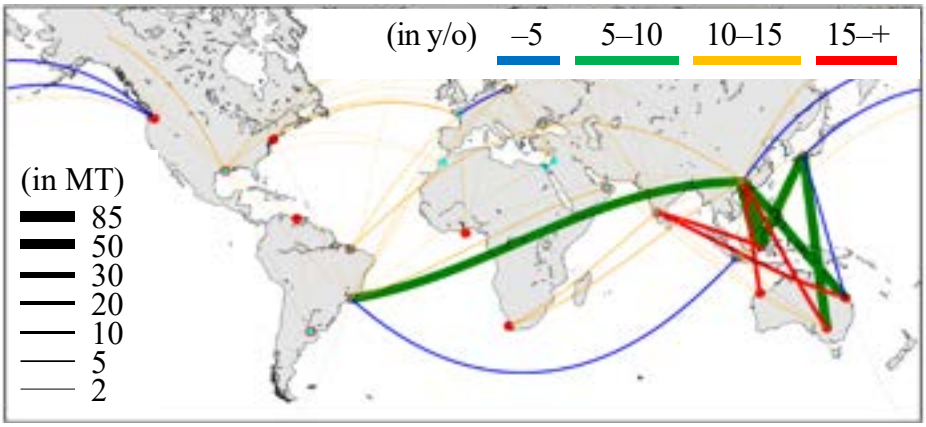

Figure 19. A sample of great circle visualization: (**a**) average DWT, (**b**) average sailing speed, and (**c**) average ship age.

The amount of cargo movement (MT) as line thickness in Figure 19. Specifically, Figure 19a presents the great circle visualization of average DWT in the simulation results. This figure has the route with an average DWT of less than 70,000, 70,000–80,000, 80,000–90,000, and more than 90,000 colored in blue, green, yellow, and red. We can confirm that the ships with the largest average DWT (>90,000) were allocated on the routes of South East Asia, East Australia, and South Australia to Japan and China.

Moreover, Figure 19b shows the great circle visualization of average sailing speed in the simulation results. This figure has the route with an average sailing speed (kn) of less than 6, 6–8, 8–10, and more than 10, colored in blue, green, yellow, and red. The visualization suggests that routes with major cargo movement; South East Asia, East Australia, and South Australia to Japan and China allocated the ships with an average sailing speed 8–10 knots.

In a similar scheme, we visualized the average ship age in the great circle format, as shown in Figure 19c. This visualization owns the route with average ship age (y/o) of less than 5, 5–10, 10–15, and more than 15, colored in blue, green, yellow, and red. This shows that the routes with the highest cargo movement (85 MT) consist of 5–10 years old ships. To conclude the presented visualization sample, we can identify that larger ships served major routes. In addition, these are typically younger ships operated at moderate speeds.

5. CASE STUDIES AND DISCUSSIONS

5.1. Case Studies intended for Capesize Dry Bulk Carrier

5.1.1. Overview of Case Studies intended for Capesize Dry Bulk Carrier

We conducted several simulations using algorithms 1 and 2: ship replacement while preserving existing ship allocation (case study 1), optimization of ship allocation using existing ships (case study 2), and optimization of ship allocation using new ships instance (case study 3). Table 30 shows an overview of case studies of Capesize dry bulk carriers. First, we analyzed the actual ship allocation to understand the current ship allocation characteristics. Case study 1 analyzed new ships to replace existing ships without changing their allocation. Case study 2 reconstructed the ship allocation using only the existing ships. Case study 3 reconstructed the ship allocation using the existing ships and new ships instance (Table 31). Finally, we summarized the results of the average DWT and sailing speed graphically in a great circle format [53-55]. The following were the objectives of the simulations:

- Target ship: Capesize dry bulk carrier (DWT 100,000 or more, 1647 ships);
- Cargo types: Iron ore and coal;
- Route: Worldwide (sailing routes served by target ship);
- Operation period: 2018;
- Assumed fuel attributes (specific fuel consumption, g/kWh; emissions factor, t-CO2/t-fuel; fuel prices, USD): HFO (175–185; 3.114; 300) and MDO (daily average fuel consumption [28,29]; 3.206; 600).

Table 30. Overview of case studies of Capesize dry bulk carrier.

Case Study	Method	Offered Ships [1]	Ship Allocation [2]	Cargo Movement [3]	Operation Conditions [4]	Fuel Attributes [5]
1	Algorithm 1	*existing*	*existing*	*2018*; *Ir*, *Co*	*existing*	*2018*
2	Algorithm 2	*existing*	*optimized*	*2018*; *Ir*, *Co*	*predicted*	*2018*
3	Algorithm 2	*existing*, *new*	*optimized*	*2018*; *Ir*, *Co*	*predicted*	*2018*

[1] *existing*: existing ships in the actual ship allocation [39,42]; *new*: new ships instance.
[2] *existing*: actual ship allocation; *optimized*: reconstructed ship allocation.
[3] *2018*: worldwide cargo movement in 2018 [39]; *Ir*: iron ore; *Co*: coal.
[4] *existing*: operation conditions in the actual ship allocation; *predicted*: predicted operation conditions by using deep learning model.
[5] *2018*: assumed fuel attributes in 2018 [48].

5.1.2. Definition of New Ships Instances in Case Studies intended for Capesize Dry Bulk Carrier

For case studies 1 and 3, we offered new ships with the same principal particulars but with the ADM of Capesize dry bulk carrier in 2021 (ADM_{C21}). Figure 20 presents the ADM of Capesize dry bulk carriers before and after common structural rules for bulk carriers (CSR-BC).

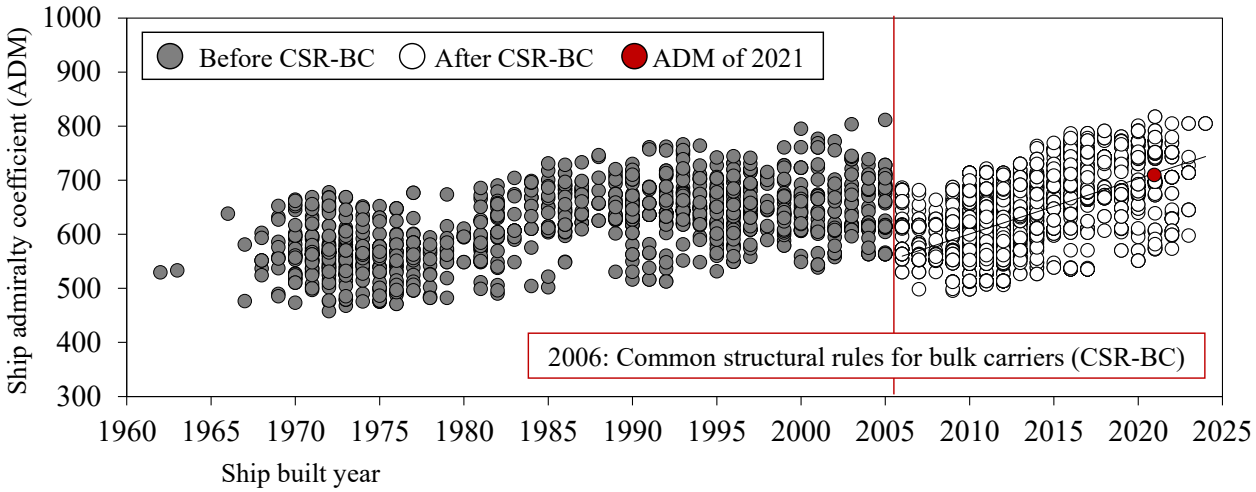

Figure 20. Ship admiralty coefficient (ADM) of Capesize dry bulk carrier before and after common structural rules for bulk carriers (CSR-BC) [42,56,57].

In case study 1, a new ship (i') was defined for each existing ship (i) of the 2018 ship allocation. The existing and new ships of Capesize dry bulk carriers are defined as I and I', respectively. Thus, the main engine power ($P_{i'}$) of the new ship i' was reduced by preserving a constant ship i design speed as follows [56]:

$$\boldsymbol{P_{i'} = P_i \times \left(\frac{ADM_i}{ADM_{C21}}\right) \quad \forall i \in I, \quad \forall i' \in I',} \tag{31}$$

where P_i is the main engine power of the existing ship i (kW), ADM_i is the ADM of the existing ship i, ADM_{C21} is the defined ADM of Capesize dry bulk carrier in 2021: 697.29, and i is an individual ship (1647 Capesize dry bulk carriers operating in 2018).

Moreover, in case study 3, the new ship specifications were sampled from the existing ships of the 2018 ship allocation. The set of sampled ships is defined as S. We defined these ships as more efficient since they had the ADM of Capesize dry bulk carrier in 2021: 697.29 (see Figure 20). Hence, the main engine power (P_s') was reduced by retaining a constant ship s design speed as follows [56]:

$$\boldsymbol{P'_s = P_s \times \left(\frac{ADM_s}{ADM_{C21}}\right) \quad \forall s \in S,} \tag{32}$$

where P_s is the main engine power of ship s (kW), ADM_s is the ADM of ship s, ADM_{C21} is the defined ADM of Capesize dry bulk carrier in 2021: 697.29, and s is an individual ship (six ships sampled from 1647 Capesize dry bulk carriers operating in 2018). Table 31 lists the specifications of the new ships. These ships had the same principal particulars as the sampled ships but lower main engine power.

Table 31. Assumed specifications of the new ships.

New Ship	*DWT* [1]	*d* (m) [1]	*B* (m) [1]	*L* (m) [1]	*v* (kn) [1]	*Age* [2]	Existing *ME* Power (kW) [3]	New Ship *ME* Power (kW) [3]	*ME* Power Reduction (%) [3]
A	100,076	12.9	43	250	14.5	1	11,400	10,414	9.5
B	183,194	18.2	45	292	14.5	1	15,815	15,317	3.2
C	208,377	18.3	50	300	14.5	1	17,300	16,795	3.0
D	261,046	18.8	57	327	14.5	1	22,324	19,446	14.8
E	297,204	21.4	55	327	14.5	1	23,280	21,042	10.6
F	403,508	23	65	361	14.5	1	29,260	25,583	14.4

[1] *DWT*: new ships' deadweight tonnage; *d*: new ships' draught; *B*: new ships' breadth; *L*: new ships' length; *v*: new ships' design speed;
[2] *Age*: assumed ship age;
[3] *ME*: main engine.

5.1.3. Actual Ship Allocation of Capesize Dry Bulk Carrier

Before conducting simulations, it is necessary to analyze the typical features of the actual ship allocation. Figure 21 proportionally illustrates the ships' average DWT and sailing speed, such that the line thickness indicates the annual cargo movement on each route, and the sorted colors represent the DWT and sailing speed variance.

In the West Australia–China routes, which have the highest cargo movement, the average DWT is 180,000–200,000, and the average sailing speed is 8.5–9.5 knots, which indicates the use of smaller ships at typically slower speeds. Additionally, the long-distance routes, such as Brazil–China, show the ships operating with an average DWT of 200,000–260,000 and an average sailing speed exceeding 9.5 knots, which indicates that the routes are served by larger ships at higher speeds.

(a) Average DWT

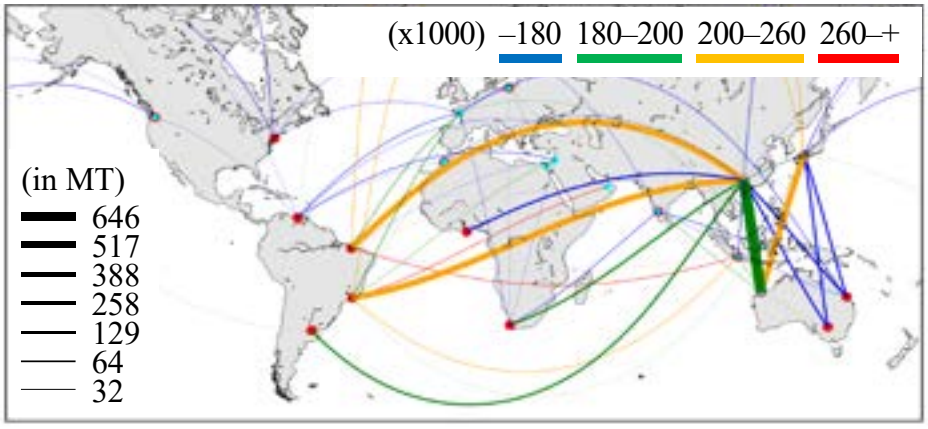

(b) Average sailing speed

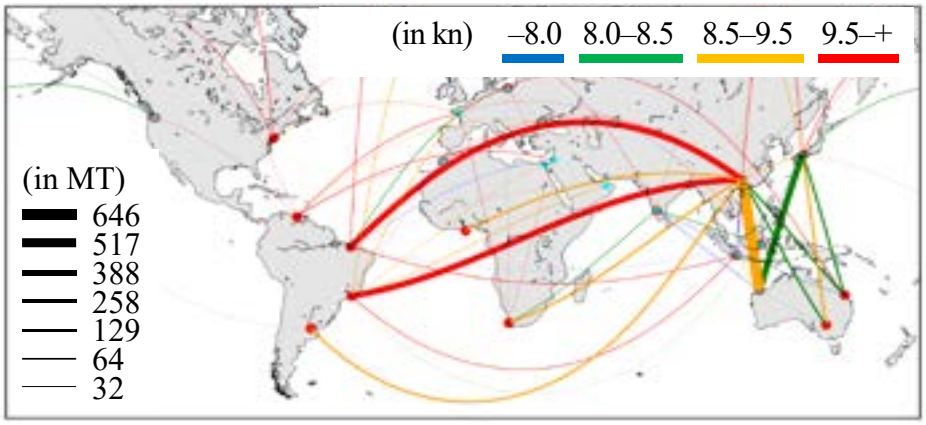

Figure 21. Actual ship allocation of Capesize dry bulk carrier: (**a**) Average DWT and (**b**) sailing speed.

5.1.4. Case study 1: Ship Replacement while Preserving the Existing Ship Allocation

5.1.4.1. Definition of Case Study 1

This case study attempted to directly replace each existing ship with a new ship without changing the actual ship allocation and then to observe the changes in the total COST and GHG emissions, including COST-optimized ship replacement while preserving the existing ship allocation (case study 1a) and GHG-optimized ship replacement while preserving the existing ship allocation (case study 1b). The following were the parameters of case study 1:

- Method: Allocation algorithm 1;
- Offered ships: A new ship with the ADM of Capesize dry bulk carrier in 2021 for each existing ship in the actual ship allocation.

5.1.4.2. Results of Case Study 1

The allocated new ship rates for cases 1a and 1b are shown in Figure 22. Both the cases show a typically high allocation rate for new ships. Figure 22a shows the major routes in which the allotted new ships take for over 40%–60% of the operation numbers. Meanwhile, Figure 22b shows that the new ships accounted for more than 60% of the worldwide operation numbers.

(a) Case study 1a (COST-optimized)

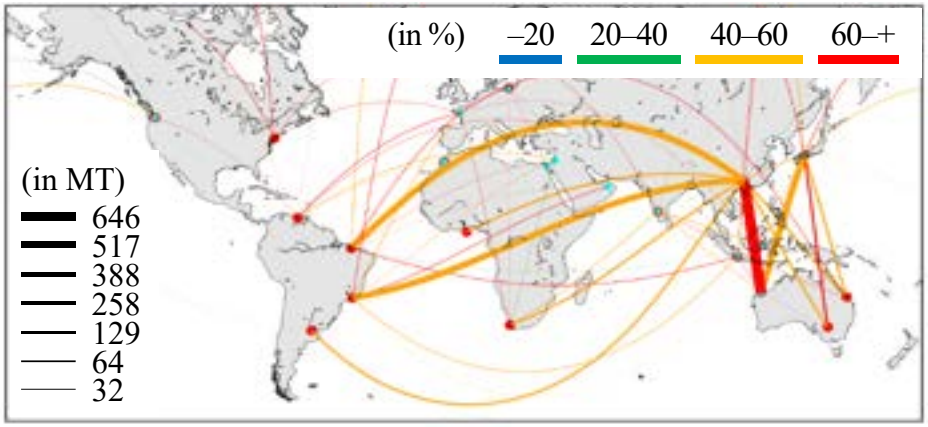

(b) Case study 1b (GHG-optimized)

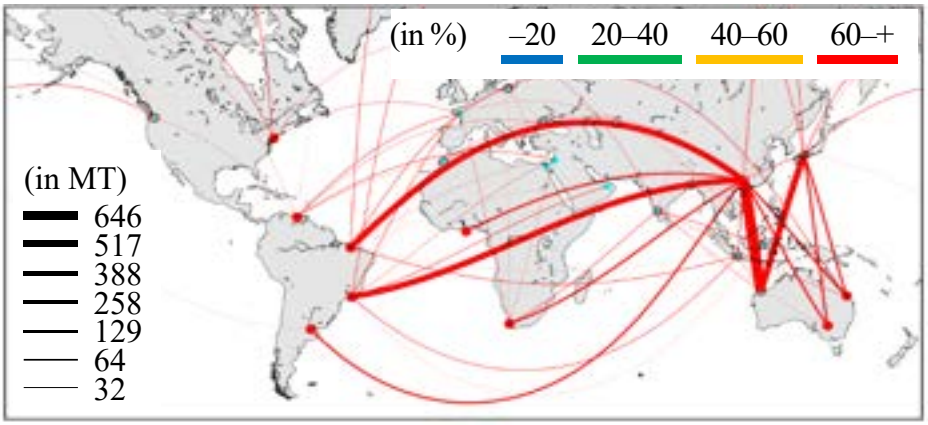

Figure 22. Ship replacement while preserving existing ship allocation of Capesize dry bulk carrier: Allocated new ship rate of (**a**) case study 1a (COST-optimized) and (**b**) case study 1b (GHG-optimized).

As shown in Table 32, minor reductions in the total COST and GHG emissions can be seen in case study 1. In case study 1a, new ships replaced 58.8% of the total number of existing ship operations, which reduced the total COST by 3.5%, and the GHG emissions were reduced by 5.6% compared to the actual ship allocation. Moreover, case study 1b allotted 87.5% of its operations to new ships, which allowed a 9.7% reduction in the GHG emissions, but the total COST increased by 0.4%.

5.1.5. Case study 2: Optimization of Ship Allocation in Time-Charter Contract using Existing Ships

5.1.5.1. Definition of Case Study 2

In this case study, we discussed optimizing the ship allocation using only the existing Capesize dry bulk carrier. The two case studies covered are: COST-optimized ship allocation using existing ships (case study 2a) and GHG-optimized ship allocation using existing ships (case study 2b). The following were the parameters for case study 2:

- Method: Allocation algorithm 2;
- Offered ships: The existing ships operated in the current ship allocation.

5.1.5.2. Results of Case Study 2

The results obtained for case study 2 are illustrated in Figure 23 and Figure 24. From Figure 23a, we can ascertain that the Brazil–China routes allotted larger ships with a DWT of more than 260,000 and an average sailing speed of more than 9.5 knots. The average DWT of ships designated to the Brazil–China routes increased, compared to the actual ship allocation, due to the use of larger ships.

In Figure 23b, the major routes are allocated to ships with an average sailing speed of 8.5–9.5 knots. Subsequently, Figure 24a depicts a similar average DWT as the actual ship allocation, and the average sailing speed shown in Figure 24b is generally slower. This analysis indicated the importance of speed reduction in optimizing the ships' fuel consumption and GHG emissions.

(a) Case study 2a (COST-optimized) average DWT

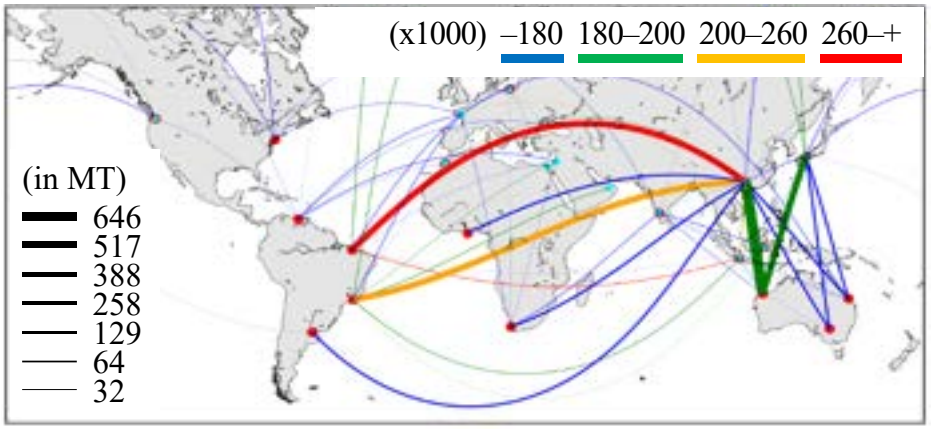

(b) Case study 2a (COST-optimized) average sailing speed

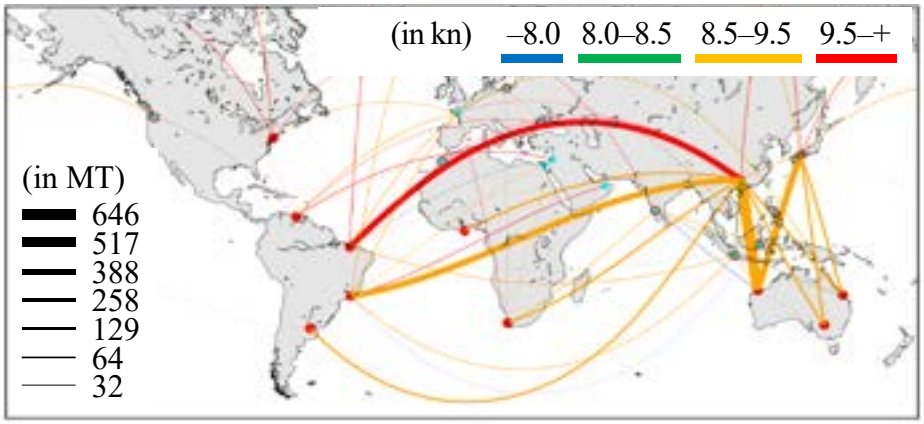

Figure 23. Ship allocation optimization in time-charter contract using existing ships of Capesize dry bulk carrier: Case study 2a (COST-optimized) (**a**) average DWT and (**b**) sailing speed.

As summarized in Table 32, case study 2a reduced the total COST by 7.3% compared to the actual ship allocation, whereas the total GHG emissions were reduced by 14.8% in case study 2b. Additionally, the ship operation numbers of case studies 2a and 2b were reduced by 1.1% and 2.2%, respectively. The operation-level alterations made such changes in the ship allocation, despite simply employing the existing ships. Nevertheless, a significant reduction in the total COST and GHG emissions could not be obtained using only the existing ships.

(a) Case study 2b (GHG-optimized) average DWT

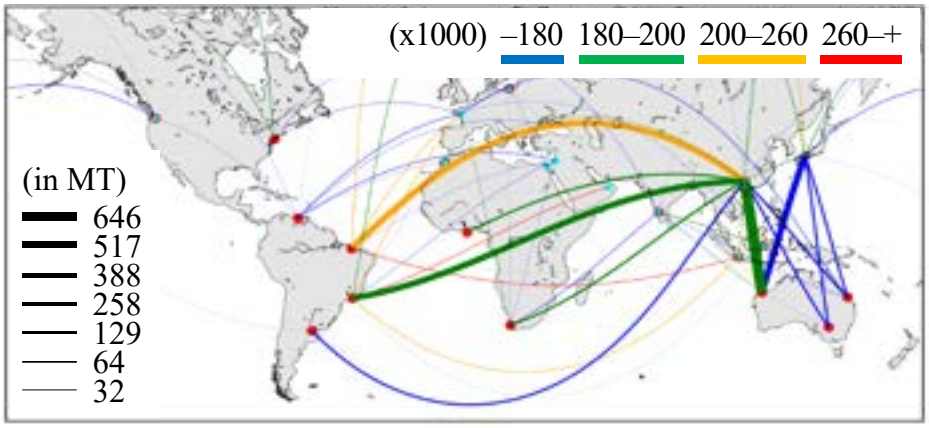

(b) Case study 2b (GHG-optimized) average sailing speed

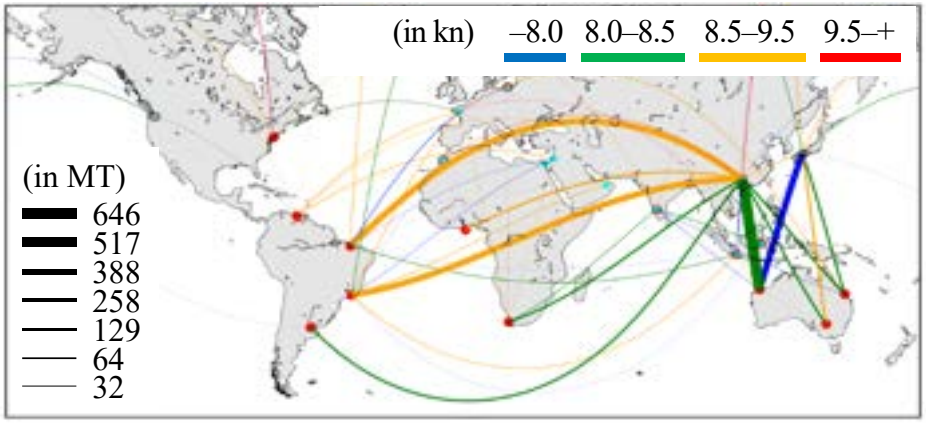

Figure 24. Ship allocation optimization in time-charter contract using existing ships of Capesize dry bulk carrier: Case study 2b (GHG-optimized) (**a**) average DWT and (**b**) sailing speed.

5.1.6. Case study 3: Optimization of Ship Allocation in Time-Charter Contract with New Ships Instance

5.1.6.1. Definition of Case Study 3

In addition to the analysis of case study 2 (Section 5.1.5), this case study presents a set of new ships. We examined the competitive new ships that could replace the existing ships by conducting simulations to optimize the ship allocation with these new ships. The following were the parameters of case study 3:

- Method: Allocation algorithm 2;
- Offered ships: The existing ships of case study 2 and new ships.

As new ships could be allotted indefinitely, we discussed the following case studies: COST-optimized ship allocation with new ships instance (case study 3a) and GHG-optimized ship allocation with new ships instance (case study 3b).

5.1.6.2. Results of Case Study 3

This case study optimized the ship allocation by allowing the existing ships to be replaced by new ships. This allowed us to ascertain the average DWT and sailing speed patterns simultaneously on a global scale. Figure 25 and Figure 26 show the ship allocation results of case study 3. From Figure 25a and Figure 26a, we can observe that both the case studies allocated ships with a similar average DWT. The major routes in Figure 25b have a uniform average sailing speed of more than 8.5 knots, similar to case study 2. The allocated ships' lower average sailing speed compared to the actual ship allocation can be seen in Figure 26b. The short- and long-distance routes allocated ships with an average sailing speed of less than 8.5 knots and 8.5–9.5 knots, respectively. This indicated that the importance of sailing speed varied depending on the sailing distance.

(a) Case study 3a (COST-optimized) average DWT

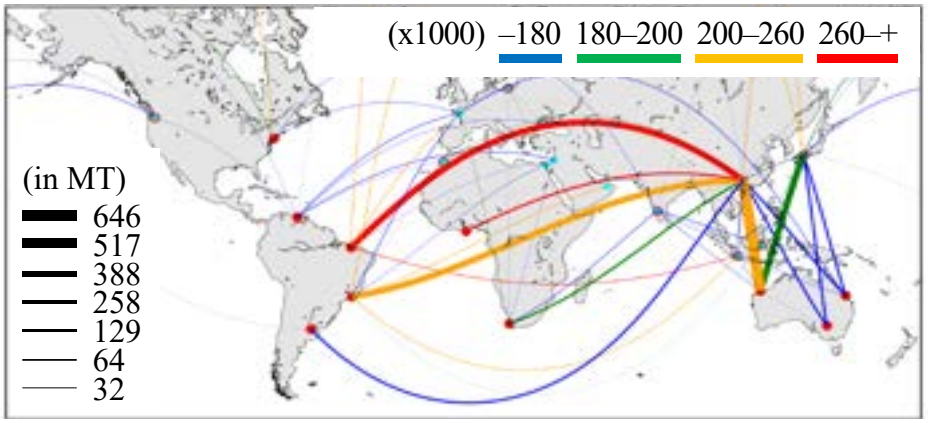

(b) Case study 3a (COST-optimized) average sailing speed

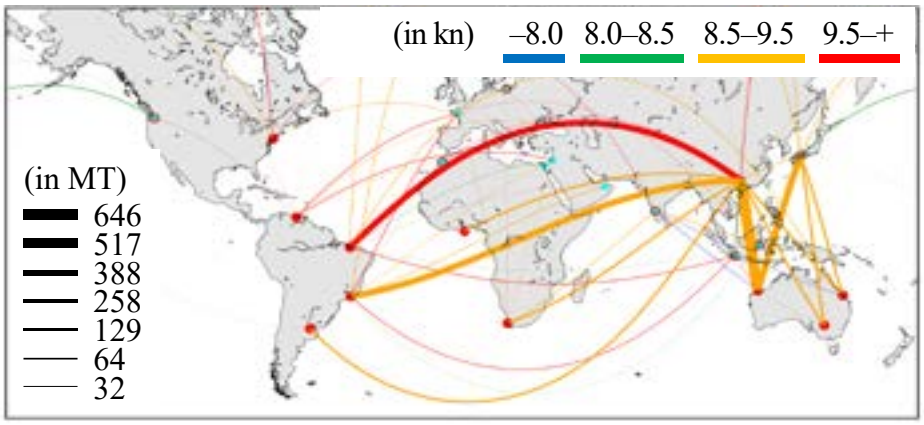

Figure 25. Ship allocation optimization in time-charter contract of Capesize dry bulk carrier with new ships instance: Case study 3a (COST-optimized) (**a**) average DWT and (**b**) sailing speed.

(a) Case study 3b (GHG-optimized) average DWT

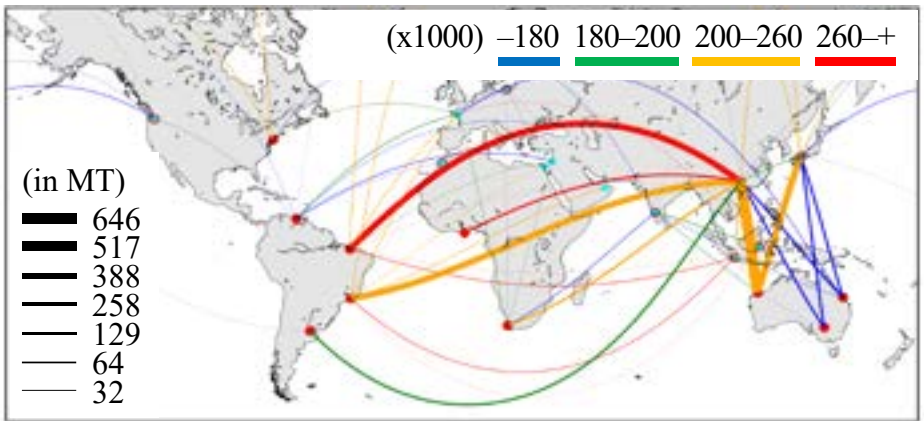

(b) Case study 3b (GHG-optimized) average sailing speed

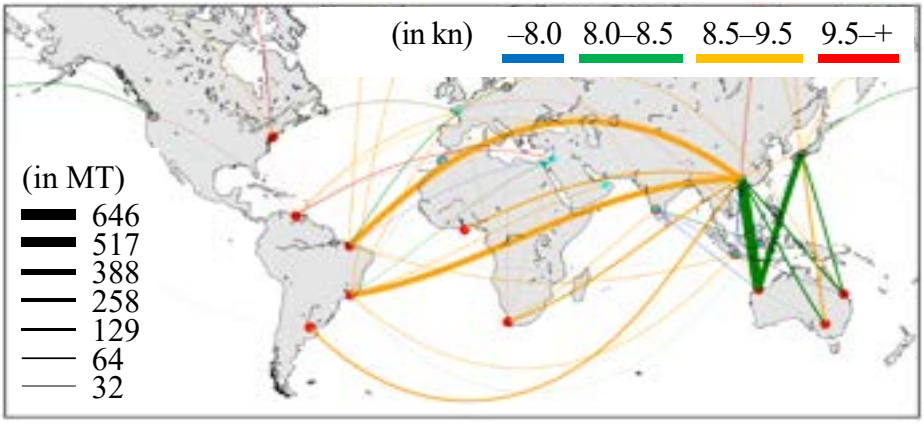

Figure 26. Ship allocation optimization in time-charter contract of Capesize dry bulk carrier with new ships instance: Case study 3b (GHG-optimized) (**a**) average DWT and (**b**) sailing speed.

In Table 32, we observe that case study 3a reduces the total COST by 9.5% compared to the actual ship allocation. These reductions were accounted for by new ships, replacing 40.9% of the existing operations. In case study 3b, the GHG emissions were reduced by 22.8%, but the total COST increased by 4.6%. To conclude, we identified a significant reduction in the total COST and GHG emissions by adding new ships.

5.1.7. Discussion 1: Significance of the Total COST and GHG Emissions Reductions

The results of each case study are compiled in Table 32. Case studies 1a and 1b employed new ships covering 58.8% and 87.5% of the worldwide operation numbers using allocation algorithm 1. However, only minor changes were typically observed compared to the actual ship allocation, with a 3.5% total COST reduction in case study 1a and a 9.7% GHG emissions reduction in case study 1b.

Case study 2 optimized the ship allocation using only the existing ships operating in the current ship allocation by deploying allocation algorithm 2. Case study 2a realized a 7.3% total COST reduction, two times which of case study 1a, compared to the actual ship allocation. For the GHG emissions aspect, case study 2b achieved a 14.8% reduction, 1.5 times that of case study 1b. A more significant reduction in the total COST and GHG emissions was achieved in case study 2 than in case study 1.

In addition, using only the existing ships, differences in the allocated ship size can be observed in the case study 2 through the average sailing distances for each ship size category, as shown in Figure 27. For ships with DWT more than 260,000, an increase in the average sailing distances can be ascertained in COST-optimized case (Case 2a), whereas GHG-optimized case (Case 2b) allocated more operations with average sailing distances similar to the actual ship allocation.

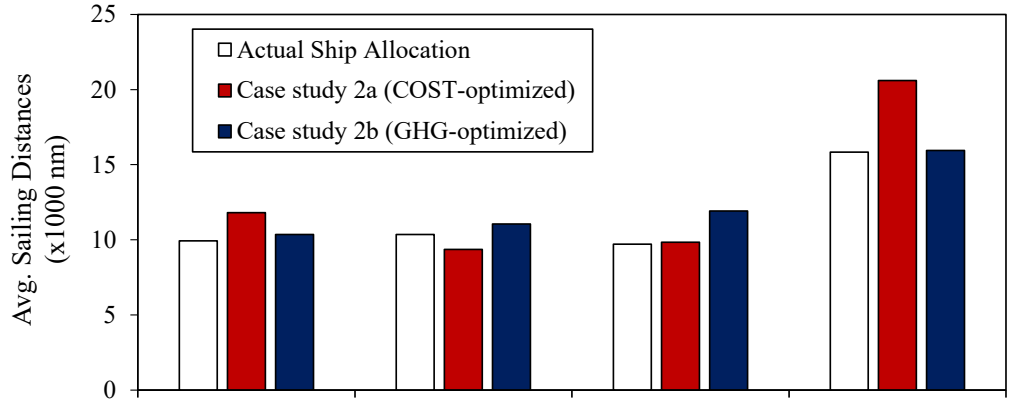

Operation Numbers

Ship DWT (x1000)	(, 180]	(180, 200]	(200, 260]	(260,]
Actual Ship Allocation	4296	2286	2053	550
Case study 2a (COST-optimized)	3841	2451	2291	508
Case study 2b (GHG-optimized)	4385	2106	1849	649

Figure 27. Average sailing distances of case study 2: ship allocation optimization in time-charter contract using existing ships of Capesize dry bulk carrier.

On the other hand, in the COST optimized case (Case 2a), ships with DWT 180,000–200,000 and 200,000–260,000 were averagely sailed less than actual ship allocation; in the contrary, these ships were averagely sailed longer distances in GHG-optimized case (Case 2b).

Case study 3 proposed new ships in applying allocation algorithm 2 under the same constraints as case study 2. The new ships were defined as being able to be allocated indefinitely, which allowed such ships with higher merits to replace the existing ships as needed. In case study 3a, 40.9% of the operation numbers were served by the new ships, allowing a 9.5% total COST reduction compared to the actual ship allocation. For GHG emissions, 48.2% of the operation numbers in case study 3b were served by the new ships. This enabled a considerable reduction of 22.8% in GHG emissions. Additionally, case study 3 allocated new ships at a considerably lower rate than case study 1. Nevertheless, the most significant reduction in the total COST and GHG emissions was actualized by presenting the new ships for the ship allocation optimization.

Table 32. Results of case studies 1, 2, and 3.

Case Studies	Total COST in Million USD (Reduction in %)	GHG Emissions in MT (Reduction in %)	Total Operation Numbers (Reduction in %)	Operation Number of Allocated New Ships (%) [1]
Actual ship allocation	10,848 (0.0)	34.9 (0.0)	9185 (0.0)	*na*
Case study 1a (COST-optimized)	10,469 (-3.5)	33.0 (-5.6)	9185 (0.0)	58.8
Case study 1b (GHG-optimized)	10,883 (−0.4)	31.6 (-9.7)	9185 (0.0)	87.5
Case study 2a (COST-optimized)	10,063 (-7.3)	32.7 (-6.6)	9091 (-1.1)	*na*
Case study 2b (GHG-optimized)	10,249 (-5.6)	29.8 (-14.8)	8989 (-2.2)	*na*
Case study 3a (COST-optimized)	9827 (-9.5)	30.3 (-13.3)	8246 (-10.3)	40.9
Case study 3b (GHG-optimized)	11,345 (−4.6)	27.0 (-22.8)	7560 (-17.7)	48.2

[1] *na*: not available–no new ship in the ship allocation.

5.1.8. Discussion 2: New Ship Demand

In the previous section, case study 3 specified that notable results could be obtained by optimizing the ship allocation with the new ships instance. The allocated new ship rates of case studies 3a and 3b are shown in Figure 28. The allocated new ship rate was observed to vary depending on the sailing distance. Similarly, in the COST- and GHG-optimized cases, more than 60% of the new ships were allocated in the West Australia–China routes, the major iron ore routes with 646 million tons of cargo movement demands.

(a) Case study 3a (COST-optimized)

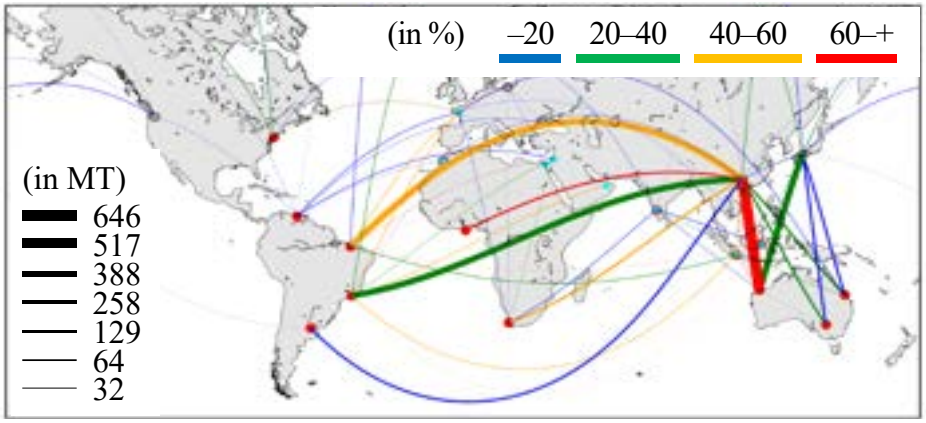

(b) Case study 3b (GHG-optimized)

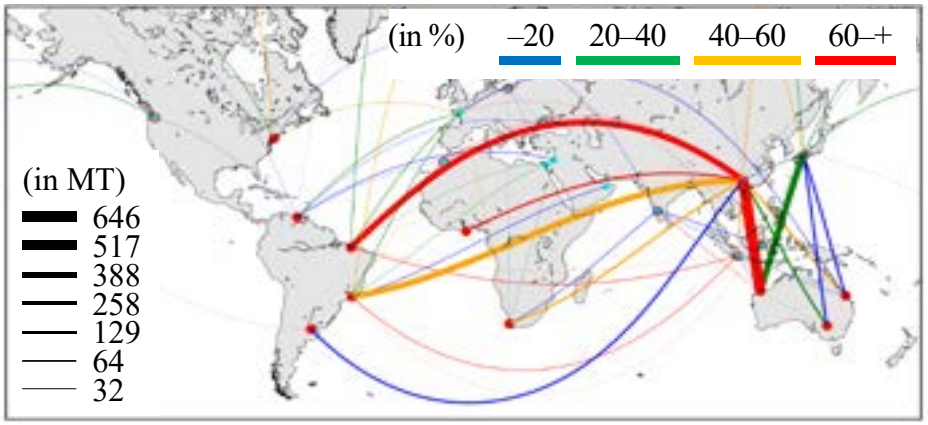

Figure 28. Ship allocation optimization of Capesize dry bulk carrier with new ships instance: Allocated new ship rate of (**a**) case study 3a (COST-optimized) and (**b**) case study 3b (GHG-optimized).

Next, we examined the distinct specifications of the demanded new ships in the West Australia–China routes. Figure 29 shows the composition of operations in the COST- and GHG-optimized ship allocations with the new ships instance. The new ship E (DWT 290,000) was the most allocated, accounting for 47.9% and 54.7% of the COST- and GHG-optimized ship allocation operations, respectively.

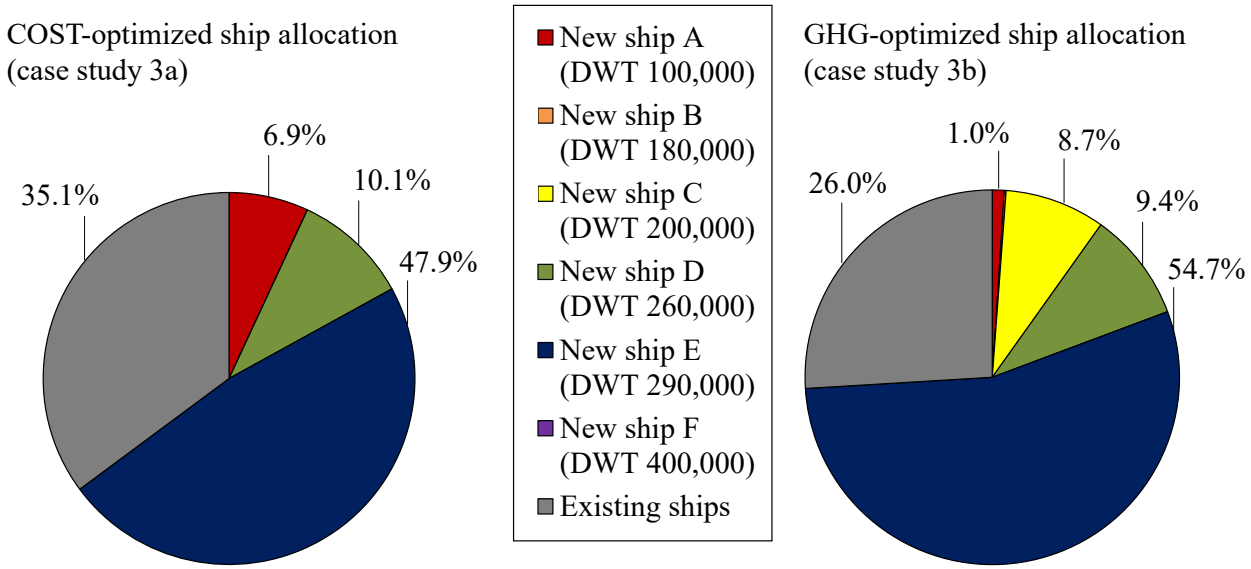

Figure 29. COST- and GHG-optimized ship allocation with new ships instance (case study 3): Composition of operations in the routes of West Australia–China.

This proved that the new ship E specification improvement, through the ADM of Capesize dry bulk carrier in 2021, presented a larger benefit than the existing ships in both the optimization cases. Moreover, looking at the significant main port restrictions of West Australia–China (Table 33), the largest new ship that entered was the new ship E, thus confirming that the demanded ship was a large iron ore bulk carrier.

Table 33. Significant main port limitations of West Australia and China.

Region	Port Name	Cargo Throughput (MT)	*L* (m) [1]	*B* (m) [1]	*d* (m) [1]
West Australia	Port Hedland	386.8	340.0	57	25.5
	Dampier	124	330.1	57	25.5
	Port Walcott	118.1	330.1	57	25.5
China	Caofeidian	77.8	362.0	65	24.3
	Jingtang	71.7	333.0	60	25.5
	Zhoushan	66.1	362.0	65	23.3
	Tianjin	62.1	340.0	60	22.2
	Rizhao	50.5	340.0	62	22.6

[1] *L*: ports' length restriction; *B*: ports' breadth restriction; *d*: ports' draught restriction.

5.2. Case Studies intended for Panamax and MiniCape Dry Bulk Carriers

5.2.1. Overview of Case Studies intended for Panamax–MiniCape Dry Bulk Carriers

We conducted several simulations using algorithms 1, 2, and 3: ship replacement while preserving existing ship allocation (case study 4), optimization of ship allocation in time- and voyage-charter contracts using existing ships (case study 5), and optimization of ship allocation time- and voyage-charter contracts with new ships instance (case study 6). Table 34 shows an overview of case studies of Panamax–MiniCape dry bulk carrier. The following were the objectives of the simulations:

- Target ship: Panamax–MiniCape dry bulk carriers (DWT 65,000-140,000, 2479 ships);
- Cargo types: Iron ore, coal, grain, and others;
- Route: Worldwide (sailing routes served by target ship);
- Operation period: 2018;
- Assumed fuel attributes (specific fuel consumption, g/kWh; emissions factor, t-CO2/t-fuel; fuel prices, USD): HFO (175–185; 3.114; 300–375) and MDO (daily average fuel consumption [28,29].

Table 34. Overview of case studies of Panamax–MiniCape dry bulk carrier.

Case Study	Method	Offered Ships [1]	Ship Allocation [2]	Cargo Movement [3]	Operation Conditions [4]	Fuel Attributes [5]
4	Algorithm 1	*existing*	*existing*	*2018*; *Ir, Co, Gr, Ot*	*existing*	*2018*
5	Algorithms 2, 3	*existing*	*optimized*	*2018*; *Ir, Co, Gr, Ot*	*predicted*	*2018*
6	Algorithms 2, 3	*existing*, *new*	*optimized*	*2018*; *Ir, Co, Gr, Ot*	*predicted*	*2018*
7	Algorithms 2, 3	*new*	*optimized*	*2030*; 2050; *Ir, Co, Gr, Ot*	*predicted*	*2030–2050*

[1] *existing*: existing ships in the actual ship allocation [40,42]; *new*: new ships instance.
[2] *existing*: actual ship allocation; *optimized*: reconstructed ship allocation.
[3] *2018*: worldwide cargo movement in 2018 [40]; *2030*: predicted worldwide cargo movement in 2030 [58]; *2050*: worldwide cargo movement in 2050 [58]; *Ir*: iron ore; *Co*: coal; *Gr*: grain; *Ot*: others.
[4] *existing*: operation conditions in the actual ship allocation; *predicted*: predicted operation conditions by using route-base average.
[5] *2018*: assumed fuel attributes in 2018; *2030–2050*: assumed fuel attributes for future scenarios.

5.2.2. *Definition of New Ships Instance in Case Studies intended for Panamax–MiniCape Dry Bulk Carriers*

For case studies 4 and 6, we offered new ships with the same principal particulars but with the ADM of Panamax–MiniCape dry bulk carriers in 2021 (ADM_{P21}). Figure 30 presents the ADM of Panamax–MiniCape dry bulk carriers before and after CSR-BC.

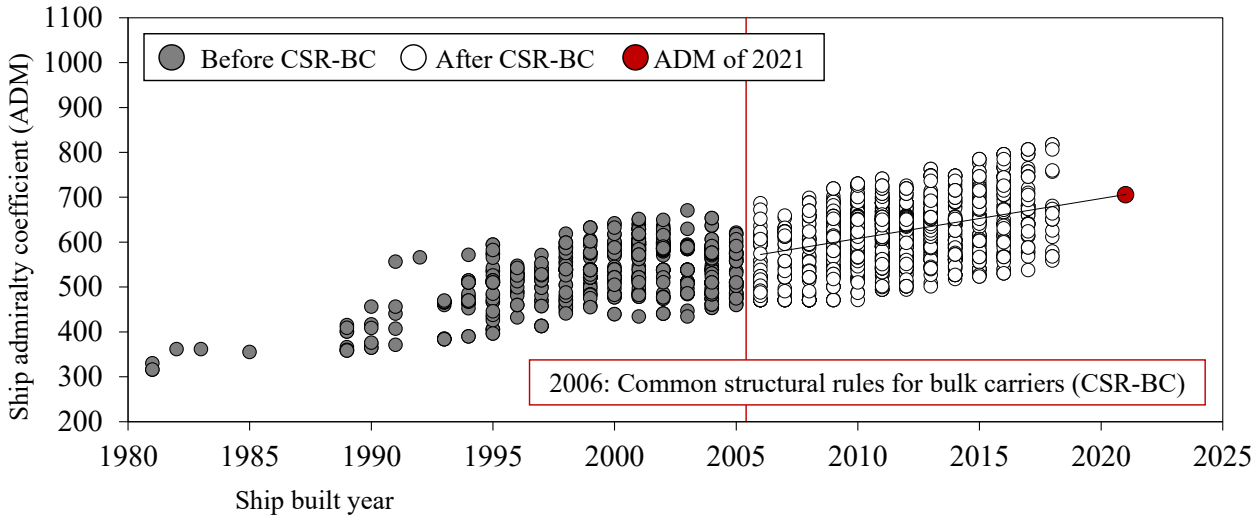

Figure 30. Ship ADM of Panamax–MiniCape dry bulk carriers before and after CSR-BC [42,56,57].

In case study 4, a new ship (i') was defined for each existing ship (i) of the 2018 ship allocation. The set of existing and new ships of Panamax–MiniCape dry bulk carriers are defined as I and I', respectively. Thus, the main engine power ($P_{i'}$) of the new ship i' was reduced by preserving a constant ship i design speed. $P_{i'}$ is calculated as the Capesize dry bulk carrier's case (Equation (31)), by replacing the ADM of Capesize dry bulk carrier in 2021 (ADM_{P21}) with the ADM of Panamax–MiniCape dry bulk carriers in 2021 (ADM_{C21}), as follows [56]:

$$\boldsymbol{P_{i'} = P_i \times \left(\frac{ADM_i}{ADM_{P21}}\right) \quad \forall i \in I, \quad \forall i' \in I',} \tag{33}$$

where P_i is the main engine power of the existing ship i (kW), ADM_i is the ADM of the existing ship i, ADM_{P21} is the defined ADM of Panamax–MiniCape dry bulk carriers in 2021: 705.96, and i is an individual ship (2479 Panamax–MiniCape dry bulk carriers operating in 2018).

Moreover, in case study 6, the new ship specifications were sampled from the existing ships of the 2018 ship allocation. The set of sampled ships is defined as S. We defined these ships as more efficient since they had the ADM of Panamax–MiniCape dry bulk carriers in 2021: 705.96 (see Figure 30). Hence, the main engine power (P_s') was reduced by retaining a constant ship s design speed. P_s' is calculated as the Capesize dry bulk carrier's case (Equation (32)) by replacing the ADM of Capesize dry bulk carrier in 2021 (ADM_{P21}) with the ADM of Panamax–MiniCape dry bulk carriers in 2021 (ADM_{C21}), as follows [56]:

$$\boldsymbol{P_s' = P_s \times \left(\frac{ADM_s}{ADM_{P21}}\right) \quad \forall s \in S,} \tag{34}$$

where P_s is the main engine power of ship s (kW), ADM_s is the ADM of ship s, ADM_{P21} is the defined ADM of Panamax–MiniCape dry bulk carriers in 2021: 705.96, and s is an individual ship (eight ships sampled from 2479 Panamax–MiniCape dry bulk carriers operating in 2018). These ships had the same principal particulars as to the sampled ships but lowered main engine power, as shown in Table 35.

Table 35. Assumed specifications of the new ships.

New Ship	*DWT* [1]	*d* (m) [1]	*B* (m) [1]	*L* (m) [1]	*v* (kn) [1]	*Age* [2]	Existing *ME* Power (kW) [3]	New Ship *ME* Power (kW) [3]	*ME* Power Reduction (%) [3]
A	66,485	12.9	36	200	14.5	1	8470	7892	6.8
B	67,508	13.2	32	225	14.5	1	9000	8051	10.5
C	75,122	13.8	32	225	14.5	1	10,750	8403	21.8
D	77,679	12.9	37	229	14.5	1	10,224	8603	15.9
E	85,001	14.0	37	229	14.5	1	9660	9198	4.8
F	95,790	14.5	38	235	14.5	1	12,950	9937	23.3
G	106,415	13.6	43	254	14.5	1	13,560	10,807	20.3
H	118,863	14.8	43	260	14.5	1	13,560	11,757	13.3

[1] *DWT*: new ships' deadweight tonnage; *d*: new ships' draught; *B*: new ships' breadth; *L*: new ships' length; *v*: new ships' design speed;
[2] *Age*: assumed ship age;
[3] *ME*: main engine.

5.2.3. Actual Ship Allocation of Panamax–MiniCape Dry Bulk Carriers

Similar to Capesize dry bulk carrier (Section 5.1.3), the typical characteristics of the actual ship allocation must be ascertained. The ships' average DWT, ship age, and sailing speed in the actual ship allocation of Panamax–MiniCape dry bulk carriers are respectively shown in Figure 31. The line thickness indicates the annual cargo movement on each route, and the sorted colors represent the variance of the DWT, ship age, and sailing speed.

In the South East Asia–China routes, which have the largest cargo movement, the average DWT is 75,000–85,000, the average ship age is 3–10 years old, and the average sailing speed is less than 8 knots, which indicates the use of smaller ships at typically slower speeds. Additionally, the long-distance routes, such as Brazil–China, show the operated ships with an average DWT of 75,000–85,000, the average ship age is 10–15 years old, and an average sailing speed was exceeding 9–10 knots, which indicates that the routes are served by older ships at higher speeds.

(a) Average DWT

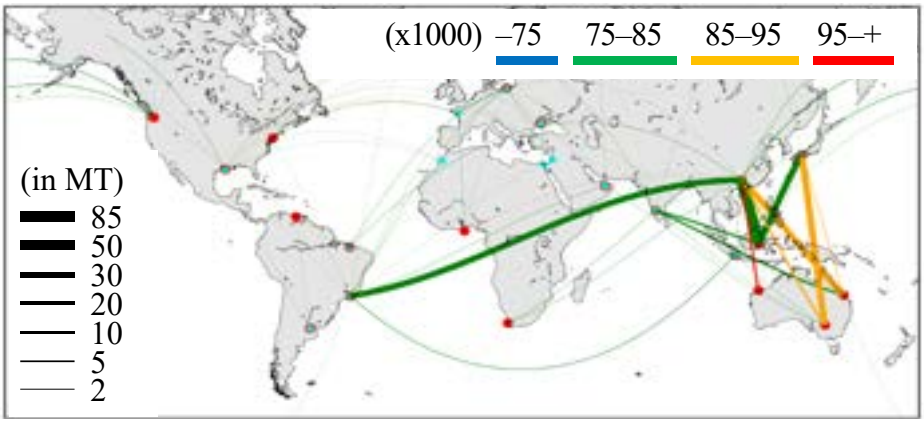

(b) Average Ship Age

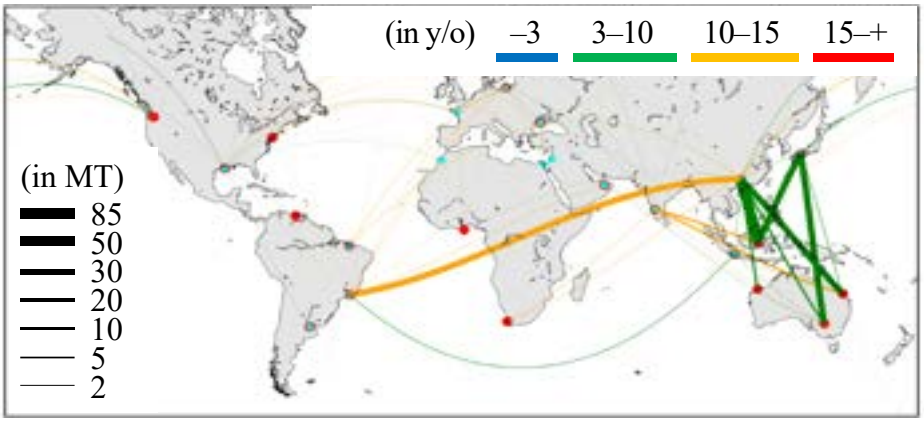

(c) Average Sailing Speed

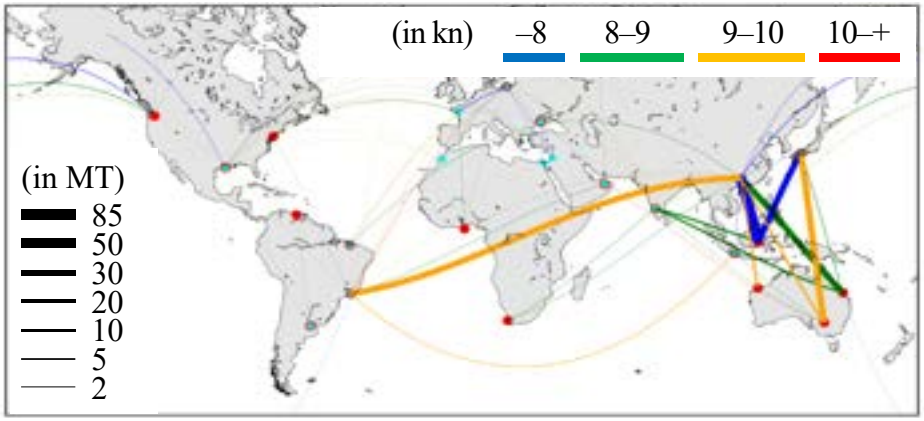

Figure 31. Actual ship allocation of Panamax–MiniCape dry bulk carriers: (**a**) Average DWT, (**b**) sailing speed, and (**c**) ship age.

5.2.4. Case study 4: Ship Replacement while Preserving the Existing Ship Allocation

5.2.4.1. Definition of Case Study 4

This case study attempted to directly replace each existing ship with a new ship without changing the actual ship allocation and then to observe the changes in the total COST and GHG emissions, including COST-optimized ship replacement while preserving the existing ship allocation (case study 4a) and GHG-optimized ship replacement while preserving the existing ship allocation (case study 4b). The following were the parameters of case study 1:

- Method: Allocation algorithm 1;
- Offered ships: A new ship with the ADM of Panamax–MiniCape dry bulk carriers in 2021 for each existing ship in the actual ship allocation.

5.2.4.2. Results of Case Study 4

The allocated new ship rates for cases 4a and 4b are shown in Figure 32. Both the cases show a typically high allocation rate for new ships. Figure 32a shows the major routes in which the allotted new ships take over 70%–90% of the operation numbers. Meanwhile, Figure 32b shows that the new ships accounted for more than 90% of the operation numbers on most routes.

(a) Case study 4a (COST-optimized)

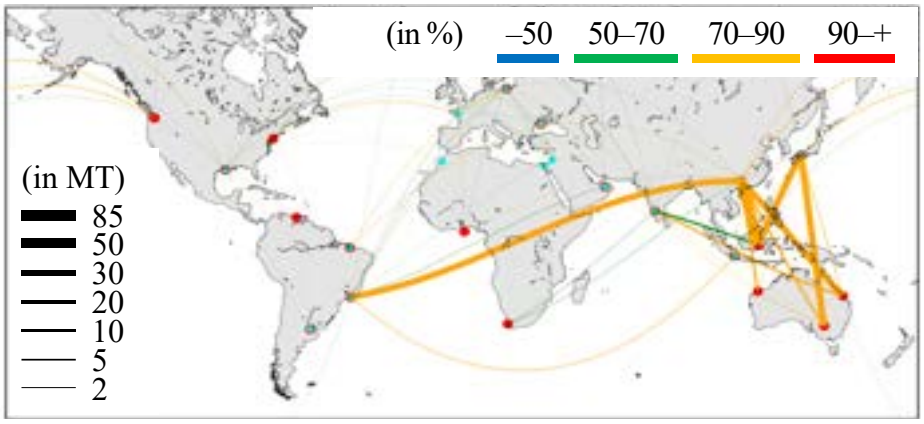

(b) Case study 4b (GHG-optimized)

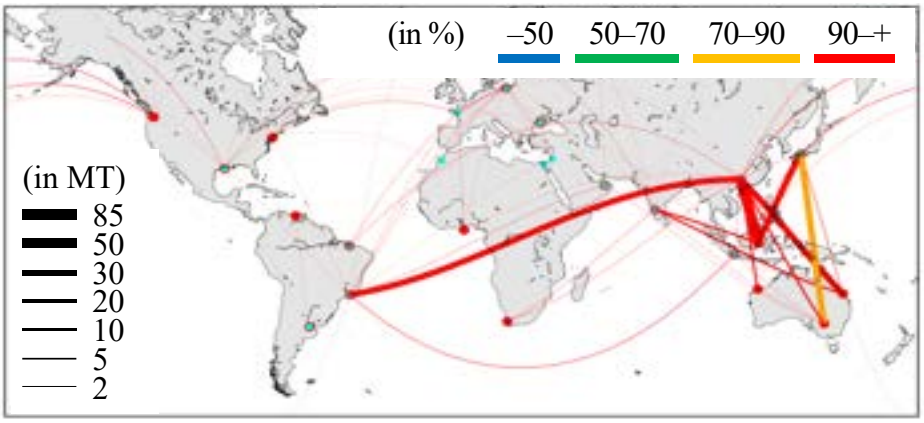

Figure 32. Ship replacement while preserving existing ship allocation of Panamax–MiniCape dry bulk carriers: Allocated new ship rate of (**a**) case study 4a (COST-optimized) and (**b**) case study 4b (GHG-optimized).

As shown in Table 36, minor reductions in the total COST and GHG emissions can be seen in case study 4. In case study 4a, new ships replaced 73.8% of the total number of existing ship operations, which reduced the total COST by 3.5%, and the GHG emissions were reduced by 3.3% compared to the actual ship allocation. Moreover, case study 4b allotted 94.9% of its operations to new ships, which allowed a 4.8% reduction in the GHG emissions, and the total COST was reduced by 3.0%.

5.2.5. Case study 5: Optimization of Ship Allocation in Time- and Voyage-Charter Contracts using Existing Ships

5.2.5.1. Definition of Case Study 5

In this case study, we discussed optimizing the ship allocation using only the existing ships of Panamax–MiniCape dry bulk carriers. The four case studies covered are: COST-optimized ship allocation in time-charter contracts using existing ships (case study 5a), GHG-optimized ship allocation in time-charter contracts using existing ships (case study 5b), COST-optimized ship allocation in voyage-charter contract using existing ships (case study 5c), and GHG-optimized ship allocation in voyage-charter contract using existing ships (case study 5d). The following were the parameters for case study 2:

- Method: Allocation algorithms 2 and 3;
- Offered ships: The existing ships of Panamax–MiniCape dry bulk carriers operating in the current ship allocation.

5.2.5.2. Results of Case Study 5

The results obtained for case study 5 are illustrated in Figure 33, Figure 34, Figure 35, and Figure 36. From Figure 33, we can ascertain the route with the largest cargo movement; South East Asia–China routes allotted larger ships with an average DWT of 85,000–95,000 and an average ship age of 3–10 years old. With the same average ship age, the average DWT of ships designated to South East Asia–China routes increased compared to the actual ship allocation due to the use of larger ships.

In Figure 34, the major routes are allocated to ships with an average ship age of 3–10 years old, including the long-distance routes of Brazil–China. Subsequently, the average DWT of ships allocated to these routes was increased compared to the actual ship allocation, with an average DWT of 85,000–95,000. In addition, South East Asia–China routes in Figure 34 depict a similar average DWT as the actual ship allocation but older ships with an average ship age of 10–15 years old. To reduce the global GHG emissions in the time-charter contract, these results indicated the importance of typically young larger ships for long-distance routes.

(a) Case study 5a (COST-optimized) average DWT

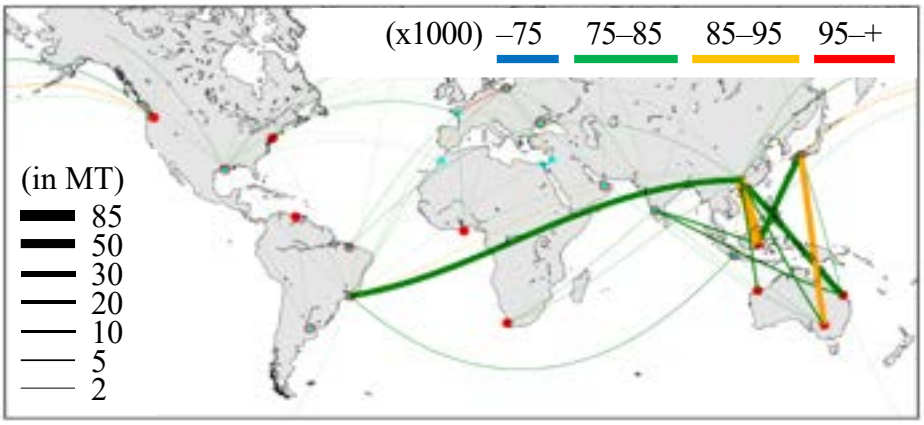

(b) Case study 5a (COST-optimized) average ship age

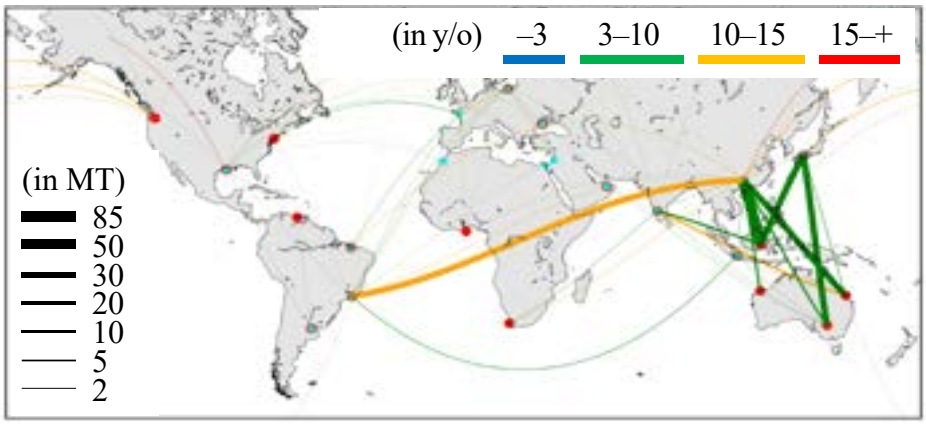

Figure 33. Ship allocation optimization in time-charter contract using existing ships of Panamax–MiniCape dry bulk carriers: Case study 5a (COST-optimized) (**a**) average DWT and (**b**) ship age.

(a) Case study 5b (COST-optimized) average DWT

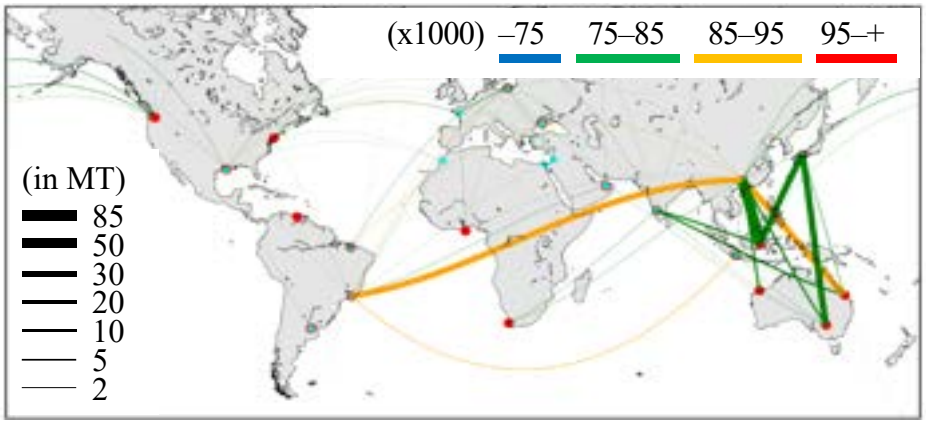

(b) Case study 5b (COST-optimized) average ship age

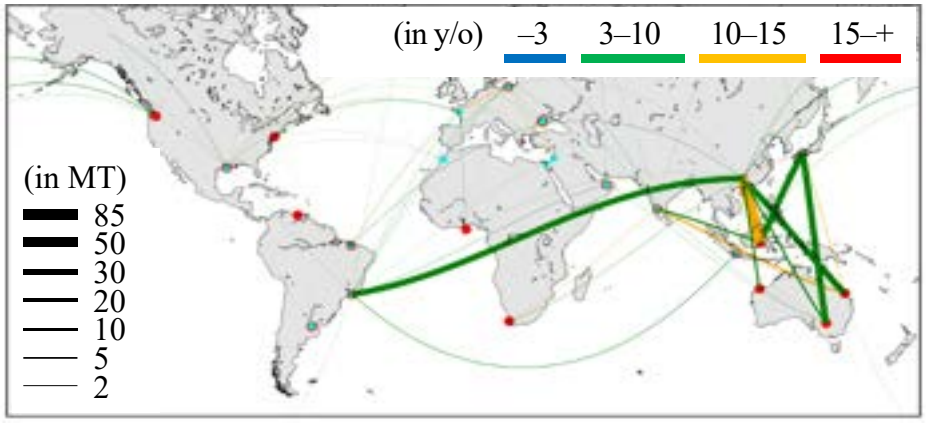

Figure 34. Ship allocation optimization in time-charter contract using existing ships of Panamax–MiniCape dry bulk carriers: Case study 5b (GHG-optimized) (**a**) average DWT and (**b**) ship age.

Furthermore, from Figure 35, we can ascertain that the major routes allocated ships with various average DWT compared to the actual ship allocation. Moreover, the average ship age ranges between 3–10 and 10–15 years old. These suggest that the ships were designated following the monthly cargo movement fluctuation. Thus, the significance of reducing the total COST for each route in the voyage-charter is diversified.

In Figure 36a, the size of allocated ships in major routes is more evenly distributed with an average DWT of 75,000–85,000 and 85,000–95,000. Subsequently, Figure 36b depicts a uniform average ship age of 3–10 years old. These results indicated the importance of younger ships in optimizing the GHG emissions.

(a) Case study 5c (COST-optimized) average DWT

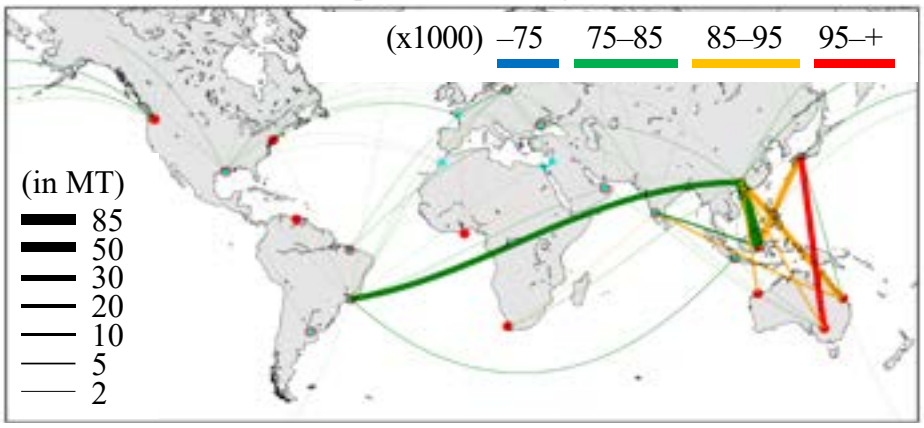

(b) Case study 5c (COST-optimized) average ship age

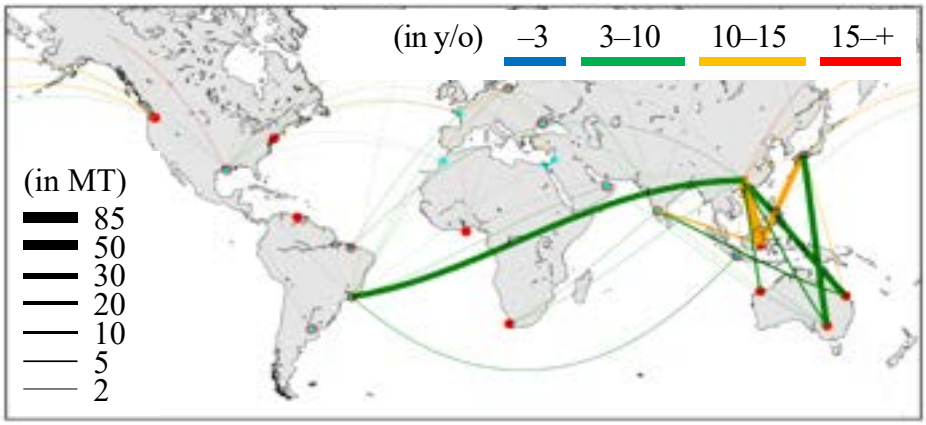

Figure 35. Ship allocation optimization in voyage-charter contract using existing ships of Panamax–MiniCape dry bulk carriers: Case study 5c (COST-optimized) (**a**) average DWT and (**b**) ship age.

(a) Case study 5d (GHG-optimized) average DWT

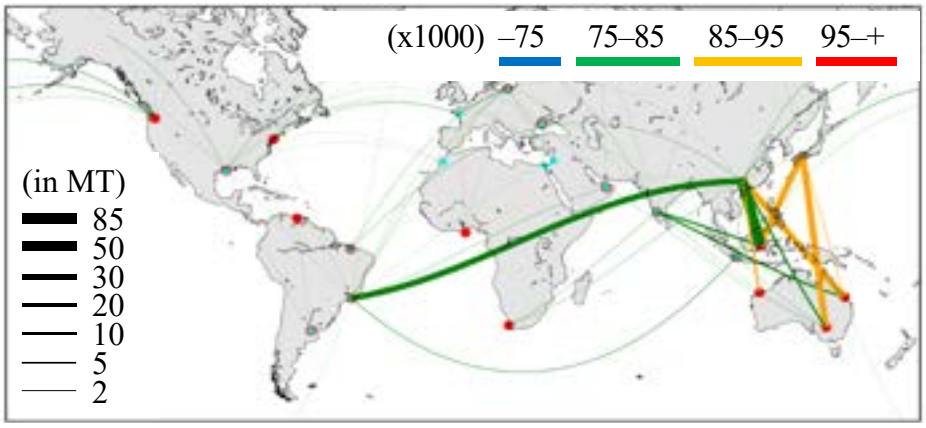

(b) Case study 5d (GHG-optimized) average ship age

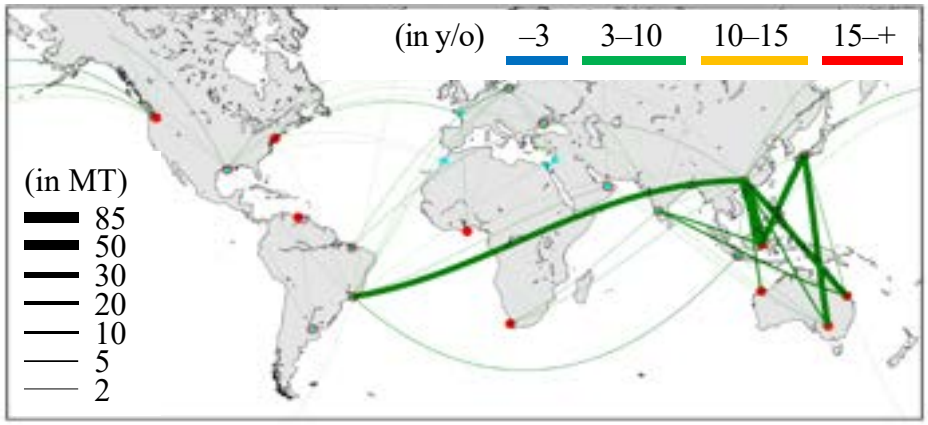

Figure 36. Ship allocation optimization in voyage-charter contract using existing ships of Panamax–MiniCape dry bulk carriers: Case study 5d (GHG-optimized) (**a**) average DWT and (**b**) ship age.

As summarized in Table 36, case study 5a reduced the total COST by 0.4% compared to the actual ship allocation, which was less reduction compared to case study 4a. Moreover, the total GHG emissions were reduced by 5.2% in case study 5b. Additionally, the ship operation numbers of case studies 5a and 5b were reduced by 6.5% and 5.0%, respectively. Next, considering the case of voyage-charter, case study 5c reduced the total COST by 7.6% compared to the actual ship allocation, whereas the total GHG emissions in case study 5d were reduced by 10.9%. In addition, the ship operation numbers of case studies 5c and 5d were reduced by 1.7% and 1.5%, respectively. The operation-level alterations made such changes in the ship allocation, despite simply employing the existing ships. Nevertheless, a significant reduction in the total COST and GHG emissions could not be obtained using only the existing ships.

5.2.6. Case study 6: Optimization of Ship Allocation in Time- and Voyage-Charter Contracts with New Ships Instance

5.2.6.1. Definition of Case Study 6

In addition to the analysis of case study 5, which is already discussed in Section 5.2.5, this case study offers a set of new ships to the optimization. We examined the competitive new ships that could replace the existing ships by conducting simulations to optimize the ship allocation with these new ships. The following were the parameters of case study 6:

- Method: Allocation algorithms 2 and 3;
- Offered ships: The existing ships of case study 5 and eight new ships with the ADM of Panamax–MiniCape dry bulk carriers in 2021.

As new ships could be allotted indefinitely, we discussed the following case studies: COST-optimized ship allocation in time-charter contract with new ships instance (case study 6a), GHG-optimized ship allocation in time-charter contract with new ships instance (case study 6b), COST-optimized ship allocation in voyage-charter contract with new ships instance (case study 6c), and GHG-optimized ship allocation in voyage-charter contract with new ships instance (case study 6d).

5.2.6.2. Results of Case Study 6

This case study optimized the ship allocation by allowing the existing ships to be replaced by new ships. This allowed us to ascertain the average DWT and sailing speed patterns simultaneously on a global scale. Figure 37 and Figure 38 present the ship allocation in the time-charter contract results of case study 6. We can observe that both case studies allocated ships with an identical average DWT of more than 95,000. Similarly, the major routes for both cases selected a ship with an average ship age of less than 3 years old. Specifically, the difference between these cases can be ascertained in the average ship age of North America–Japan routes. Figure 37b and Figure 38b show that ships with average ship age 10–15 and less than 3 years old were allocated in these minor routes. With new ships instance, these indicated that the importance of DWT and ship age were equal in a time-charter contract.

(a) Case study 6a (COST-optimized) average DWT

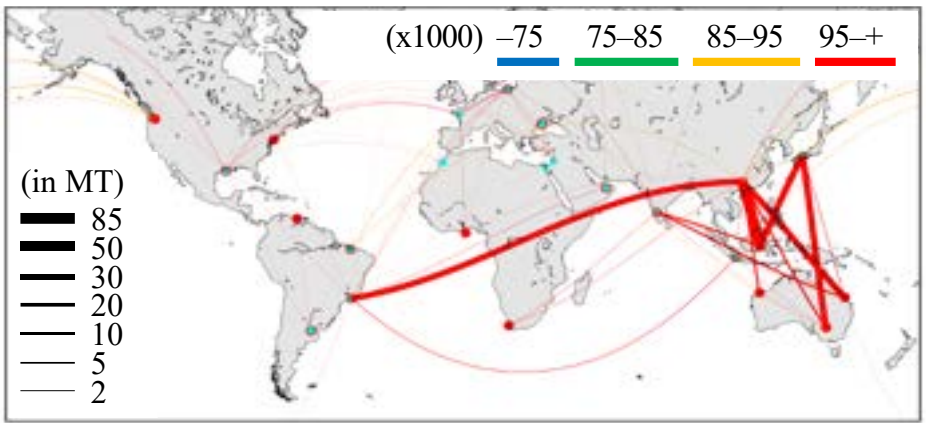

(b) Case study 6b (COST-optimized) average ship age

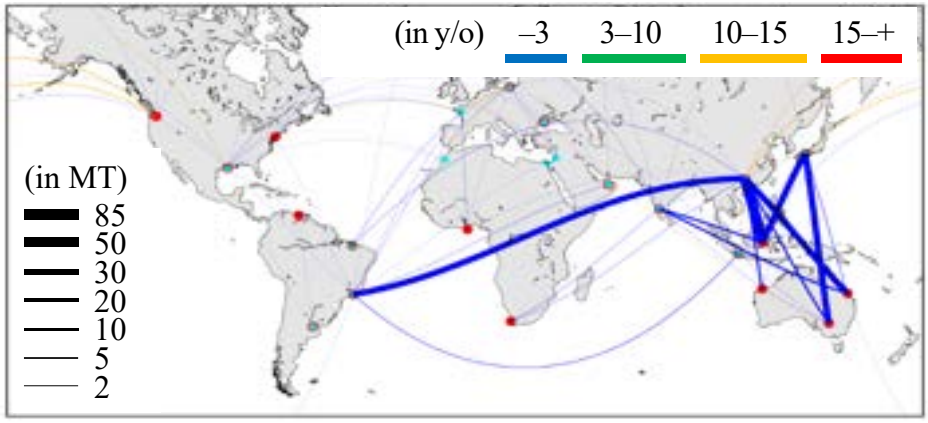

Figure 37. Ship allocation optimization in time-charter contract of Panamax–MiniCape dry bulk carriers with new ships instance: Case study 6a (COST-optimized) (**a**) average DWT and (**b**) ship age.

(a) Case study 6b (GHG-optimized) average DWT

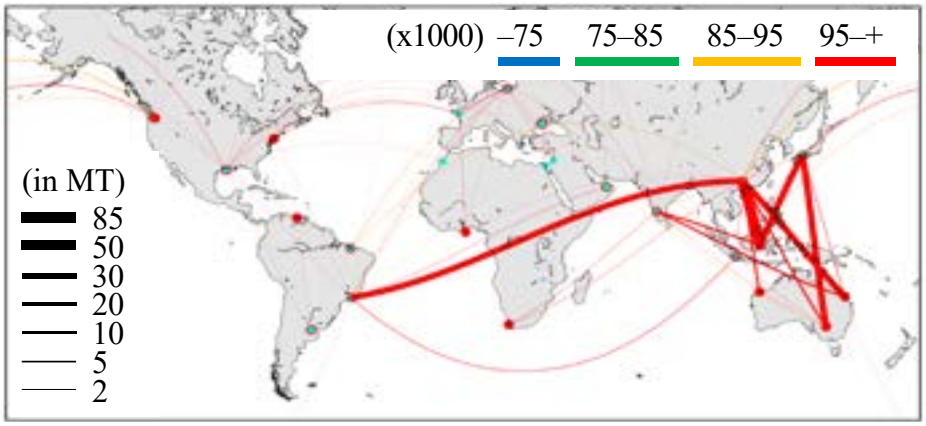

(b) Case study 6b (GHG-optimized) average ship age

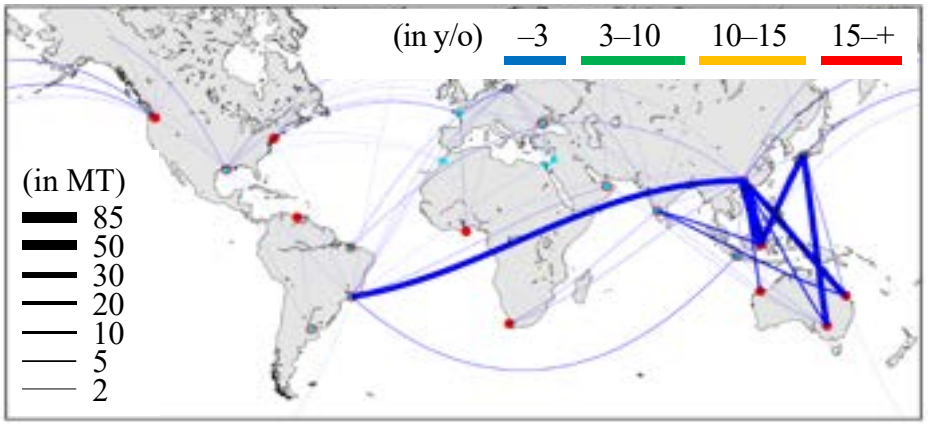

Figure 38. Ship allocation optimization in time-charter contract of Panamax–MiniCape dry bulk carriers with new ships instance: Case study 6b (GHG-optimized) (**a**) average DWT and (**b**) ship age.

Moreover, Figure 39 and Figure 40 present the ship allocation in voyage-charter contract results of case study 6. From Figure 39 a and Figure 40a, we can observe that both case studies allocated ships with a similar average DWT. South East Asia–China and Brazil–China routes allocated ships with the average DWT of 85,000–95,000 and 75,000–85,000, respectively. Additionally, larger ships with an average DWT of more than 95,000 were designated for Australia–China and Australia–Japan routes.

Furthermore, Figure 39b and Figure 40b show disparity in the allocated ships' average ship age. Ships with an average age of 14–15 years old can be observed in the South East Asia–China and South East Asia –Japan routes of Figure 39b. On the other hand, Figure 40b depicts a globally uniform average ship age of fewer than 3 years old.

With new ships instance, these indicated that the importance of DWT is equally proportionated to the monthly cargo movement of each route. In addition, the significance of new ships in reducing the GHG emissions was shown by the allocated ships that consist of an only younger ships.

(a) Case study 6c (COST-optimized) average DWT

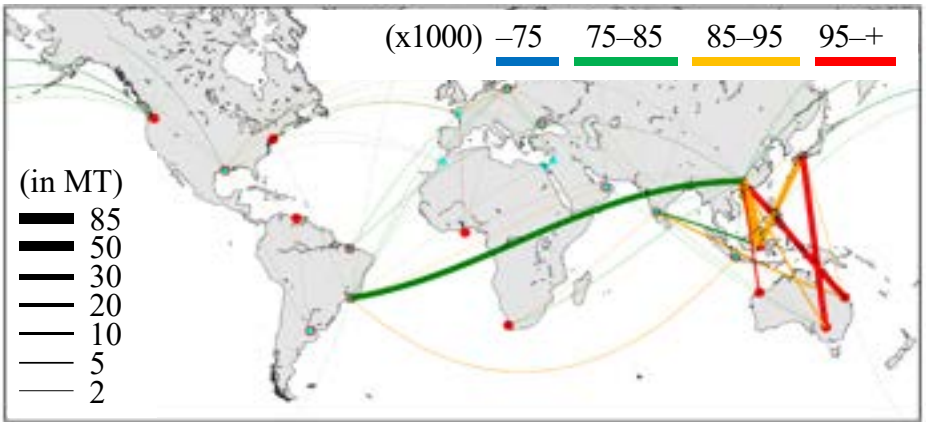

(b) Case study 6c (COST-optimized) average ship age

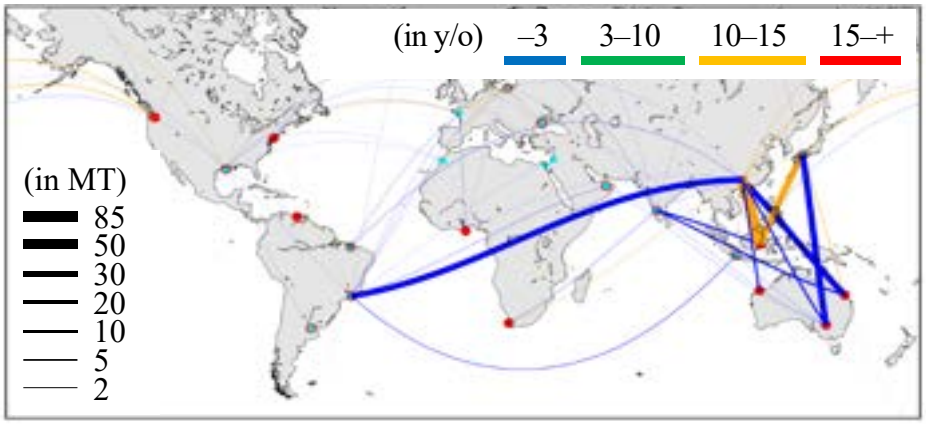

Figure 39. Ship allocation optimization in voyage-charter contract of Panamax–MiniCape dry bulk carriers with new ships instance: Case study 6c (COST-optimized) (**a**) average DWT and (**b**) ship age.

(a) Case study 6d (GHG-optimized) average DWT

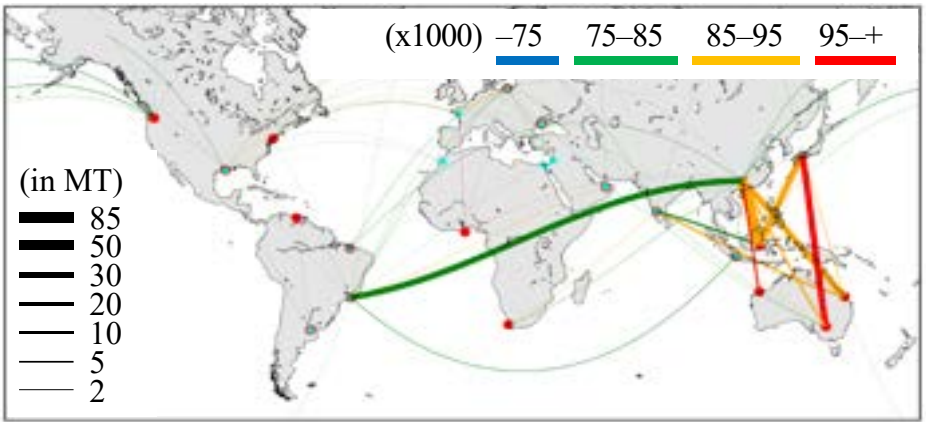

(b) Case study 6d (GHG-optimized) average ship age

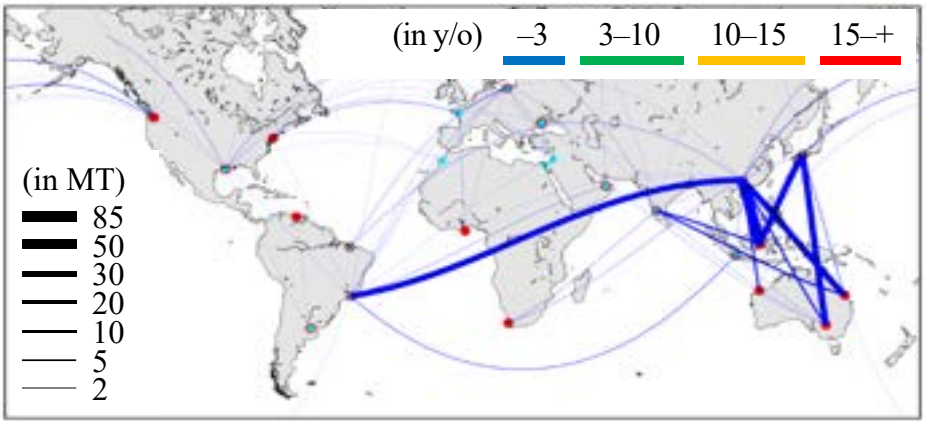

Figure 40. Ship allocation optimization in voyage-charter contract of Panamax–MiniCape dry bulk carriers with new ships instance: Case study 6d (GHG-optimized) (**a**) average DWT and (**b**) ship age.

In Table 36, we observe that case study 6a reduced the total COST by 12% compared to the actual ship allocation. These reductions were accounted for by new ships, replacing 68% of the existing operations. In case study 6b, the GHG emissions were reduced by 20.9% by the allocated new ships of 77.4%.

Similarly, considering the voyage-charter, case study 6c reduced the total COST by 13.7% compared to the actual ship allocation, whereas the total GHG emissions in case study 6d were reduced by 21.4%. Case studies 6c and 6d take new ships into their ship allocation by 70.7% and 85.2%, respectively. To conclude, we identified a significant reduction in the total COST and GHG emissions by adding new ships.

5.2.7. Discussion 3: Significance of the Total COST and GHG Emissions Reductions in Time- and Voyage-Charter Contracts

The total GHG emissions and COST resulting from case studies 4, 5, and 6 are shown in Table 36. Applying algorithm 1 to the existing ship allocation, case studies 4a and 4b offered new ships with the same specification as the existing ships but higher ADM. However, it can be ascertained that only minor reductions in total GHG emissions and COST have resulted from those case studies.

Table 36. Results of case studies 4, 5, and 6.

Case Studies	Total COST in Million USD (Reduction in %)	GHG Emissions in MT (Reduction in %)	Total Operation Numbers (Reduction in %)	Operation Number of Allocated New Ships (%) [1]
Actual ship allocation	9747 (0.0)	30.1 (0.0)	16,110 (0.0)	*na*
Case study 4a (COST-optimized)	9405 (-3.5)	29.1 (-3.3)	16,110 (0.0)	73.8
Case study 4b (GHG-optimized)	9453 (-3.0)	28.6 (-4.8)	16,110 (0.0)	94.9
Case study 5a (COST-optimized)	9711 (-0.4)	29.1 (-3.2)	15,067 (-6.5)	*na*
Case study 5b (GHG-optimized)	9749 (0.0)	28.5 (-5.2)	15,307 (-5.0)	*na*
Case study 5c (COST-optimized)	9002 (-7.6)	27.2 (-9.6)	15,844 (-1.7)	*na*
Case study 5d (GHG-optimized)	9101 (-6.6)	26.8 (-10.9)	15,873 (-1.5)	*na*
Case study 6a (COST-optimized)	8574 (-12.0)	24.3 (-19.3)	12,595 (-21.8)	68.0
Case study 6b (GHG-optimized)	8647 (-11.3)	23.8 (-20.9)	12,466 (-22.6)	77.4
Case study 6c (COST-optimized)	8411 (-13.7)	24.3 (-19.4)	15,092 (-6.3)	70.7
Case study 6d (GHG-optimized)	8498 (-12.8)	23.6 (-21.4)	15,096 (-6.3)	85.2

[1] *na*: not available–no new ship in the ship allocation.

Moreover, applying algorithm 2, case studies 5a and 5b deliver lower reductions in total GHG emissions and COST compared to case studies 4a and 4b. On the other hand, using algorithm 3, case studies 5c and 5d result in even higher reductions. Referring to Section 5.1.7, this pattern differs from the Capesize dry bulk carrier cases. Furthermore, we observe the average economic days taken from the operation-level schedule of the allocated ships in case study 5, as shown in Table 37.

Table 37. Average economic days taken from case study 5

Case Studies [1]	Average Laden *SD*	Average Ballast *SD*	Average Loading *PS*	Average Unloading *PS*	Total Average *ED*
Actual Ship Allocation	162.0	116.5	14.6	20.1	313.1
Case study 5a (COST-optimized)	140.5	141.5	13.5	18.7	314.2
Case study 5b (GHG-optimized)	139.9	140.7	13.8	19.0	313.4
Case study 5c (COST-optimized)	146.1	114.4	14.3	19.7	294.6
Case study 5d (GHG-optimized)	145.8	114.6	14.4	19.7	294.5

[1] *SD*: sailing days (d); *PS*: port staying time (d); *ED*: economic days (d).

It can be observed that optimization using algorithm 2 and annual cargo movement demand in case studies 5a and 5b, assuming all ships operating in time-charter contract, resulted in longer ballast operation time. This condition is caused by the assumption that a ship went round-trip, back and forth to the origin port. On the contrary, optimization using algorithm 3 and monthly cargo movement demand in the case studies 5c and 5d were able to allocate ships that acquired similar average ballast sailing days as the actual ship allocation. Furthermore, we can ascertain that this method is the most suitable to simulate the actual ship allocation of the Panamax–Minicape dry bulk carrier.

Finally, optimization with new ships instance of case studies 6a, 6b, 6c, and 6d results lowest total GHG emissions and COST compared to other case studies. These case studies offered new ships with ADM in 2021, considering eight different DWT categories. Those guaranteed lower total GHG emissions and COST while the new ships can be allocated indefinitely. Moreover, using algorithm 3, case studies 6c and 6d are ascertained to achieve even higher reductions in total GHG emissions and COST compared to case studies 6a and 6b.

5.2.8. Discussion 4: New Ship Demand in Time- and Voyage-Charter Contracts

In the previous section, case study 6 specified that notable results could be obtained by optimizing the ship allocation with the new ships instance. The allocated new ship rates of case studies 6a–6d are shown in Figure 41. The allocated new ship rate was observed to vary depending on the sailing distance. Generally, in the GHG-optimized cases of 6b and 6d, more than 60% of the new ships were allocated in the South East Asia–China routes, with the largest cargo movement demands.

(a) Case study 6a (COST-optimized)

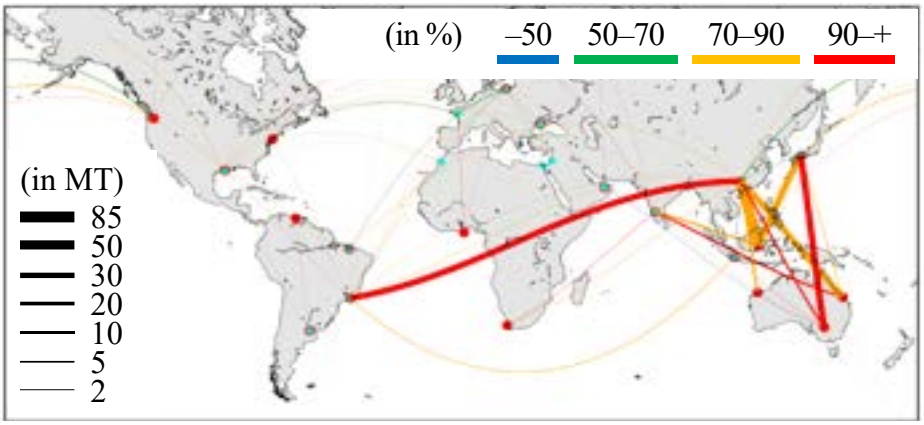

(b) Case study 6b (GHG-optimized)

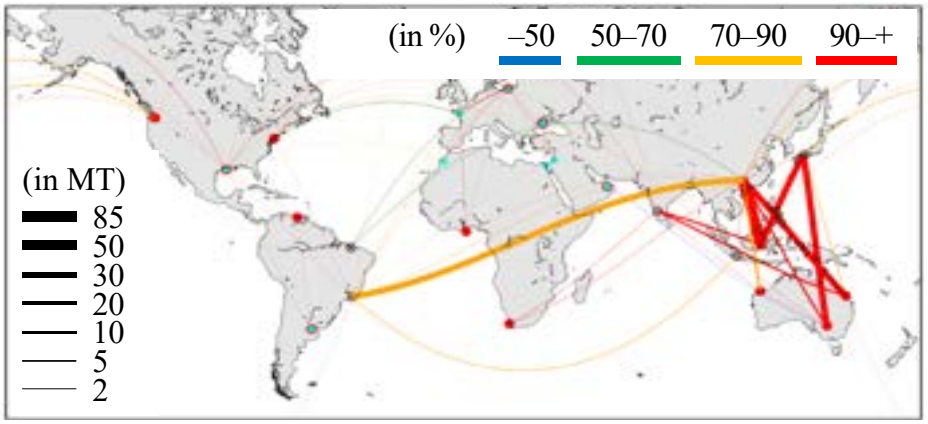

Continued

(c) Case study 6c (COST-optimized)

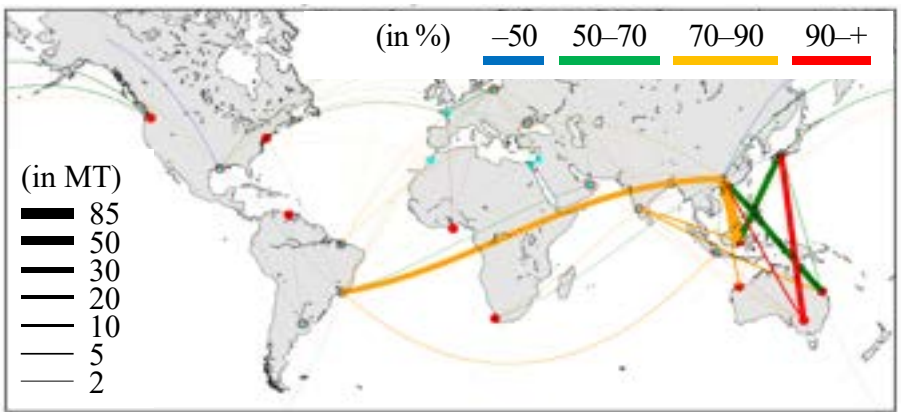

(d) Case study 6d (GHG-optimized)

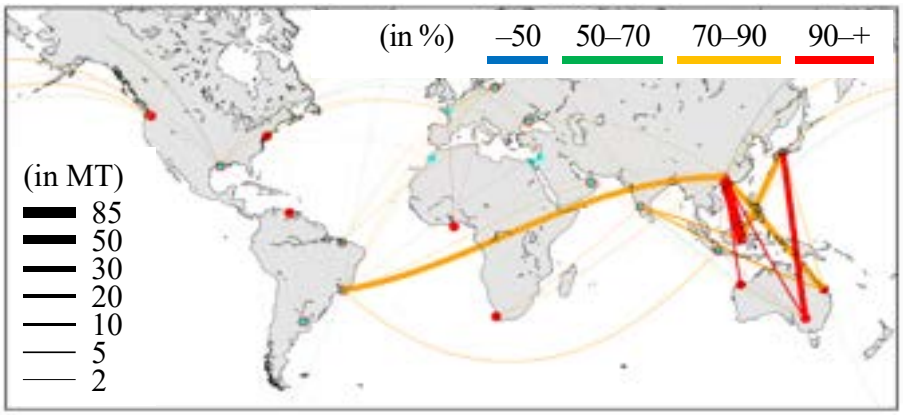

Figure 41. Ship replacement while preserving existing ship allocation of Panamax–MiniCape dry bulk carrier: Allocated new ship rate of (**a**) case study 6a (COST-optimized), (**b**) case study 6b (GHG-optimized) (**c**) case study 6c (COST-optimized), (**d**) case study 6d (GHG-optimized).

Next, Figure 42 shows the composition of operations in the case studies 6a–6d. In the case of the time-charter contract, the largest new ship, new ship H (DWT 110,000), was the most allocated, accounting for 40% and 43.7% of the operations of the case studies 6a and 6b, respectively. On the other hand, the case studies of 6c and 6d allocated new ships evenly with the dominance of new ship C. This ship was allocated mostly for 20.8% and 25.2% of the operations in the case studies 6c and 6d. These proved that the new ship H and new ship C specification improvement, through the ADM of Panamax–MiniCape dry bulk carrier in 2021, to be the most competitive in the optimization case of time- and voyage-charter contracts, respectively. Moreover, looking at the size limitations of significant routes with the highest annual cargo movement demand (see Table 38), the largest new ship that entered was the new ship H, thus confirming that the demanded ship was a larger bulk carrier to carry iron ore, coal, and other cargo types.

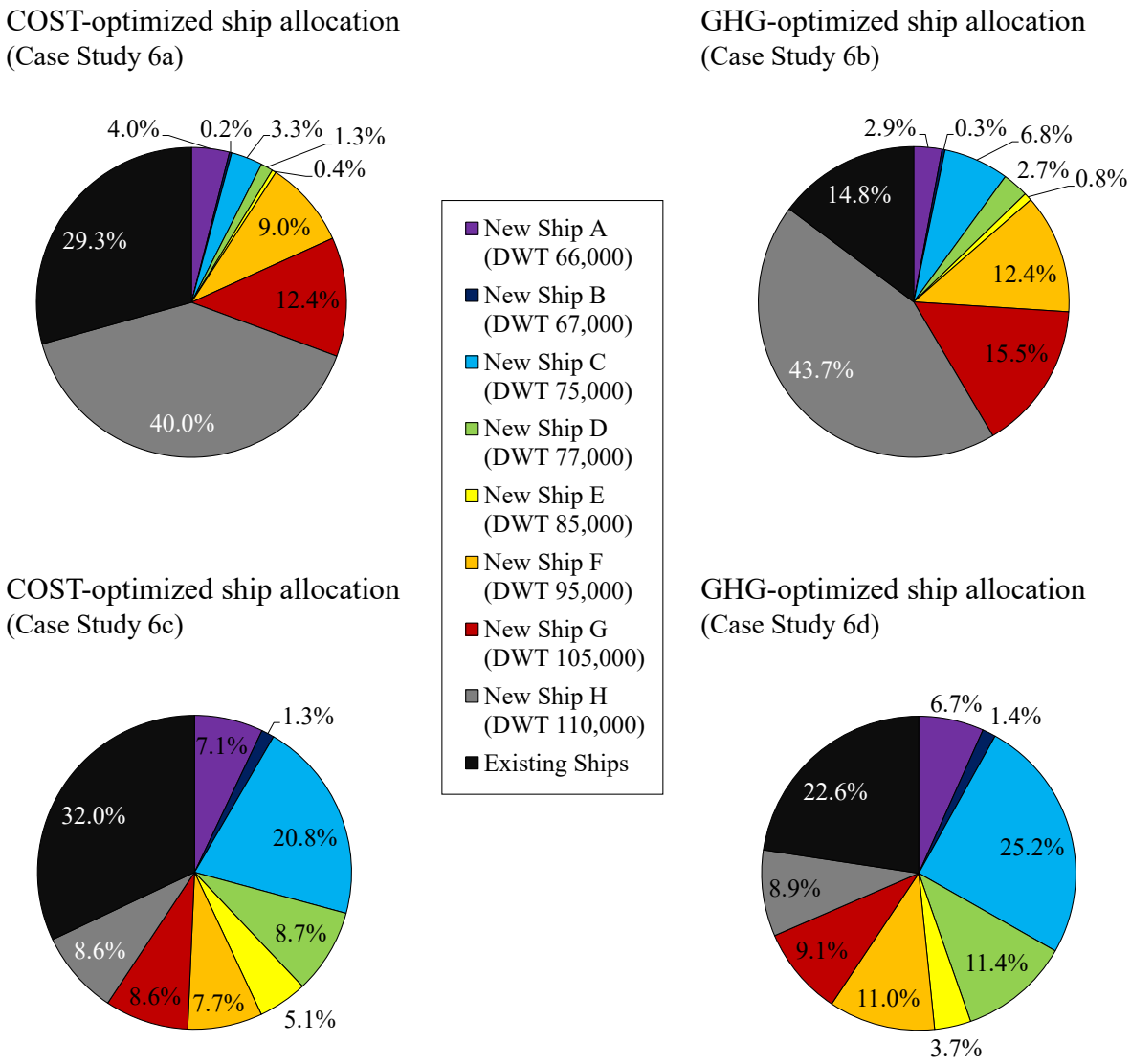

Figure 42. COST- and GHG-optimized ship allocation with new ships instance (case study 6): Composition of operations in the worldwide routes.

Table 38. Size limitations of significant routes with highest annual cargo movement demand.

Origin Port	Destination Port [1]	Cargo Type	Annual *CARGO* (t/y) [2]	*L* (m) [2]	*B* (m) [2]
Newcastle	*Japan-A*	Coal	7,725,659	300	50
Newcastle	*Japan-B*	Coal	12,899,395	300	50
Newcastle	*Japan-D*	Coal	8,431,933	300	50
Newcastle	*Japan-E*	Coal	7,097,576	300	50
Newcastle	Taichung	Coal	5,739,793	300	50
Newcastle	*Chinese Taipei-A*	Coal	4,715,928	292	45
Newcastle	Kaohsiung	Coal	4,557,594	300	50
Fujairah	Mesaieed	Others	5,667,613	292	45
Fujairah	Middle East	Others	4,150,019	292	45
Cape Preston	Ningbo	Iron Ore	8,059,747	300	48

[1] Port cluster of *Japan-A*: 19 ports of Gushikawa, Hakata, Hibikishinko, etc.; *Japan-B*: 26 ports of Etajima, Hashihama, Higashi-Harima, etc.; *Japan-D*: 12 ports of Hachinohe, Haramachi, Ishinomaki, etc.; *Japan-E*: 9 ports of Ishikawa, Maizuru, Misumi, etc. *Chinese Taipe-A*: 8 ports of Taipei, Hualien, Suao, etc.
[2] *CARGO*: annual cargo movement demand (t/y); *L*: new ships' length; *B*: new ships' breadth.

Furthermore, in the case of voyage-charter contracts, new ship C with a DWT of 75,000 is the most allocated in both COST- and GHG-optimized cases. Figure 43 represents the average monthly cargo movement demand used in the ship allocation with the new ships instance. It can be ascertained that the monthly cargo movement demand, on average, lay under 75,000 tons. This condition confirms the competitiveness of new ship C since this size category is the largest possible to transport the monthly cargo movement.

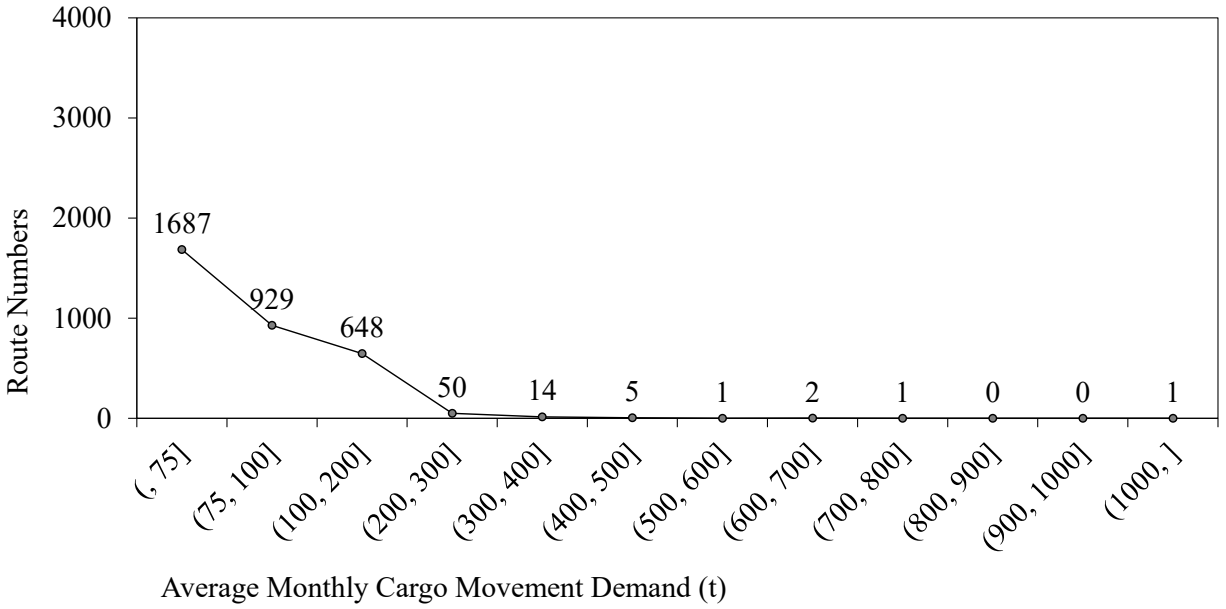

Figure 43. Average monthly cargo movement demand used in the ship allocation with new ships instance (case studies 6c and 6d).

5.3. Case Studies intended for Panamax Dry Bulk Carrier of Specific Ship Operator

5.3.1. Overview of Case studies intended for Future Scenario

In the previous sections, we presented the case studies considering worldwide ship allocation. These tend to give wide perspective towards the implementation of our system. Given that worldwide applicability have been explored, this study conduct the case study of ships operated by specific ship operator.

We conducted case studies using algorithms 2 and 3, optimization of ship allocation time- and voyage-charter contracts intended for the Panamax dry bulk carriers of Ship Operator **A** (case study 7). The aim was to confirm the different results delivered by the proposed algorithms. The following were the objectives of the simulations:

- Target ship: Panamax dry bulk carriers of Ship Operator **A** (DWT 74,000-93,000, 32 ships);
- Cargo types: Iron ore, coal, grain, and others;
- Route: Worldwide (sailing routes served by target ship);
- Operation period: 2018;

- Assumed fuel attributes (specific fuel consumption, g/kWh; emissions factor, t-CO2/t-fuel; fuel prices, USD): HFO (175–185; 3.114; 300–375) and MDO (daily average fuel consumption [28,29]; 3.206; 600).

Table 39 presents the size categories consisting of ship lists of Ship Operator **A**. Herein, we are able to reconstruct the ship allocation considering COST- or GHG-optimized using the proposed algorithms. Because GHG emissions are linear to fuel consumption, this section discusses the actual ship allocation and several case studies focusing on COST-optimized cases of ship allocation using only existing ships in the time-charter (Case 7a) and voyage-charter (7b) contracts, and ship allocation with new ships presence in voyage-charter contract (Case 8).

Table 39. Size categories consisted in ship list of Ship Operator **A**.

Ship Size Category	Ship Numbers	*DWT* [1]	*L* [1] (m)	*B* [1] (m)	Avg. Ship Age
A	8	75,000	225	32.3	17.1
B	10	82,000	229	32.3	8.5
C	9	85,000	229	35.0	5.9
D	4	93,000	229	38.0	10.3

[1] typical DWT: deadweight tonnage; L: length; B: breadth.

5.3.2. Actual Ship Allocation of Panamax Dry Bulk Carriers of Ship Operator A

The cargo types in the actual ship allocation of Ship Operator **A** are shown in Figure 44, indicating that the majority of transported cargo types were grain and coal, where the major CARGO is in the Brazil–China routes.

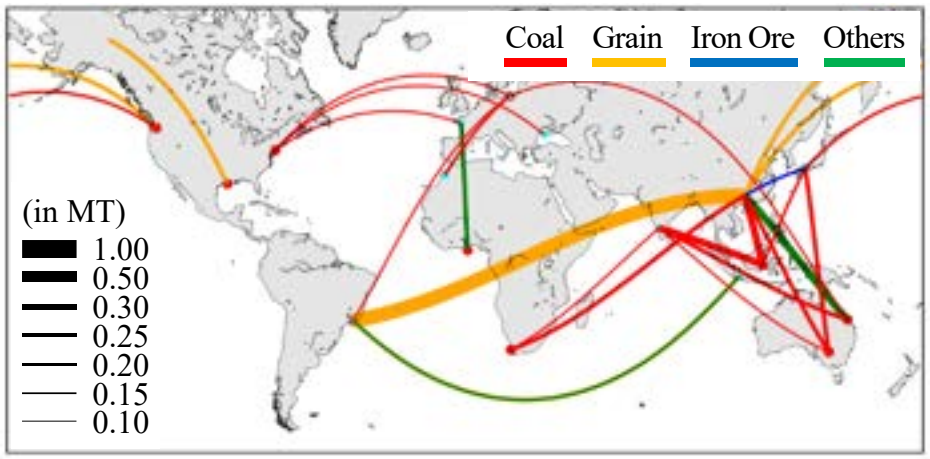

Figure 44. Visualization of actual ship allocation of panamax dry bulk carrier of Ship Operator **A**.

5.3.3. Case study 7: Optimization of Ship Allocation in Time- and Voyage-Charter Contracts using Existing Ships

5.3.3.1. Definition of Case Study 7

This simulation is arranged to evaluate the proposed algorithm 3, which is an optimization for reconstructing ship allocation in voyage-charter contracts. Worldwide, Ship Operator **A** operated 32 ships carrying four types of cargo, mainly in the voyage-charter scheme. Hence, the total COST and GHG emissions resulting from the simulations are observed. This case study covered a ship allocation optimization using only the existing ships of Ship Operator **A**, following these parameters:

- Method: Allocation algorithms 2 and 3; an optimization for reconstructing ship allocation in time- and voyage charter contract;
- Offered ships: The existing ships operating in the actual ship allocation.

5.3.3.2. Results of Case Study 7

The results obtained for case study 7 are listed in Table 40. Case study 7a used algorithm 2 to allocate a ship by assuming it operated in a time-charter contract; therefore, a ship went round-trip, resulting in similar sailing distances back and forth to the origin port. Thus, this algorithm results in a longer ballast sailing day compared to the actual condition and fails to transport all CARGO. Hence, this scheme is considered unsuitable for simulating the actual contract that occurs in the actual ship allocation.

Table 40. Results of case studies 7a and 7b.

Ship Allocation	Annual CARGO (MT)	Annual Operation Numbers	Annual GHG Emissions (MT)	Annual COST (Million USD)	Avg. Annual Laden Sailing Days (d)	Avg. Annual Ballast Sailing Days (d)
Actual	13.7	191	0.427	139.3	180.4	148.6
Case 7a	**11.3**	**156**	0.411	141.3	153.8	**178.7**
Case 7b	13.7	191	0.398	133.7	169.9	**139.5**

Subsequently, case 7b, using algorithm 3, allocated a ship by assuming that it operated in a voyage-charter contract; thus, it made it possible for a ship to serve the next closer sailing route after its trip to a destination port. This algorithm results in a shorter ballast sailing day compared to the results of algorithm 2. In conclusion, we can observe that all the CARGO is transported, and there is reduction in total COST and GHG

emissions. Specifically, Figure 45 presents the economic days of the sample ship. At the operation level, we confirmed that using algorithm 3 (case 7b) resulted in ballast sailing days similar to the actual ship allocation.

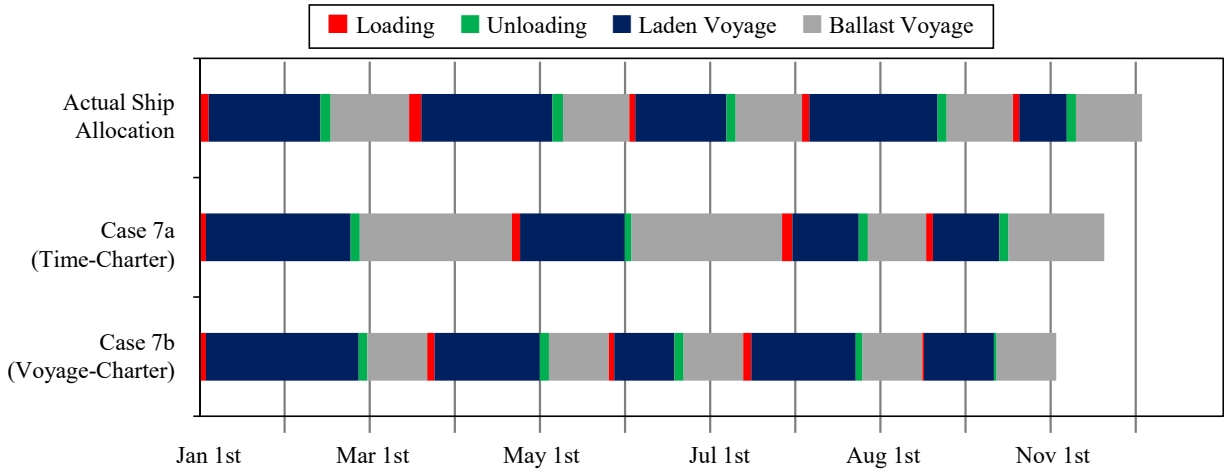

Figure 45. Economic days of a sample ship of Ship Operator **A**.

5.3.4. Case study 8: Optimization of Ship Allocation in Voyage-Charter Contract with New Ships Instance

5.3.4.1. Definition of Case Study 8

This simulation was conducted to examine the demanded new ship specifications by inputting new ships into the simulation. We sampled new ships from each size category that occurred during the actual ship allocation (see Table 39). These ships were proposed to have a higher efficiency for a lower main engine power. This was determined by calculating the ADM [42,56,57], as shown in Figure 46. These ships can be allocated indefinitely, allowing the replacement of the existing ship operations. Hence, ships with high competitiveness against the existing ships can be observed.

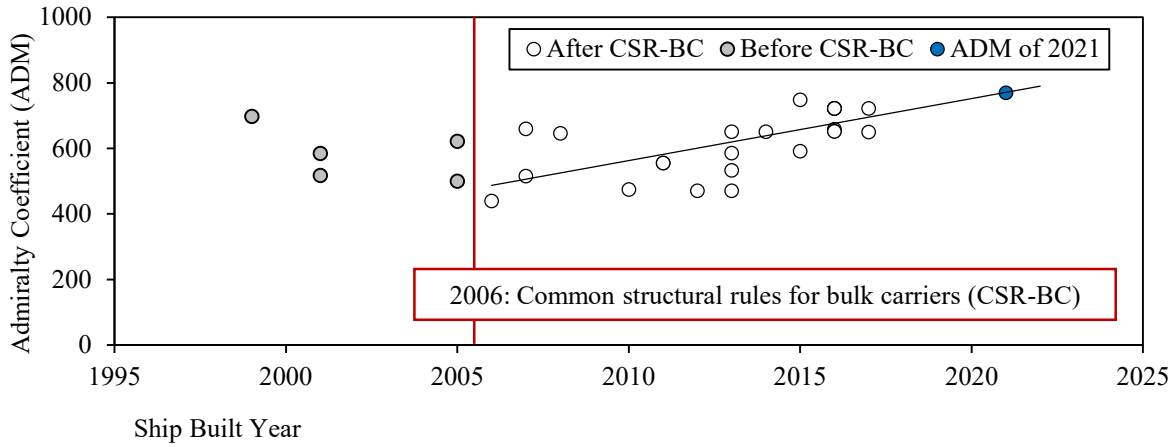

Figure 46. Admiralty coefficient of ships of Ship Operator A.

Extended from case study 7, this case study proposes new ships for COST-optimized ship allocation in voyage-charter contracts, following these parameters:

- Method: Allocation algorithm 3: Optimization for reconstructing ship allocation in voyage-charter contracts.
- Offered ships: Existing ships in case study 7 and four new ships sampled from each size categories consisted in existing ships, as shown in Table 41.

Table 41. Proposed new ship specifications.

New Ship	*DWT* [1]	*d* [1] (m)	*B* [1] (m)	*L* [1] (m)	*v* [1] (kn)	*ME* [2] (kW)	*Age* [3]
A	75,000	14.0	32.3	225	14.5	**7746**	1
B	82,000	14.5	32.3	229	14.5	**8023**	
C	85,000	14.5	35.0	229	14.5	**8464**	
D	93,000	14.9	38.0	229	14.5	**9105**	

[1] *DWT*: new ships' deadweight tonnage; *d*: new ships' draught; *B*: new ships' breadth; *L*: new ships' length; *v*: new ships' design speed;

[2] *ME*: main engine;

[3] *Age*: assumed ship age.

5.3.4.2. Results of Case Study 8

As new ships can be allocated indefinitely, case study 8 optimized ship allocation by allowing existing ships to be replaced by new ships. Changes in the composition of the ship allocation can be observed, as shown in Table 42.

Table 42. Allocated ships and operation numbers in case study 8.

Ship Size Category	Actual Ship Allocation		Case 8 (Voyage-Charter with New Ships)	
	Ship Numbers	Operation Numbers	Ship Numbers	Operation Numbers **(Changes)**
A	8	48	9	71 (+**23**)
B	10	59	11	66 (+**7**)
C	9	44	6	38 (**-6**)
D	4	30	3	12 (**-18**)
Other	1	10	1	4 (**-6**)
Total	32	191	30	191

In this context, an increase in the number of ships allocated to size categories A and B can be observed. This condition, as a result of significant routes, was served by ships with these size categories, as shown in Figure 47.

(a) Actual Ship Allocation

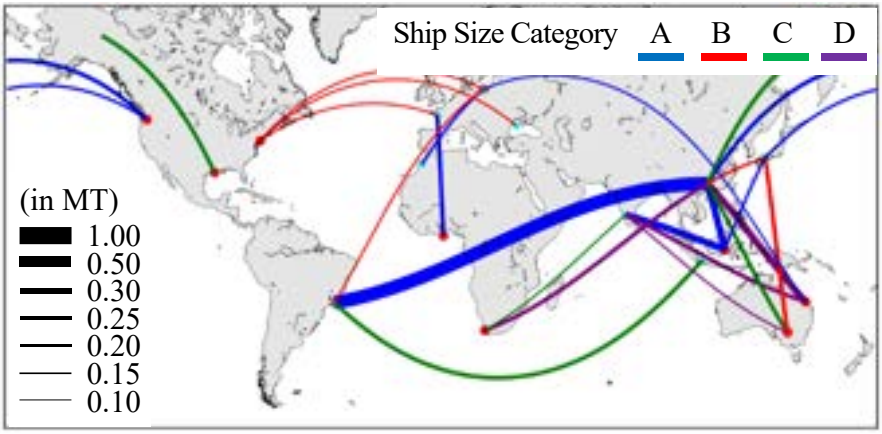

(b) Case 8: Voyage-Charter Optimization with New Ships Presence

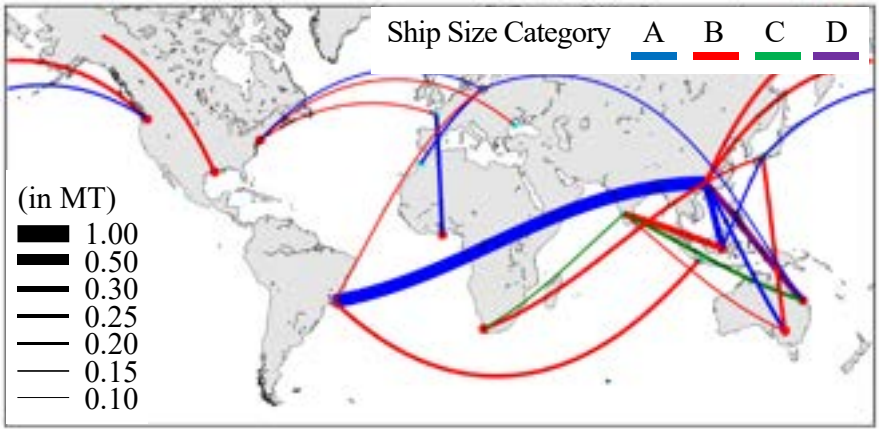

Figure 47. Visualization of actual ship allocation and ship allocation optimization of case study 8.

Moreover, considering the ship ages in actual ship allocation, ships with size category A are fairly older (more than 15 years old); thus, this emphasizes the importance of introducing new ships with higher efficiency, as shown in Figure 48.

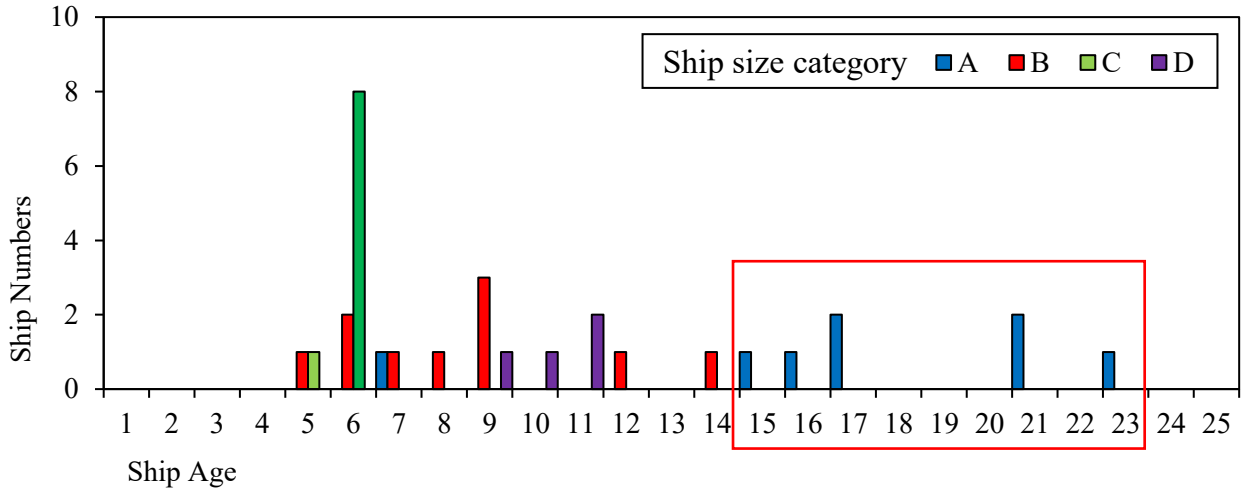

Figure 48. Ship age of ships in the actual ship allocation of Ship Operator **A**.

5.4. Case Studies intended to examine Competitive Ship Dimension of Panamax and MiniCape Dry Bulk Carriers

5.4.1. Overview of Case Studies intended to examine Competitive Ship Dimension of Panamax Dry Bulk Carrier

In this section, we aimed to examine the changes in the allocated ships dimension by presenting only new ships to allocate worldwide CARGO of Panamax–MiniCape dry bulk carriers. This case was aimed to examine the changes in the allocated ships dimension.

We conducted case studies using algorithms 2 and 3, optimization of ship allocation time- and voyage-charter contracts intended for the proposed new ships which sampled from the ship dimension consisted in worldwide ship allocation of Panamax–MiniCape dry bulk carrier, as shown in Table 43. The following were the objectives of the simulations:

- Target ship: Panamax and MiniCape dry bulk carriers (DWT 65,000-140,000, 6 ships);
- Cargo types: Iron ore, coal, grain, and others;
- Route: Worldwide (sailing routes served by Panamax and MiniCape dry bulk carriers);
- Operation period: 2018;

- Assumed fuel attributes (specific fuel consumption, g/kWh; emissions factor, t-CO2/t-fuel; fuel prices, USD): HFO (175–185; 3.114; 300–375) and MDO (daily average fuel consumption [28,29].

Table 43. Assumed specifications of the new ships.

New Ship	*DWT* [1]	*d* (m) [1]	*B* (m) [1]	*L* (m) [1]	*v* (kn) [1]	*Age* [2]	Existing *ME* Power (kW) [3]	New Ship *ME* Power (kW) [3]	*ME* Power Reduction (%) [3]
A	66,485	12.9	36	200	14.5	1	8470	7892	6.8
B	75,122	13.8	32	225	14.5	1	10,750	8403	21.8
C	85,001	14.0	37	229	14.5	1	9660	9198	4.8
D	95,790	14.5	38	235	14.5	1	12,950	9937	23.3
E	106,415	13.6	43	254	14.5	1	13,560	10,807	20.3
F	118,863	14.8	43	260	14.5	1	13,560	11,757	13.3

[1] *DWT*: new ships' deadweight tonnage; *d*: new ships' draught; *B*: new ships' breadth; *L*: new ships' length; *v*: new ships' design speed;
[2] *Age*: assumed ship age;
[3] *ME*: main engine.

5.4.2. Case study 9: Optimization of Ship Allocation in Time- and Voyage-Charter Contracts using only New Ships

5.4.2.1. Definition of Case Study 9

Herein, we conducted several simulations using algorithms 2 and 3: optimization of ship allocation time- and voyage-charter contracts with all new ships instance (case study 9). These new ships were offered to transport the worldwide cargo of Panamax and MiniCape dry bulk carriers. Hence, this case study covered a ship allocation optimization using only the new ships, following these parameters:

- Method: Allocation algorithms 2 and 3; an optimization for reconstructing ship allocation in time- and voyage charter contract;
- Offered ships: The new ships sampled from the existing ships consisted in the actual ship allocation (Table 43).

5.4.2.2. Results of Case Study 9

The results obtained for case study 9 are listed in Table 44. It can be observed that both time- and voyage-charter contracts scheme were able to reduce the total COST and GHG emissions compared to the actual ship allocation. This results considered linear to the discussion which already discussed in Section 5.2.7.

Table 44. Results of case study 9.

Case Studies	Total COST in Million USD (Reduction in %)	GHG Emissions in MT (Reduction in %)	Total Operation Numbers (Reduction in %)	Operation Number of Allocated New Ships (%) [1]
Actual ship allocation	9747 (0.0)	30.1 (0.0)	16,110 (0.0)	*na*
Time-Charter COST-optimized	8574 (-12.0	24.3 (-19.3)	12,595 (-21.8)	100
Time-Charter GHG-optimized	8646 (-11.3	23.8 (-20.9)	12,466 (-22.6)	100
Voyage-Charter COST-optimized	8411 (-13.7)	24.3 (-19.4)	15,092 (-6.3)	100
Voyage -Charter GHG-optimized	8498 (-12.8	23.6 (-21.5)	15,096 (-6.3)	100

[1] *na*: not available–no new ship in the ship allocation.

Specifically, Figure 49 indicated the changes in the allocated ships dimension. It can be observed that the largest operation numbers was belong to the ships with DWT 75,000 in the actual ship allocation. In the time-series scheme, both COST- and GHG-optimized allocated largest ships possible with DWT 115,000. On the other hand, an optimization assuming the ships operating in voyage-charter was majorly allocate ships with DWT 85,000.

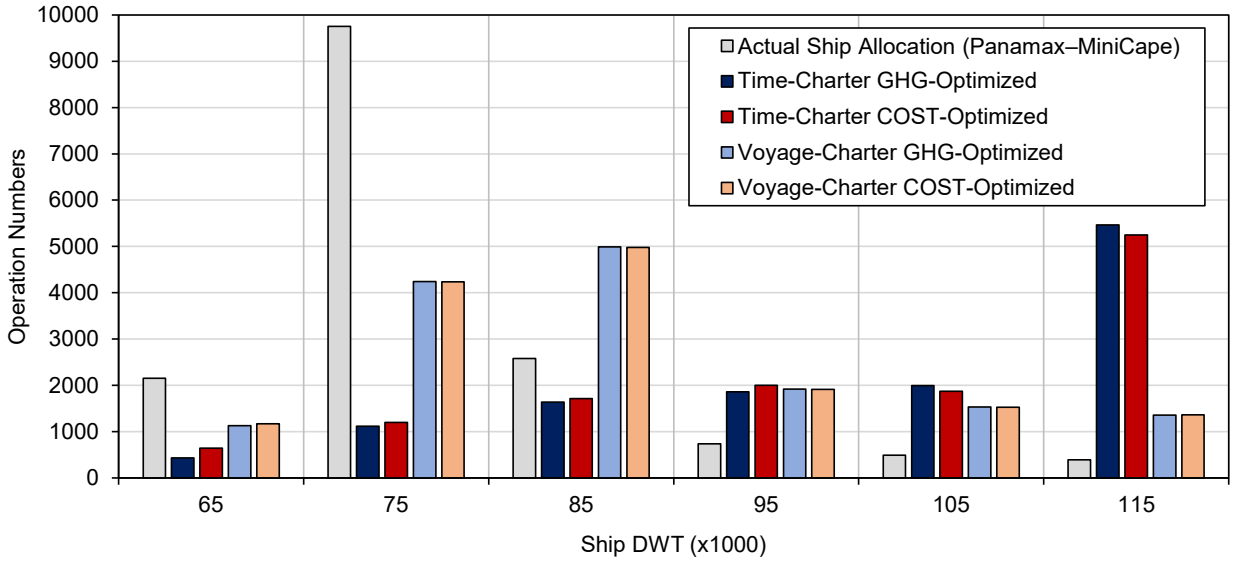

Figure 49. Changes in the allocated ships dimension of case study 9.

5.5. Case Studies intended for Future Scenario

5.5.1. Overview of Case studies intended for Future Scenario

We conducted several simulations using algorithms 2 and 3: optimization of ship allocation time- and voyage-charter contracts with all new ships instance (case study 6). Figure 38 shows an overview of case studies of Panamax–MiniCape dry bulk carrier. The following were the objectives of the simulations:

- Target ship: New ships of case study 6;
- Cargo types: Iron ore, coal, grain, and others;
- Route: Worldwide (sailing routes served by target ship);
- Operation period: 2018;
- Assumed fuel attributes (specific fuel consumption, g/kWh; emissions factor, t-CO2/t-fuel; fuel prices, USD): HFO (175–185; 3.114; 300–375), MDO (daily average fuel consumption [28,29]; 3.206; 600), LNG (148; 2.750; 590), and MeOH (350; 1.375; 400).

Table 45. Overview of case studies intended for future scenario.

Case Study	Method	Offered Ships [1]	Ship Allocation [2]	Cargo Movement [3]	Operation Conditions [4]	Fuel Attributes [5]
9	Algorithms 2, 3	*new*	*optimized*	*2030*; 2050; *Ir, Co, Gr, Ot*	*predicted*	*2030–2050*

[1] *new*: new ships instance.

[2] *optimized*: reconstructed ship allocation.
[3] *2030*: predicted worldwide cargo movement in 2030 [58]; *2050*: worldwide cargo movement in 2050 [58]; *Ir*: iron ore; *Co*: coal; *Gr*: grain; *Ot*: others.
[4] *predicted*: predicted operation conditions by using route-base average.
[5] *2030–2050*: assumed fuel attributes for future scenarios.

5.5.2. *Case study 10: Optimization of Ship Allocation in Time- and Voyage-Charter Contracts intended for Future Scenario*

5.5.2.1. Definition of Case Study 10

This section examined the potential ship allocation to achieve IMO GHG reduction strategy [28,29,49-51]. The minimum ambition sets a target of GHG emissions reduction by at least 50% by 2050 compared to 2008. Figure 50 shows the linear projection of the GHG emissions target from 2008 to 2050. We defined discrete case studies to cover short- and long-term scenarios of 2030 and 2050, respectively. The following were the parameters of case study 10:

- Method: Allocation algorithms 2 and 3;
- Offered ships: Eight new ships of case study 6 with the future ADM (2030 and 2050) fueled with the alternative fuels with lower emission factors (LNG and MeOH).

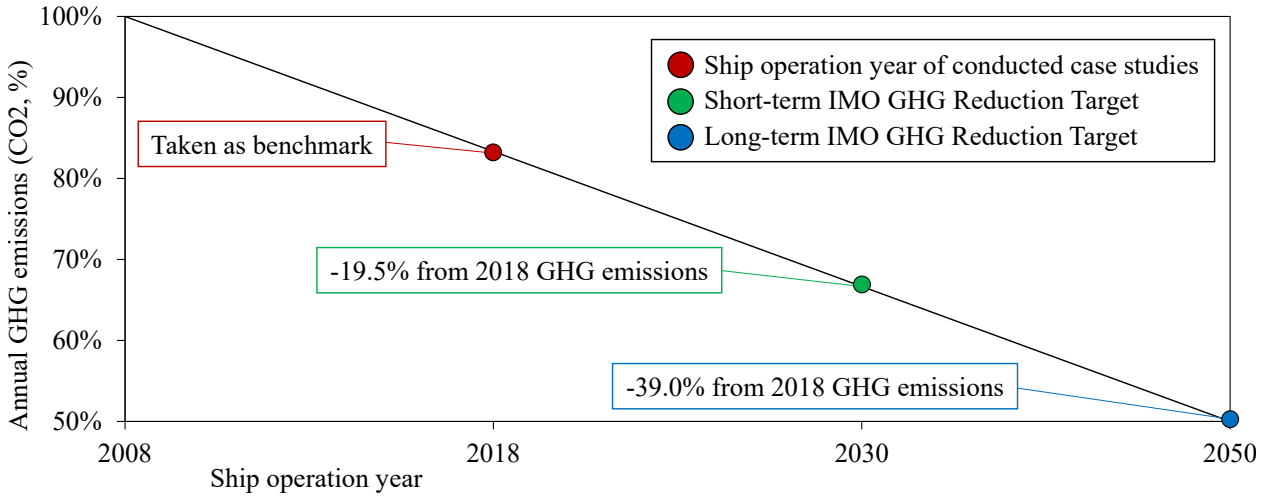

Figure 50. Linear projection of the GHG emissions target from 2008 to 2050 [49-51].

Eight new ship specifications were sampled as case study 6. We defined these ships considering the ADM of Panamax–MiniCape dry bulk carriers in 2030 and 2050: 786.17 and 964.42, respectively, as shown in Figure 51. Similar to case study 6, the main

engine power (P_s') of these new ships was reduced by retaining a constant ship s design speed [56]. Thus, the defined specifications of the new ships in 2030 and 2050 are listed in Table 46.

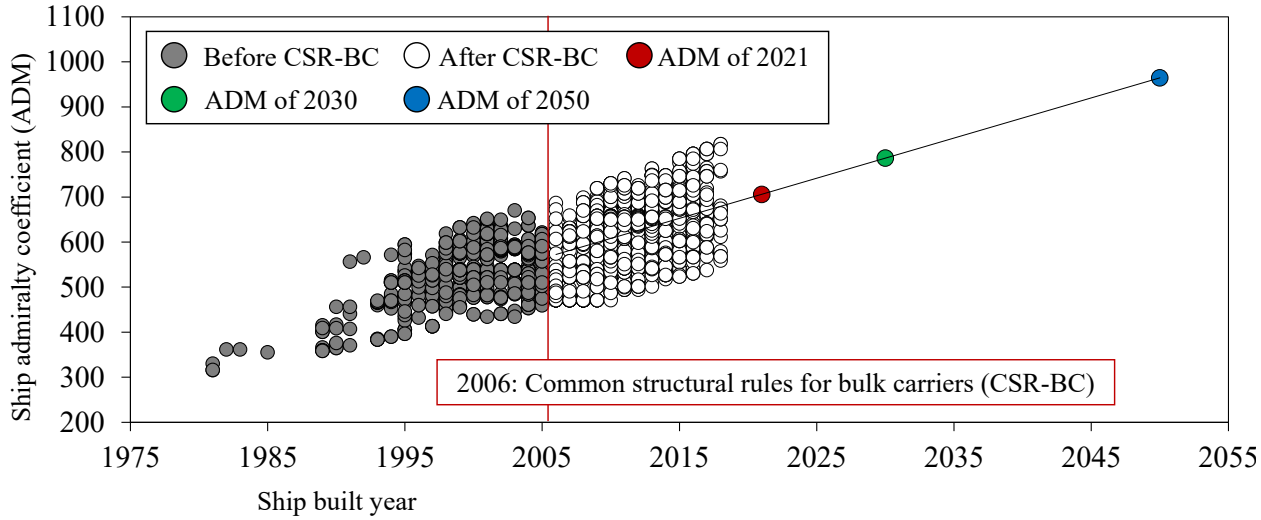

Figure 51. ADM of Panamax and MiniCape in 2030 and 2050 [42,56,57].

Table 46. Defined specifications of the new ships in 2030 and 2050.

New Ship	*DWT* [1]	*d* (m) [1]	*B* (m) [1]	*L* (m) [1]	*v* (kn) [1]	*Age* [2]	Existing *ME* Power (kW) [3]	*ME* Power in 2030 (kW) [3]	*ME* Power in 2050 (kW) [3]
A	66,485	12.9	36	200	14.5	1	8470	7087	5777
B	67,508	13.2	32	225	14.5	1	9000	7230	5893
C	75,122	13.8	32	225	14.5	1	10,750	7546	6151
D	77,679	12.9	37	229	14.5	1	10,224	7725	6298
E	85,001	14.0	37	229	14.5	1	9660	8783	7160
F	95,790	14.5	38	235	14.5	1	12,950	8923	7274
G	106,415	13.6	43	254	14.5	1	13,560	9705	7911
H	118,863	14.8	43	260	14.5	1	13,560	10,558	8606

[1] *DWT*: new ships' deadweight tonnage; *d*: new ships' draught; *B*: new ships' breadth; *L*: new ships' length; *v*: new ships' design speed;
[2] *Age*: assumed ship age;
[3] *ME*: main engine.

Moreover, we offer the abovementioned ships to be fueled by low-carbon fuels. To conclude what has already been discussed in Section 4.4.2, the attributes of total COST and GHG emissions will be altered by considering new fuel attributes for the main engine,

as shown in Table 47. Each of these fuels will be used by the offered ships separately to observe its effect on the global GHG emissions reduction.

Table 47. Properties of various main engine's fuel types in 2030–2050 [28].

Fuel Type	Main Engine Type [1]	Specific Fuel Consumption (g/kWh)	Emission Factors (t-CO2 / t-fuel)	Fuel Price (USD)
HFO	*SSD*	175	3.114	375
Methanol	*SSD*	350	1.375	400
LNG	*LNG-Otto*	148	2.750	590

[1] *SSD*: Slow-speed Diesel; *LNG-Otto*: Slow-speed Dual-fuel.

Furthermore, for this case study, we projected the future annual and monthly cargo movement demand with the assumption that the growth of cargo movement demand is linear between 2030 and 2050 by referring to the Energy Transition Outlook by DNVGL [40,58], as shown in Figure 52.

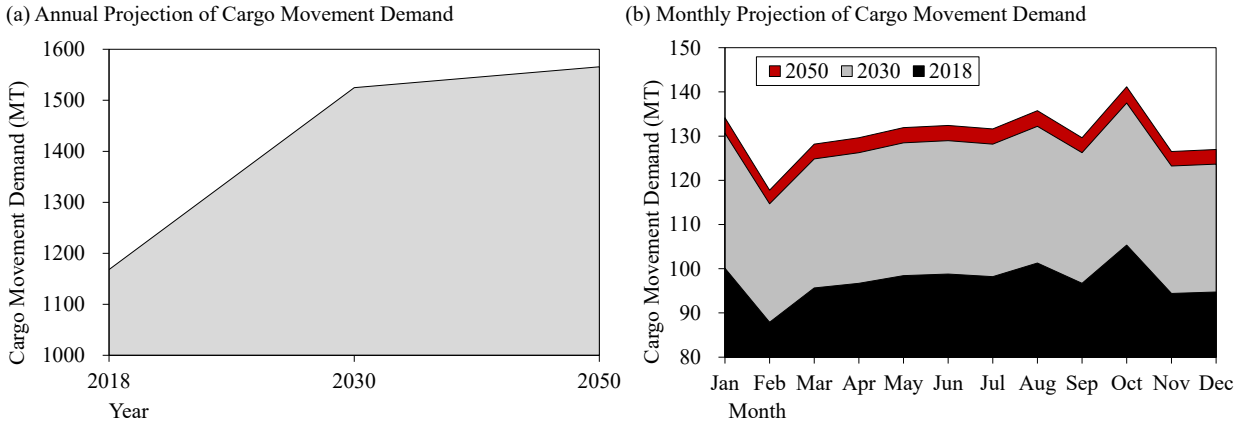

Figure 52. Projection of Cargo Movement Demand [40,58]: (**a**) annual and (**b**) monthly.

As the offered ships could be allocated indefinitely, we discussed the following case studies covered for each term: GHG-optimized ship allocation in time-charter contract using new ships in 2030 fueled by HFO, LNG, and MeOH (case study 10a), GHG-optimized ship allocation in voyage-charter contract using new ships in 2030 fueled by HFO, LNG, and MeOH (case study 10b), GHG-optimized ship allocation in time-charter contract using new ships in 2050 fueled by HFO, LNG, and MeOH (case study 10c), and GHG-optimized ship allocation in voyage-charter contract using new ships in 2050 fueled by HFO, LNG, and MeOH (case study 10d).

5.5.2.2. Results of Case Study 10

This case study formed the future ship allocation in 2030 and 2050 using only new ships. In addition, this case study neglects the capital cost that could occur to construct the offered new ships specification, such as the costs of shipbuilding, new engine type, and administration. In this case study, we offer ships fueled by HFO, LNG, and MeOH to transport the cargo movement of 2030 and 2050. Since this case study offered one-year-old new ships with operation conditions adopted from R-AVG of 2018, this will result in the same average ship age and sailing speed as the actual ship allocation. Thus, we will observe that the average DWT in the future ship allocation consisted of all new ships.

Figure 53 shows the case study 10a results of the ship allocation optimization in the time-charter contract using new ships in 2030. First, we can observe an increase in cargo movement compared to actual ship allocation since this case study used projected cargo movement in 2030. Furthermore, we can observe identical results for all fuel cases. The major routes for all cases resulted in an average DWT of more than 95,000.

Moreover, Figure 54 presents case study 10b results of the ship allocation optimization in voyage-charter contract using new ships in 2030. Contrary to the results of the time-charter contract, these cases allocated ships with various average DWT. In South East Asia–China routes, larger ships with an average DWT of more than 95,000 were allocated. In addition, Brazil–China routes allocated smaller ships with an average DWT of 85,000–95,000. To conclude, despite the variation in average DWT of the allocated ships, the ship allocation in the voyage-charter contract shows identical average DWT for all fuel types.

(a) Case study 10a (GHG-optimized) HFO-fueled

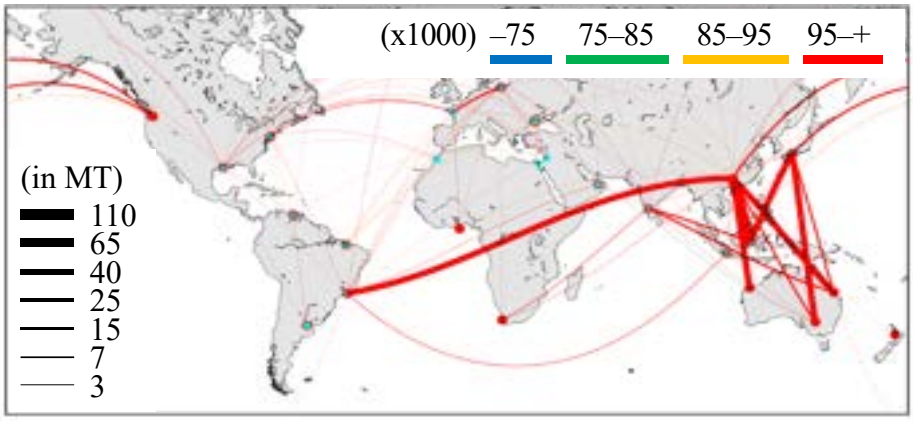

(b) Case study 10a (GHG-optimized) LNG-fueled

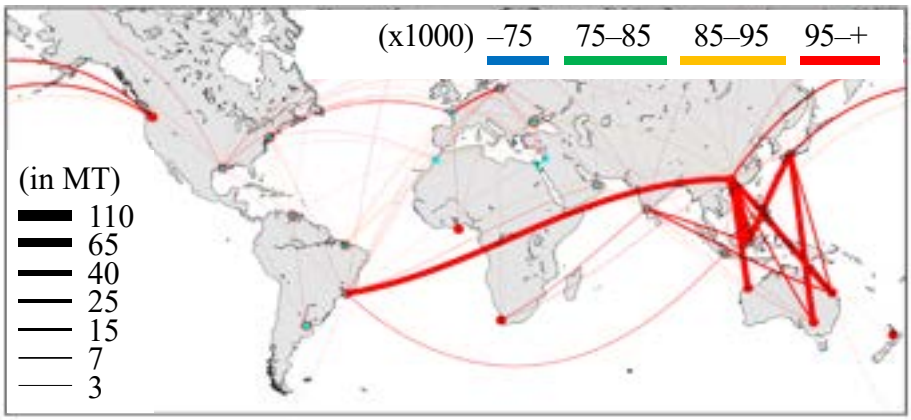

(c) Case study 10a (GHG-optimized) MeOH-fueled

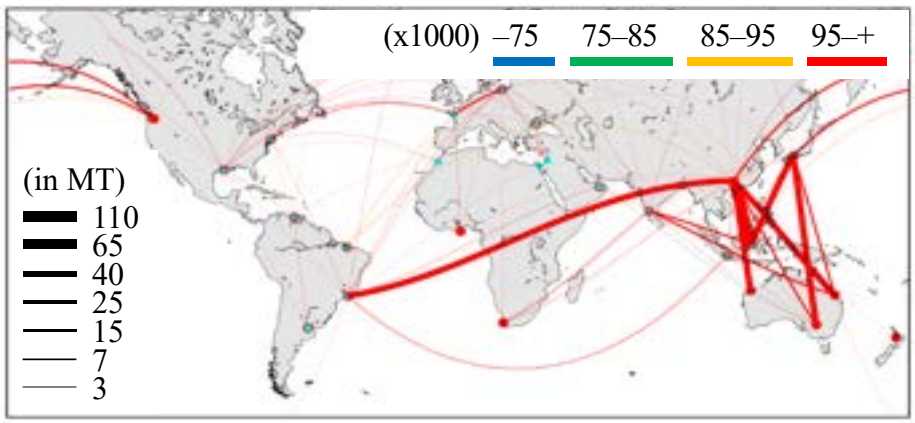

Figure 53. Ship allocation optimization in time-charter contract using new ships in 2030: Case study 10a (GHG-optimized) average DWT using (**a**) HFO, (**b**) LNG, and (**c**) MeOH.

(a) Case study 10b (GHG-optimized) HFO-fueled

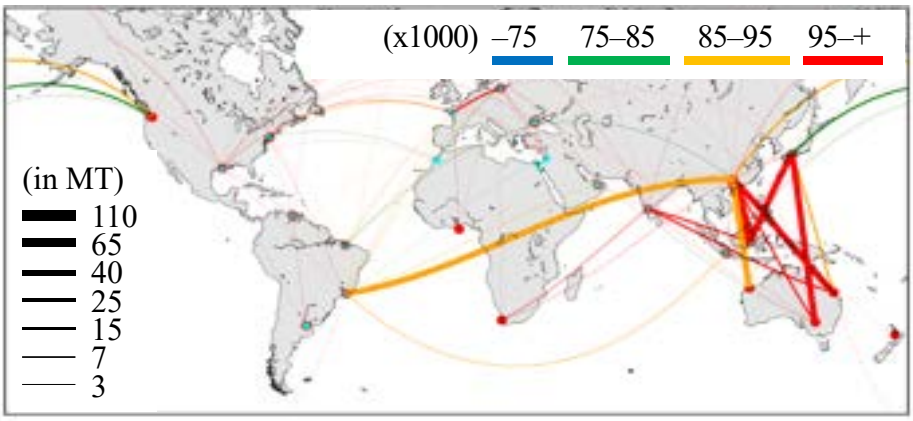

(b) Case study 10b (GHG-optimized) LNG-fueled

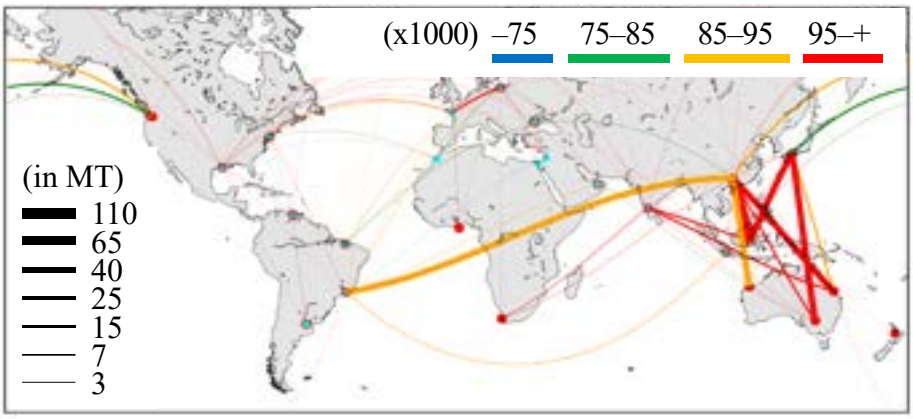

(c) Case study 10b (GHG-optimized) MeOH-fueled

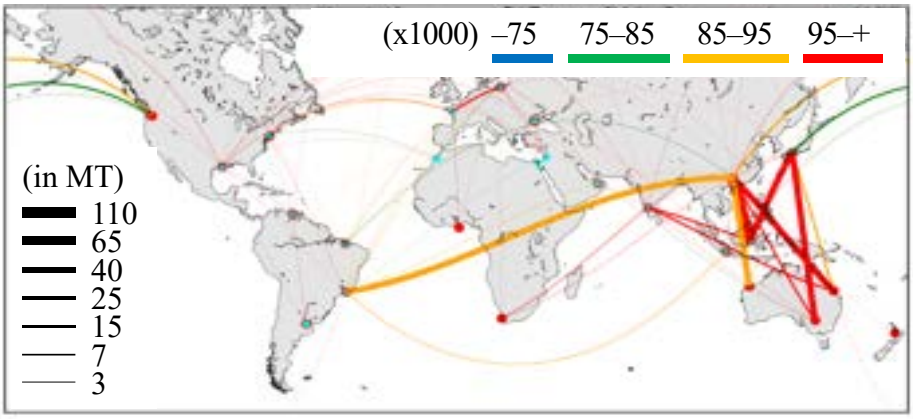

Figure 54. Ship allocation optimization in voyage-charter contract using new ships in 2030: Case study 10b (GHG-optimized) average DWT using (**a**) HFO, (**b**) LNG, and (**c**) MeOH.

Furthermore,

(a) Case study 10c (GHG-optimized) HFO-fueled

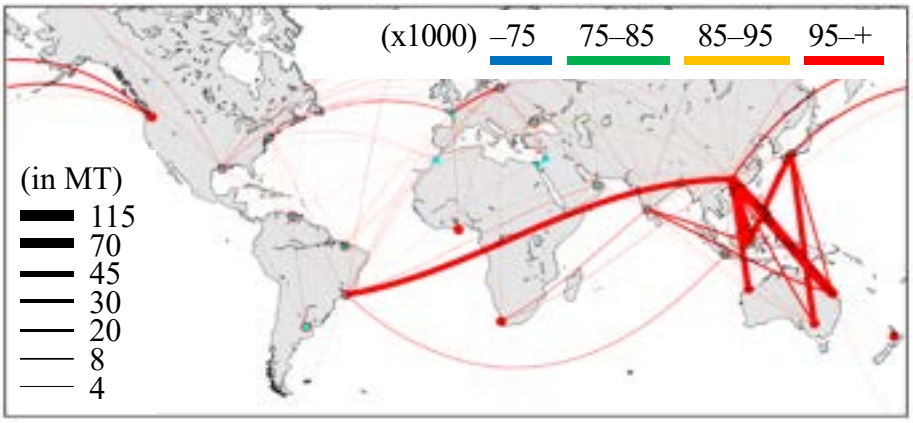

(b) Case study 10c (GHG-optimized) LNG-fueled

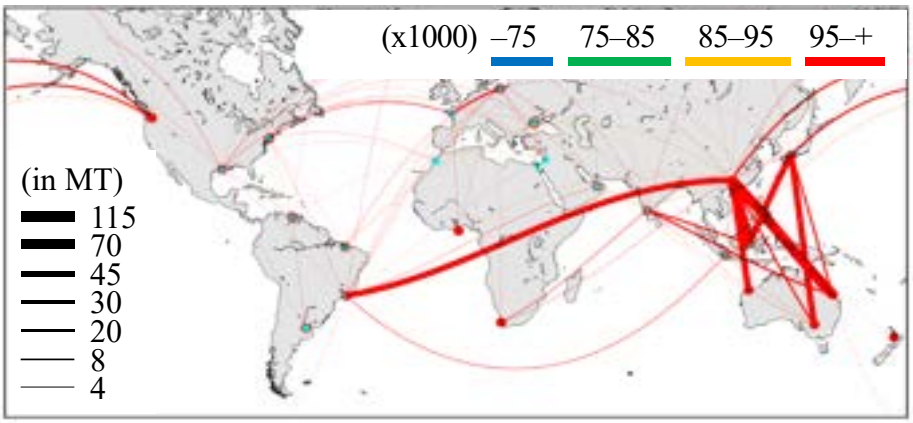

(c) Case study 10c (GHG-optimized) MeOH-fueled

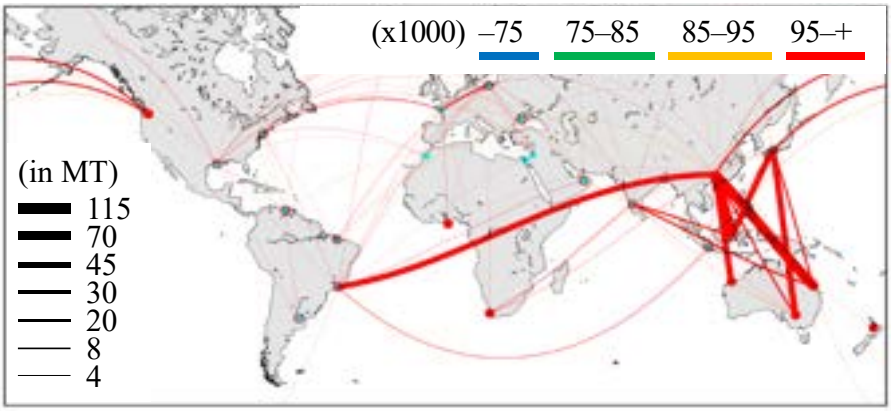

Figure 55 shows the case study 10c results of the ship allocation optimization in the time-charter contract using new ships in 2050. Initially, we can observe an increase in cargo movement compared to case studies 9a and 9b since this case study used projected

cargo movement in 2050. The results represented in

(a) Case study 10c (GHG-optimized) HFO-fueled

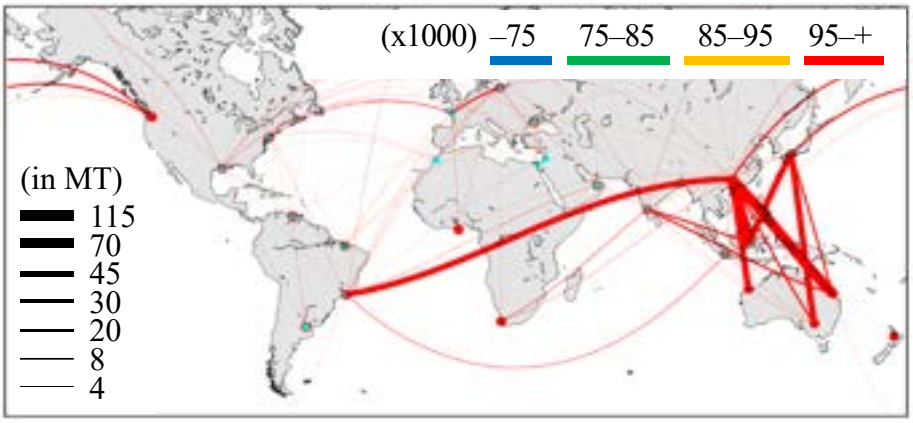

(b) Case study 10c (GHG-optimized) LNG-fueled

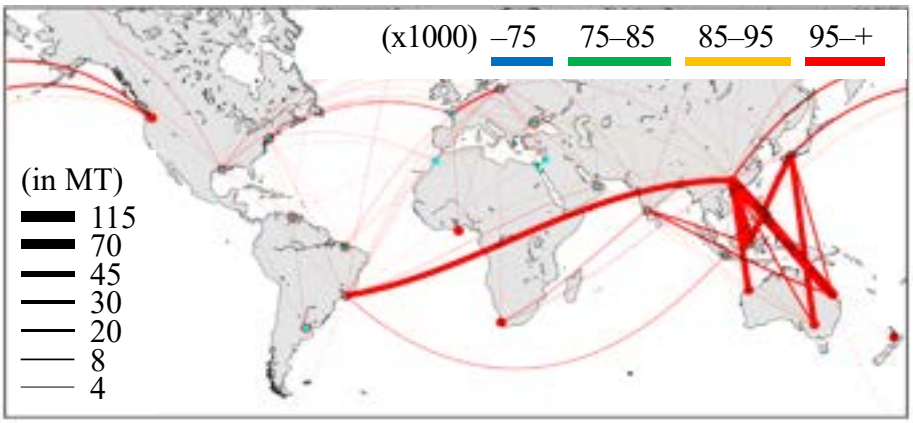

(c) Case study 10c (GHG-optimized) MeOH-fueled

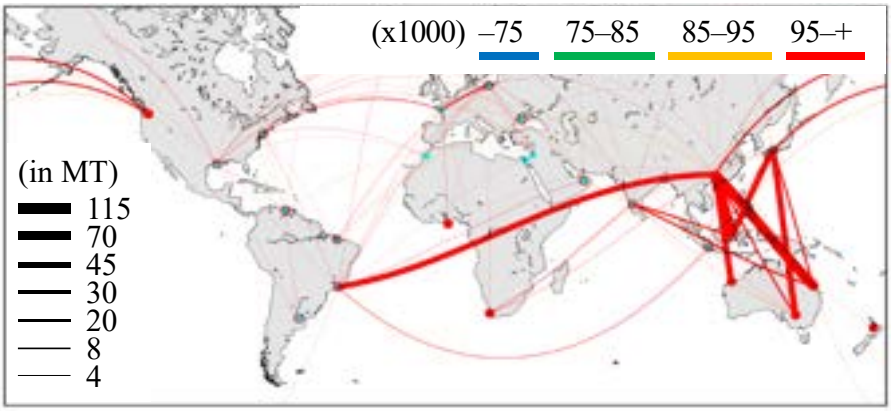

Figure 55 agree with the abovementioned case study 10a. Identically, major routes allocated larger ships with an average DWT of more than 95,000, whereas both of these cases allocated the ships in the scheme time-charter contract.

(a) Case study 10c (GHG-optimized) HFO-fueled

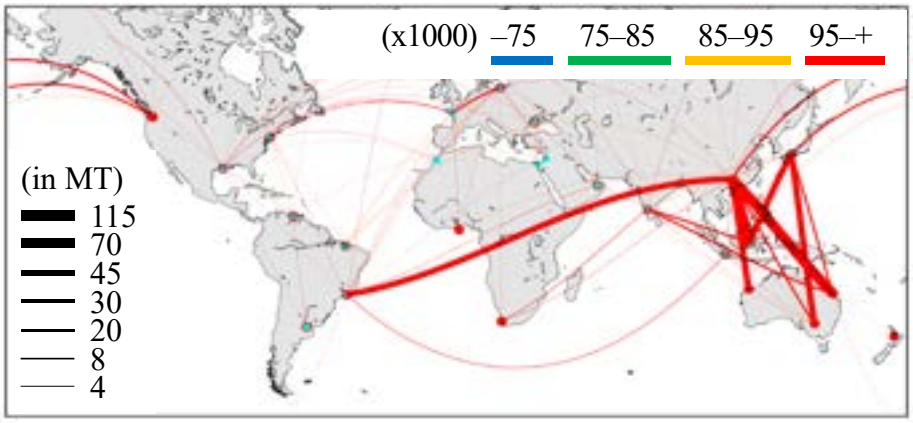

(b) Case study 10c (GHG-optimized) LNG-fueled

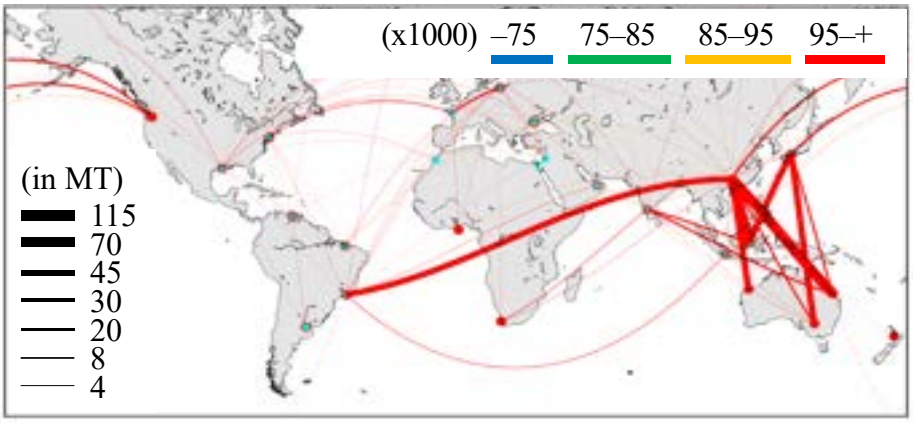

(c) Case study 10c (GHG-optimized) MeOH-fueled

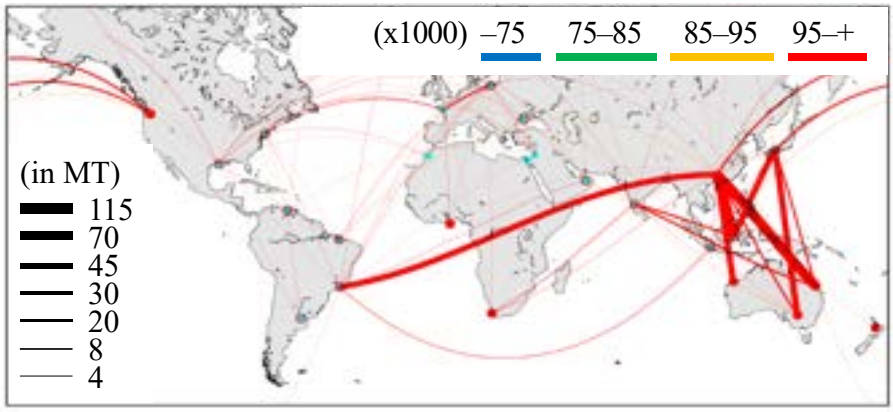

Figure 55. Ship allocation optimization in time-charter contract using new ships in 2050: Case study 10c (GHG-optimized) average DWT using (**a**) HFO, (**b**) LNG, and (**c**) MeOH.

Finally, Figure 56 suggests the case study 10d results of the ship allocation optimization in voyage-charter contract using new ships in 2050. A similar trend of average DWT is also shown here since all these cases allocated ships in the same scheme.

(a) Case study 10d (GHG-optimized) HFO-fueled

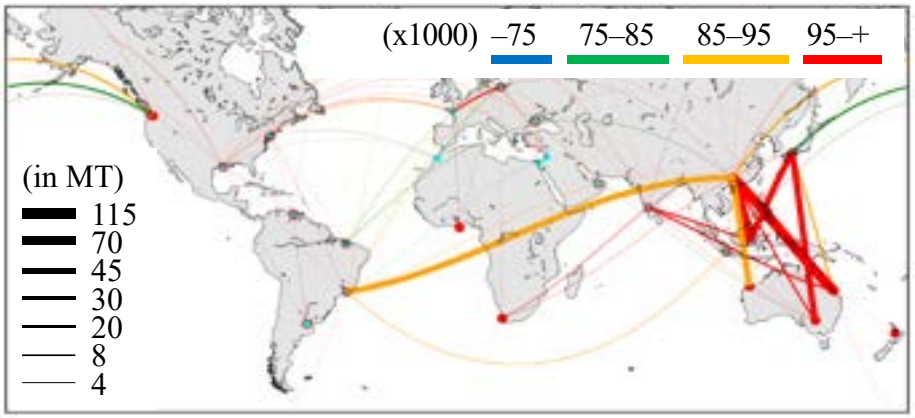

(b) Case study 10d (GHG-optimized) LNG-fueled

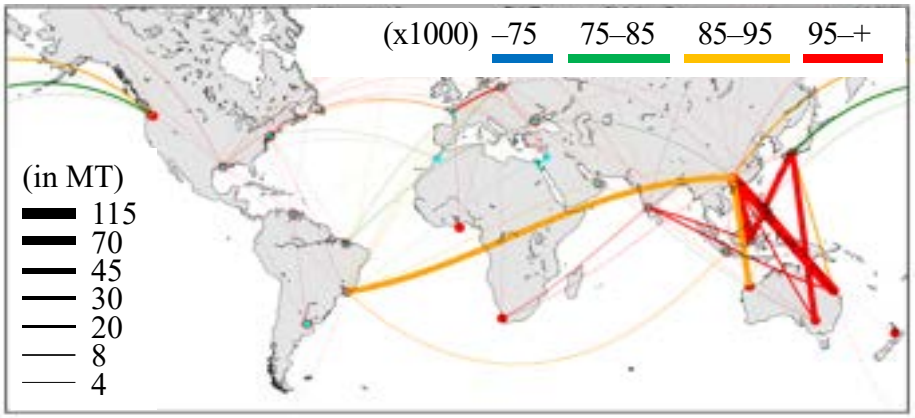

(c) Case study 10d (GHG-optimized) MeOH-fueled

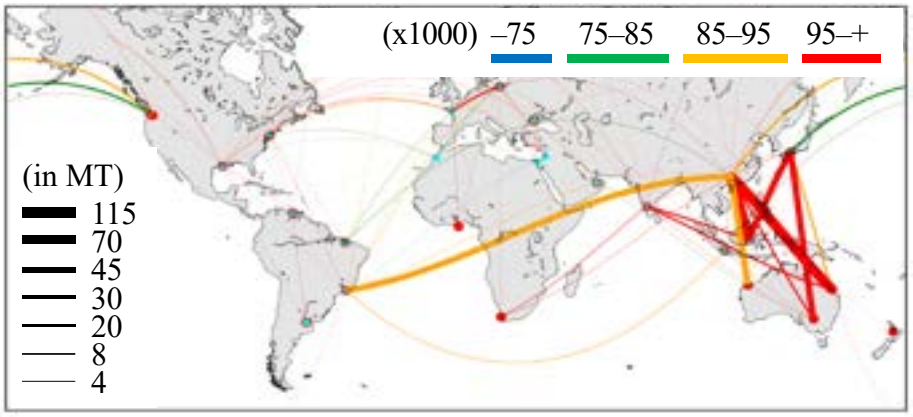

Figure 56. Ship allocation optimization in voyage-charter contract using new ships in 2050: Case study 10d (GHG-optimized) average DWT using (**a**) HFO, (**b**) LNG, and (**c**) MeOH.

5.5.3. Discussion 5: Future Potential Emissions Reductions by using Fuels with Lower Emissions Factors

The total GHG emissions resulting from case study 10 are shown in Table 48. Applying the algorithms 2 and 3 following short- (2030) and long-term (2050) future scenarios, case study 9 offered only new ships with the same specification as new ships introduced in case study 6, but higher ADM considering linear projection to 2030 and 2050. Therefore, neglecting the capital costs of the new ships, major GHG emissions can be ascertained for all fuel type cases.

Table 48. Total GHG emissions of case study 10.

Case Studies	Operation Period	Cargo Movement Demand in t (Increase in %)	GHG Emissions in MT (Reduction in %)	GHG-Effective in t-GHG/t-CARGO (Reduction in %)
Actual ship allocation	2018	1168.2 (0.0)	30.1 (0.0)	0.0257 (0.0)
Case study 10a (HFO-fueled)	2030	1525.0 (30.5)	28.2 (-6.2)	0.0185 (-28.1)
Case study 10a (LNG-fueled)	2030	1525.0 (30.5)	23.0 (-23.5)	0.0151 (-41.4)
Case study 10a (MeOH-fueled)	2030	1525.0 (30.5)	25.8 (-14.2)	0.0169 (-34.2)
Case study 10b (HFO-fueled)	2030	1525.0 (30.5)	27.6 (-8.4)	0.0181 (-29.8)
Case study 10b (LNG-fueled)	2030	1525.0 (30.5)	22.5 (-25.1)	0.0148 (-42.6)
Case study 10b (MeOH-fueled)	2030	1525.0 (30.5)	25.2 (-16.1)	0.0165 (-35.7)
Case study 10c (HFO-fueled)	2050	1565.7 (34.0)	25.1 (-16.6)	0.0160 (-37.8)
Case study 10c (LNG-fueled)	2050	1565.7 (34.0)	20.7 (-31.1)	0.0132 (-48.6)
Case study 10c (MeOH-fueled)	2050	1565.7 (34.0)	23.1 (-23.3)	0.0147 (-42.8)
Case study 10d (HFO-fueled)	2050	1565.7 (34.0)	24.6 (-18.3)	0.0157 (-39.0)
Case study 10d (LNG-fueled)	2050	1565.7 (34.0)	20.3 (-32.4)	0.0130 (-49.5)
Case study 10d (MeOH-fueled)	2050	1565.7 (34.0)	22.6 (-24.8)	0.0144 (-43.9)

Moreover, using LNG as the main engine's fuel, case studies 9a and 9b suggest the highest reduction in total GHG emissions. Referring to these results, Figure 57 represents the annual GHG emissions reduction using LNG. It can be ascertained that using new ships with ADM of 2050 and LNG as the main engine's fuel were not adequate to achieve the IMO GHG reduction target.

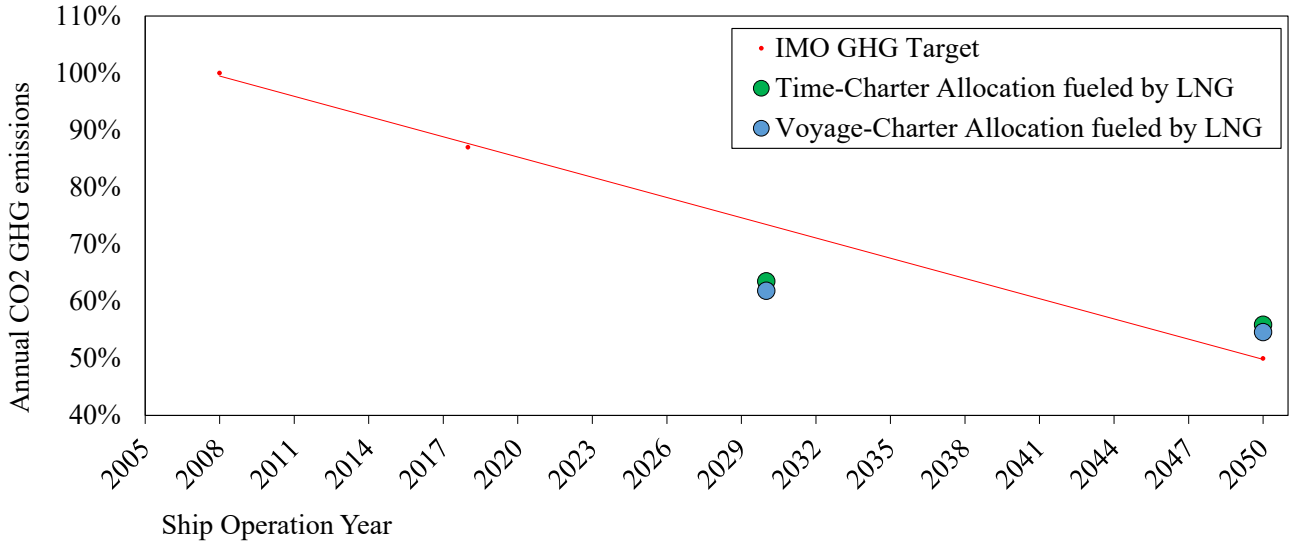

Figure 57. Annual GHG emissions reductions by using LNG (case studies 9a and 9b).

Finally, we examine the effectiveness of an extended ADM by 10% and 20% projected from the linear ADM of Panamax–MiniCape dry bulk carriers, as shown in Figure 58. In this context, the main engine power of the offered ships was reduced accordingly. Figure 59 shows the results of annual GHG emissions reductions by using LNG with an extended ADM of 10% and 20%. It can be observed that the IMO GHG reduction target can be achieved by allocating the ships with the extended ADM by 20%.'

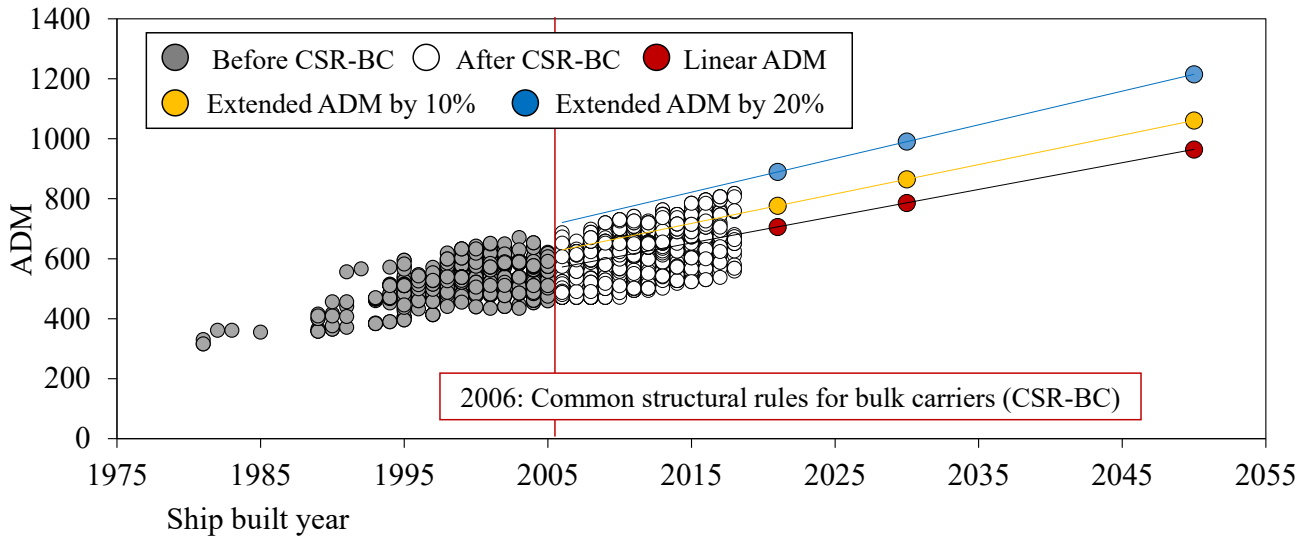

Figure 58. The extended ADM by 10% and 20% projected from the linear ADM of Panamax–MiniCape dry bulk carriers.

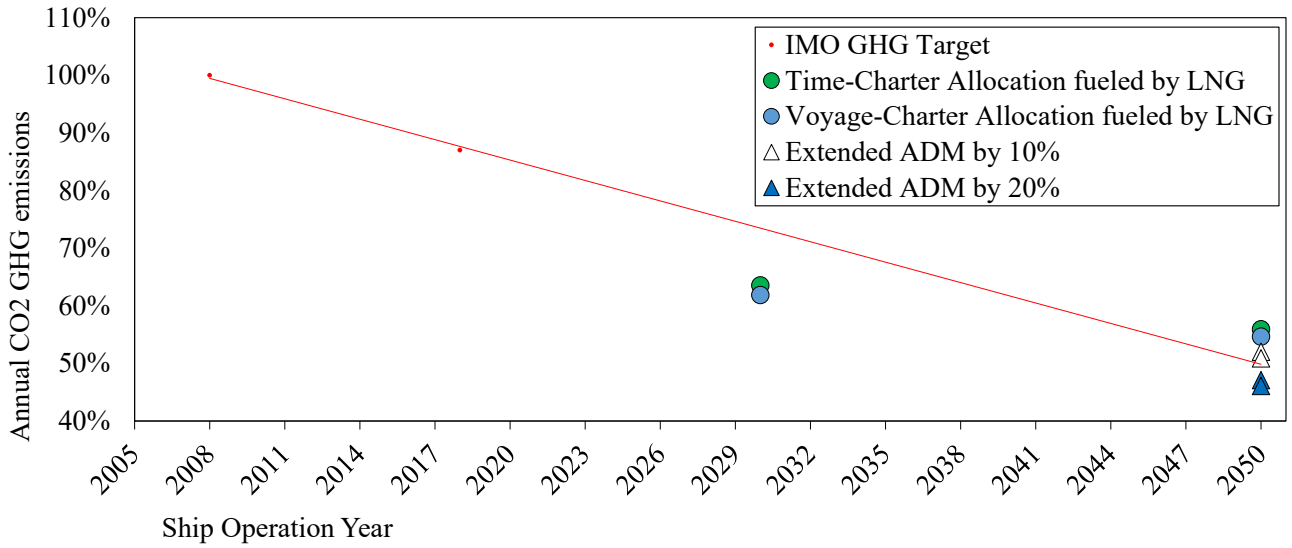

Figure 59. Annual GHG emissions reductions by using LNG (case studies 9a and 9b) with an extended ADM by 10% and 20%.

6. CONCLUDING REMARKS

In this study, we have proposed an enhancement to our basic ship-planning support system. We expanded the scope of our simulations to a worldwide scale, which allowed a broad comprehension of the demand ship specifications. In addition, we developed a ship allocation algorithm to consider the detailed COST and GHG emissions attributes. The system consisted of three distinct models and an algorithm to resemble the ship allocation bidding process: a global network model, cargo movement model, ship model, and ship allocation algorithm. The global network model defined the main ports and port clusters, resulting in a cluster of ports and their attributes, port and route limitations, and sailing distances. The cargo movement model specified the cargo movement and cargo types between the ports. The ship model represented each ship and its specifications. This model predicted the operating conditions: draught rate, average sailing speed, and port staying time for each ship serving a particular route.

Ultimately, as the core of our system, the ship allocation algorithm reconstructed the operation-level ship allocation. It calculated COST and GHG emissions for each ship, and a greedy algorithm was used to resemble the ship allocation. This study proposed three algorithms: ship replacement while preserving the existing ship allocation and optimization for reconstructing the ship allocation in time- and voyage-charter contracts scheme. Allocation algorithm 1 offered a new ship with enhanced performance for each existing ship without changing the current ship allocation. Additionally, we reallocated the ship by applying allocation algorithms 2 and 3, which optimized the total COST and GHG emissions assuming the ships operated in time- or voyage-charter contracts manner. We conducted discrete simulations: optimization using only the existing ships operating in the actual ship allocation and with new ships instance. The ship allocation optimization indicated that significant reductions in the total COST and GHG emissions were not achievable using only the existing ships. Using the developed system, we could recreate an operation-level ship allocation considering various scenarios.

Finally, we confirmed the demanded new ship specifications by presenting the new ships instance. However, this study is only feasible for the current constraints of the Capesize and Panamax–MiniCape dry bulk carriers operating in the time- and voyage-charter contract, despite the presented results. The application of the proposed system for the accumulated ship size categories such as Handymax–Capesize dry bulk carriers are considered future tasks.

Likewise, considering the importance of weather routing, the weather correction factor in the main engine's actual power calculation, which was previously assumed constant, is possibly varied [59]. Hence, further studies are crucial to assess the applicability of our system beyond these limitations.

REFERENCES

1. Stopford, M. *Maritime economics 3e*; Routledge: 2008.
2. Fan, J.; Han, F.; Liu, H. Challenges of big data analysis. *National science review* **2014**, *1*, 293-314.
3. Alharthi, A.; Krotov, V.; Bowman, M. Addressing barriers to big data. *Business Horizons* **2017**, *60*, 285-292.
4. Saggi, M.K.; Jain, S. A survey towards an integration of big data analytics to big insights for value-creation. *Information Processing & Management* **2018**, *54*, 758-790.
5. IMO. AIS transponders. Available online: https://www.imo.org/en/OurWork/Safety/Pages/AIS.aspx (accessed on 28 September 2021).
6. Svanberg, M.; Santén, V.; Hörteborn, A.; Holm, H.; Finnsgård, C. AIS in maritime research. *Marine Policy* **2019**, *106*, 103520.
7. Bauk, S. A Review of NAVDAT and VDES as Upgrades of Maritime Communication Systems. *Advances in Marine Navigation and Safety of Sea Transportation* **2019**, 81-82.
8. IMO. Voyage Data Recorders. Available online: https://www.imo.org/en/OurWork/Safety/Pages/VDR.aspx (accessed on 28 September 2021).
9. Munim, Z.H.; Dushenko, M.; Jimenez, V.J.; Shakil, M.H.; Imset, M. Big data and artificial intelligence in the maritime industry: a bibliometric review and future research directions. *Maritime Policy & Management* **2020**, *47*, 577-597.
10. Mirović, M.; Miličević, M.; Obradović, I. Big data in the maritime industry. *NAŠE MORE: znanstveni časopis za more i pomorstvo* **2018**, *65*, 56-62.
11. Zaman, I.; Pazouki, K.; Norman, R.; Younessi, S.; Coleman, S. Challenges and opportunities of big data analytics for upcoming regulations and future transformation of the shipping industry. *Procedia engineering* **2017**, *194*, 537-544.
12. Sanchez-Gonzalez, P.-L.; Díaz-Gutiérrez, D.; Leo, T.J.; Núñez-Rivas, L.R. Toward digitalization of maritime transport? *Sensors* **2019**, *19*, 926.
13. Yang, C.-H.; Chang, P.-Y. Forecasting the demand for container throughput using a mixed-precision neural architecture based on CNN–LSTM. *Mathematics* **2020**, *8*, 1784.
14. Jugović, A.; Komadina, N.; Perić Hadžić, A. Factors influencing the formation of freight rates on maritime shipping markets. *Pomorstvo* **2015**, *29*, 23-29.
15. Akar, O.; Esmer, S. Cargo demand analysis of container terminals in Turkey. *Journal of ETA Maritime Science* **2015**, *3*, 117-122.
16. Gökkuş, Ü.; Yıldırım, M.S.; Aydin, M.M. Estimation of container traffic at seaports by using several soft computing methods: a case of Turkish Seaports. *Discrete Dynamics in Nature and Society* **2017**, *2017*.
17. Jia, H.; Prakash, V.; Smith, T. Estimating vessel payloads in bulk shipping using AIS data. *International Journal of Shipping and Transport Logistics* **2019**, *11*, 25-40.

18. Zhou, X.; Hu, Q. Estimation of Shipment Size in Seaborne Iron Ore Trade. *TransNav: International Journal on Marine Navigation and Safety of Sea Transportation* **2019**, *13*.
19. Kanamoto, K.; Murong, L.; Nakashima, M.; Shibasaki, R. Can maritime big data be applied to shipping industry analysis? Focussing on commodities and vessel sizes of dry bulk carriers. *Maritime Economics & Logistics* **2021**, *23*, 211-236.
20. Prochazka, V.; Adland, R.; Wolff, F.-C. Contracting decisions in the crude oil transportation market: Evidence from fixtures matched with AIS data. *Transportation Research Part A: Policy and Practice* **2019**, *130*, 37-53.
21. Sharma, R.; Sha, O. Development of an integrated market forecasting model for shipping, and shipbuilding parameters. In Proceedings of the Proceedings of the RINA—International Conference on Computer Applications in Shipbuilding, Portsmouth, UK, 2007; pp. 18-20.
22. Wada, Y.; Yamamura, T.; Hamada, K.; Wanaka, S. Evaluation of GHG Emission Measures Based on Shipping and Shipbuilding Market Forecasting. *Sustainability* **2021**, *13*, 2760.
23. Wada, Y.; Hamada, K.; Hirata, N. Shipbuilding capacity optimization using shipbuilding demand forecasting model. *Journal of Marine Science and Technology* **2021**, 1-19.
24. Wada, Y.; Hamada, K.; Hirata, N.; Seki, K.; Yamada, S. A system dynamics model for shipbuilding demand forecasting. *Journal of Marine Science and Technology* **2018**, *23*, 236-252.
25. Lee, S.; Jung, I. Development of a Platform Using Big Data-Based Artificial Intelligence to Predict New Demand of Shipbuilding. *The Journal of The Institute of Internet, Broadcasting and Communication* **2019**, *19*, 171-178.
26. Fujikubo, M. Digital Twin for Ship Structures: Research Project in Japan (Plenary Lecture Presentation). **2019**.
27. Breinholt, C.; Ehrke, K.-C.; Papanikolaou, A.; Sames, P.C.; Skjong, R.; Strang, T.; Vassalos, D.; Witolla, T. SAFEDOR–the implementation of risk-based ship design and approval. *Procedia-Social and Behavioral Sciences* **2012**, *48*, 753-764.
28. Faber, J.; Hanayama, S.; Zhang, S.; Pereda, P.; Comer, B.; Hauerhof, E.; Yuan, H. Fourth IMO greenhouse gas study. *Retrieved from the International Maritime Organization website: https://docs. imo. org* **2020**.
29. Smith, T.; Jalkanen, J.; Anderson, B.; Corbett, J.; Faber, J.; Hanayama, S.; O'keeffe, E.; Parker, S.; Johanasson, L.; Aldous, L. Third imo ghg study. **2015**.
30. Arifin, M.D.; Hamada, K.; Hirata, N.; Ihara, K.; Koide, Y. Development of ship allocation models using marine logistics data and its application to bulk carrier demand forecasting and basic planning support. *Journal of the Japan Society of Naval Architects and Ocean Engineers* **2018**, *27*, 139-148.
31. Sirimanne, S.N.; Hoffman, J.; Juan, W.; Asariotis, R.; Assaf, M.; Ayala, G.; Benamara, H.; Chantrel, D.; Hoffmann, J.; Premti, A. *Review of maritime transport 2019*; tech. rep: 2019.

32. Zhang, X.; Lam, J.S.L.; Iris, Ç. Cold chain shipping mode choice with environmental and financial perspectives. *Transportation Research Part D: Transport and Environment* **2020**, *87*, 102537.
33. Venturini, G.; Iris, Ç.; Kontovas, C.A.; Larsen, A. The multi-port berth allocation problem with speed optimization and emission considerations. *Transportation Research Part D: Transport and Environment* **2017**, *54*, 142-159.
34. Arslan, A.N.; Papageorgiou, D.J. Bulk ship fleet renewal and deployment under uncertainty: A multi-stage stochastic programming approach. *Transportation Research Part E: Logistics and Transportation Review* **2017**, *97*, 69-96.
35. Lin, D.-Y.; Liu, H.-Y. Combined ship allocation, routing and freight assignment in tramp shipping. *Transportation Research Part E: Logistics and Transportation Review* **2011**, *47*, 414-431.
36. Yang, D.; Wu, L.; Wang, S.; Jia, H.; Li, K.X. How big data enriches maritime research–a critical review of Automatic Identification System (AIS) data applications. *Transport Reviews* **2019**, *39*, 755-773.
37. Andersson, P.; Ivehammar, P. Dynamic route planning in the Baltic Sea Region–A cost-benefit analysis based on AIS data. *Maritime Economics & Logistics* **2017**, *19*, 631-649.
38. Bai, X.; Cheng, L.; Iris, Ç. Data-driven financial and operational risk management: Empirical evidence from the global tramp shipping industry. *Transportation Research Part E: Logistics and Transportation Review* **2022**, *158*, 102617, doi:https://doi.org/10.1016/j.tre.2022.102617.
39. IHS MARKIT / TheTradeNet Market Intelligence Network (MINT). Available online: https://www.marketintelligencenetwork.com/ (accessed on 28 September 2021).
40. AXSMarine / AXSDry. Available online: https://public.axsmarine.com/axsdry/ (accessed on 28 September 2021).
41. Wada, Y.; Hamada, K.; Kamata, T.; Nanao, J.; Watanabe, D.; Majima, T. Evaluation of AIS data and port calling data using ship operation data of a shipping company. In Proceedings of the International Association of Maritime Economists (IAME), The Hong Kong Polytechnic University, 2020.
42. IHS MARKIT Sea-web Ships. Available online: https://maritime.ihs.com/entitlementportal/home/information/seaweb_ships (accessed on 28 September 2021).
43. IHS MARKIT Sea-web Ports. Available online: https://maritime.ihs.com/EntitlementPortal/Home/Information/Seaweb_Ports (accessed on 28 September 2021).
44. *IHS Fairplay Ports and Terminals Guide 2013 - 2014 (Book and CD Set)*; Jane's Information Group: 2012.
45. Authority, P.C. *OP NOTICE TO SHIPPING No. N-1-2018*; N-1-2018, Vessel Requirements: 2018.

46. Greiner, R. Ship operating costs: Current and future trends. In *Technical Report*; Moore Stephens LLP. Singapore: 2013.
47. Asariotis, R.; Benamara, H.; Finkenbrink, H.; Hoffmann, J.; Lavelle, J.; Misovicova, M.; Valentine, V.; Youssef, F. *Review of Maritime Transport, 2011*; 9211128412; 2011.
48. Clarksons Research Shipping Intelligence Network. Available online: https://sin.clarksons.net/ (accessed on 28 September 2021).
49. Rutherford, D.; Comer, B. The International Maritime Organization's initial greenhouse gas strategy. **2018**.
50. Comer, B.; Chen, C.; Rutherford, D. Relating short-term measures to IMO's minimum 2050 emissions reduction target. *International Council on Clean Transportation. Retrieved from* **2018**.
51. Rutherford, D.; Mao, X.; Comer, B. Potential CO2 reductions under the energy efficiency existing ship index. *International council on clean transportation. Working paper* **2020**, 2020-2027.
52. Japan Port Association: Port Logistics Information. Available online: https://www.phaj.or.jp/distribution/14port /price.html (accessed on 28 September 2021).
53. Whitaker, J. Basemap. Available online: https://github.com/matplotlib/basemap (accessed on 28 September 2021).
54. Whitaker, J. Plotting data on a map (Example Gallery). Available online: https://matplotlib.org/basemap/users/examples.html (accessed on 28 September 2021).
55. Fiorini, M.; Capata, A.; Bloisi, D.D. AIS data visualization for maritime spatial planning (MSP). *International Journal of e-Navigation and Maritime Economy* **2016**, *5*, 45-60.
56. Papanikolaou, A. *A holistic approach to ship design*; Springer: 2019.
57. International Association of Classification Societies (IACS). Available online: https://www.iacs.org.uk/publications/common-structural-rules/ (accessed on 28 September 2021).
58. DNVGL, R.N.E. Maritime Forecast to 2050. **2020**.
59. Perera, L.P.; Soares, C.G. Weather routing and safe ship handling in the future of shipping. *Ocean Engineering* **2017**, *130*, 684-695.

ACKNOWLEDGEMENTS

I am thankful to my supervisors Prof. Kunihiro Hamada and Assistant Professor Noritaka Hirata, Graduate School of Advanced Science and Engineering, Hiroshima University, for their noble guidance and valuable suggestions.

I would like to acknowledge Prof. Mitsuru Kitamura and Associate Prof. Eiji Shintaku for providing me the valuable suggestions regarding my dissertation.

Special thanks to colleagues in the Transportation and Environmental Systems Program, Mohammad Danil Arifin, Gunawan, Timothy Reinaldo Sihombing, Ibadurrahman, and Ede Mehta Wardhana. Their company in Japan will always be remembered.

I would like to thank all my colleagues in the Laboratory of Transportation System Innovation, who was always there during my doctoral program. Their company in the field and laboratory will always be remembered. Specifically, I would also like to express my gratitude to Yusuke Miyake, Shun Kawamura, and Takashi Saito for assisting me in sorting the data.

Most importantly, I am grateful to all my friends and family members for encouraging and supporting me whenever I needed them.

this page intentionally left blank